THE ROLE OF *SCN2A* IN AUTISM SPECTRUM DISORDER

A HUMAN *IN VITRO* INVESTIGATION OF THE AUTISM SPECTRUM DISORDER
RISK GENE *SCN2A*

By

CHAD BROWN, B.Sc, M.Sc.

A Thesis Submitted to the School of Graduate Studies in Partial Fulfilment of the
Requirements for the Degree Doctor of Philosophy

McMaster University

DOCTOR OF PHILOSPHY (2022)   McMASTER UNIVERSITY

Biochemistry and Biomedical Sciences   Hamilton, ON

TITLE: A human *in vitro* investigation of the autism
                                spectrum disorder risk gene *SCN2A*

AUTHOR: Chad Brown, B.Sc, M.Sc.

SUPERVISOR: Dr. Karun Singh

NUMBER OF PAGES: ccxxvi, 226

LAY ABSTRACT

Autism spectrum disorder (ASD) is an umbrella term that includes several neurodevelopmental disorders affecting 1 in 55 children. Children with ASD often have their quality of life impacted through impaired social communication and interactions, and repetitive behaviors. Currently, there is a lack of understanding about what causes ASD, which makes treating ASD difficult. Because of this, many treatments focus on behavioural deficits. ASD is thought to be a disorder of incorrect information processing within the brain that arises from changes in connections between brain cells (neurons). Researchers have discovered that one of the major risk factors of developing ASD is changes in the DNA (risk variants). There are over 1000 genes identified in ASD with changes. Many of these changes to DNA in varying genes have led to changes in connections between neurons. In this thesis, we collaborated with Dr. Stephen Scherer (Hospital for Sick Children, Toronto) to investigate a known ASD-risk gene with unreported genetic variants (changes in the DNA sequence). We studied the gene named *Voltage-Gated Sodium Channel Type II Alpha Subunit (SCN2A)* and found that a severe variant affecting this channel changed typical development by altering native neuron properties and connections similar to if the neuron did not have the gene there. We also discovered that no two variants behave the same, even with similar categorization, their location within the DNA sequence matters. Additionally, we discovered signalling networks that were altered in neurons that contained the severe variant in *SCN2A*. Many of these pathways were previously associated with ASD but in the context of other genes. However, for this specific variant and the current state of the knowledge around this gene, we provided new information potentially

aiding in target treatment opportunities. This thesis generates new insights into how differing disruptions in *SCN2A*'s DNA can disrupt development through changing neuronal communication. It further provides insights into how altered neuronal communication can affect signalling networks which are core to normal neurodevelopment.

ABSTRACT

Autism spectrum disorder (ASD) encompasses a group of heterogeneous disorders that affect approximately 1% of children worldwide. ASD is characterized by two core symptoms, the first being deficits in social communication and interaction, and the second being restrictive and repetitive behaviours. Although environmental and genetic factors are known to contribute to the development of ASD, the etiology remains unknown. Genetic sequencing studies have implicated over 1000 genes with risk variants that are ASD-associated. Recent sequencing studies have highlighted that *SCN2A*, a gene that encodes the Voltage-Gated Sodium Channel Type II Alpha Subunit habours a large proportion of genetic risk variants for ASD. An emphasis was put on this gene because many of the top genes regulate transcription and cytoskeletal dynamics and not sodium flux aiding in regulating neuron excitability. Initial investigations of complete loss of *Scn2a* in mice led to perinatal lethality where heterozygous loss exhibited many behavioural phenotypes associated with ASD. Through our collaboration with Dr. Stephen Scherer (Hospital for Sick Children, Toronto) we identified two *de novo* truncating point variants in *SCN2A*. In our study, we focused on using human iPSC-derived neurons for disease modelling. We found these two variants caused a reduction in synapses suggesting that neuronal communication may be altered. Furthermore, electrophysiological characterization of the neurons harbouring the differing *SCN2A* variants showcased that loss-of-function (LoF) variants can produce differential phenotypes based on their location. Beyond the initial ion channel characterization, we wanted to probe whether cellular pathways were altered directly or indirectly by atypical neuronal activity. Proteomics of neurons expressing the

more severe variant, p.R607*, found differentially expressed proteins (DEP)s that were upregulated and downregulated. Moreover, these DEPs were enriched and clustered into cellular pathways that were altered, with one of these clusters representing mitochondrial function. We functionally validated these findings in the same neurons and found corroboration between the molecular and cellular data of impaired mitochondria. Lastly, we used Clustered regularly interspaced short palindromic repeats (CRISPR)-Cas9 gene editing to generate an isogenic model to validate our findings of the less severe p.G1744* variant. Together, this will aid in the discovery of new variant categorizations and targeted treatments for rescues of atypical neural connectivity or pathways that are altered downstream.

ACKNOWLEDGEMENTS

TABLE OF CONTENTS

LIST OF FIGURES & TABLES

xv

LIST OF ABBREVIATIONS

ADOS-2	Autism diagnostic observation schedule – 2nd edition
AIS	Axon initial segment
AMPA	α-amino-3-hydroxy-5-methyl-4-isoxazolepropionic acid
AMPAR	α-amino-3-hydroxy-5-methyl-4-isoxazolepropionic acid receptor
ANK2	Ankyrin 2
ASD	Autism spectrum disorder
ASCL1	Achaete-scute family BHLH transcription factor 1
ASO	Antisense oligonucleotide
ATP	Adenosine triphosphate
BDNF	Brain-derived neurotrophic factor
BFIS	Benign familial infantile seizures
B/P	Blocking and permeabilizing solution
CACNA1C	Calcium channel, voltage-gated, L-type, alpha-1C subunit
CARS-2	Childhood autism rating scale – 2nd edition
CDC	Centres for disease control and prevention
CHD8	Chromodomain helicase DNA binding protein 8
CNS	Central nervous system
CNV	Copy number variant
CREBBP	CREB binding protein

CRISPR	Clustered regularly interspaced short palindromic repeats
CYFIP1	Cytoplasmic FMRP-interacting protein 1
DAPI	4′,6-diamidino-2-phenylindole
ddPCR	Digital droplet polymerase chain reaction
DEP	Differentially expressed protein
DIV	Day *in vitro*
DLX2	Distal-less homeobox 2
DSB	Double-stranded break
EA	Episodic ataxia
EB	Embryoid body
EE	Epileptic encephalopathy
eIF4E	Eukaryotic translation initiation factor 4E
eIF4G	Eukaryotic translation initiation factor 4G
DNA-PKcs	DNA-dependent protein kinase catalytic subunit
DSM	Diagnostic and statistical manual of mental disorders
eQTL	Expression quantitative trait-associated loci
ESC	Embryonic stem cell
ETC	Electron transport chain
E/I	Excitation/inhibition
FDA	Food and drug administration
FMR1/FMRP	Fragile X messenger ribonucleoprotein 1

FXS	Fragile X syndrome
GABA	γ-Aminobutyric acid
GDNF	Glial cell line-derived neurotrophic factor
GFP	Green fluorescent protein
GPM6A	Neuronal glycoprotein M6A
GO	Gene ontology
GoF	Gain-of-function
GWAS	Genome-wide association studies
HCD	Higher energy collision-induced dissociation
HDR	Homology-directed repair
HEK	Human embryonic kidney
ID	Intellectual disability
IEE	Infantile epileptic encephalopathy
iNeuron	Induced neuron
iNI	Neuron supplement media
iPSC	Induced pluripotent stem cell
KI	Knockin
KLF4	Kruppel like factor 4
KO	Knockout
$K_V1.1$/ $K_V1.2$	Voltage-gated potassium channel subfamily A, member 1 and 2
LoF	Loss-of-function

LTP	Long-term potentiation
MAP2	Microtubule associated protein 2
MEA	Multielectrode array
MECP2	Methyl-CpG binding protein 2
MELAS	Mitochondrial encephalomyopathy lactic acidosis and stroke-like episodes
mGluR	Metabotropic glutamate receptor
MS	Mass spectrometry
mtDNA	Mitochondrial deoxyribonucleic acid
mTOR	Mammalian target of rapamycin signaling pathway
MYC	MYC proto-oncogene, BHLH transcription factor
NANOG	Homeobox transcription factor nanog
Na$_V$s/SCNxA	Family of voltage-gated sodium channels
Na$_V$1.2	Voltage-gated sodium channel type II alpha protein
Na$_V$1.5	Voltage-gated sodium channel type V alpha protein
Na$_V$1.6	Voltage-gated sodium channel type VIII alpha protein
NCAM1	Neural cell adhesion molecule 1
NDD	Neurodevelopmental disorder
NGN2	Neurogenin2
NGS	Next generation sequencing
NGLN	Neuroligin

NHEJ	Non-homologous end joining
NMDA	N-Methyl-D-aspartate
NMDAR	N-Methyl-D-aspartate receptor
NPC	Neural progenitor cell
NXRN	Neurexin
OCT4	Octamer-binding transcription factor 4
PAM	Protospacer-adjacent motif
PBS	Phosphate buffered saline
PDD-NOS	Pervasive developmental disorder- not otherwise specified
pQTL	Protein quantitative trait loci
RNP	Ribonucleotide protein
RPLC	reverse-phase liquid chromatography
S6K1/2	Ribosomal protein S6 kinase 1 and 2
SCN1A/2A/3A/8A	Sodium channel, voltage-gated, type I/II/III/VIII, alpha subunit
SFARI	Simons foundation autism research initiative
sgRNA	Single-guide RNA
SHANK1-3	SH3 and multiple ankyrin repeat domains 1, 2, and 3
SOD1	Superoxide dismutase 1
SOX2	SRY-box transcription factor 2
SNP	Single nucleotide polymorphism
SNV	Single nucleotide variant

ssODN	Single-stranded oligodeoxynucleotides donor
SYN1	SynapsinI
SYNGAP1	Synaptic Ras GTPase activating protein 1
TALEN	Transcription activator-like effector nucleases
TMT	Tandem mass tags
tracrRNA	trans-activating CRISPR RNA
TSC1	TSC complex subunit 1
TSC2	TSC complex subunit 2
UBE3A	Ubiquitin protein ligase E3A
VZ	Ventricular zone
WES	Whole exome sequencing
WGS	Whole genome sequencing
ZFN	Zinc finger nucleases

CHAPTER 1: INTRODUCTION

1.1 Autism spectrum disorder

1.1.1 Clinical presentation, etiology, and diagnosis

Autism spectrum disorder (ASD) is a heterogeneous neurodevelopmental disorder that encompasses other disorders with varying severities that are characterized by impaired social communication and interactions, and repetitive or restricted behaviours (Miles, 2011). According to the Centres for Disease Control and Prevention (CDC 2022), diagnosis is often detected between 2-5 years of age with early detection at 6 months, and final diagnosis often being much later in age (Brian et al., 2019; Miles, 2011; Zwaigenbaum and Penner, 2018). Unfortunately, as the etiology is unknown, diagnosis can be difficult with some children being diagnosed in their adolescents. The Diagnostic and Statistical Manual of Mental Disorders (DSM) is a guideline that health care professionals use to classify development, intellectual and psychiatric disorders. Previously, children with ASD were categorized differently under the DSM-4; there were three distinct categories: Autistic disorder, Asperger's syndrome, and pervasive developmental disorder- not otherwise specified (PDD-NOS) (Miles, 2011). As of 2013 the updated DSM-5 now describes children with autism under the broad spectrum of autism spectrum disorder (Brentani et al., 2013). To date, there are several diagnostic tests used to assess for ASD. Health care professionals often use a collaborative and multidimensional approach which includes medical history, DSM-5 criteria, sensory assessment, interviews with the child's caregiver, and behavioural assessment of the child (Brian et al., 2019). The most commonly used

diagnostic test is the Autism Diagnostic Observation Schedule – 2nd edition (ADOS-2) which uses behavioural observations of the child (Brian et al., 2019). Coding observations and direct interactions with the child are examined, to supplement this test clinicians will often opt to use the Childhood Autism Rating Scale – 2nd edition (CARS-2) if children are clinically referred (Falkmer et al., 2013; Zwaigenbaum and Penner, 2018). The other commonly used diagnostic test is the Autism Diagnostic Interview-Revised (ADI-R), tests like these rely on caregiver interviews (Brian et al., 2019). As these diagnostic tests cannot be used alone to diagnose ASD, when used carefully they provide high sensitivity and specificity when identifying children with or without ASD ($\geq$80% correct identification) (Brian et al., 2019; Randall et al., 2018).

One of the most common neurodevelopmental disorders is ASD, worldwide prevalence estimates are between 1% – 1.5% (Baxter et al., 2015; Christensen et al., 2018). As diagnostic tools and next-generation sequencing (NGS) improve estimates have continued to increase. More recently, a surveillance prevalence report estimated that as many as 1 in 44 children are diagnosed with ASD (Maenner et al., 2021). Additionally, ASD is known to have a high sex-biased, with boys being 4.2 times more likely to be diagnosed than girls (Maenner et al., 2021). Depending on the severity of ASD, children may have comorbidities that add to the difficulties of having good outcomes with health, education, employment, and relationships (Farley et al., 2009; Volkmar et al., 2017). Researchers performed a meta-analysis on the long-term overall outcome of 828 individuals with ASD (Steinhausen et al., 2016). They found that 19.7% of cases had good

to very good outcomes, 31.1% of causes had a fair outcome, and 47.7% of cases had poor

to very poor outcomes (Steinhausen et al., 2016). This emphasized that roughly half of the

individuals with ASD had unfavorable long-term outcomes.

Although the cause of ASD is unknown, it is understood that genetic and

environmental factors significantly contribute (Wang et al., 2017). It is poorly understood

if the genetic risk is modulated by prenatal, perinatal, and postnatal environmental factors;

however, several studies have shown links between premature and overdue pregnancy and

increased ASD-risk along with other NDDs (Agrawal et al., 2018; Schieve et al., 2018).

Additionally, maternal immune activation during pregnancy is associated with increased

ASD-risk (Croen et al., 2019; Malkova et al., 2012). What is clear to researchers is that

genetic risk accounts for at least 20% of cases with new estimates up to 30% with the

advancements in genetic sequencing techniques (Hallmayer et al., 2011; Srivastava et al.,

2019; Ziats et al., 2021). Often, variants that are detected from ASD and NDD cohorts alter

the expression and function of the proteins encoded. Reports suggest over 700 genes have

been implicated in ASD highlighting the heterogeneity of the disorder (Saxena and

Chahrour, 2017). Many genes are found to harbour more variants than others, however,

cellular function is disrupted unbiasedly, with variants affecting proteins in scaffolding,

neuronal communication, and transcription regulation (Grove et al., 2019; Satterstrom et

al., 2020).

Since the etiology and pathobiology of ASD are poorly understood there remains

no effective treatments. Treatments instead target the symptoms of ASD including

approaches for behavioural, educational, and psychological (Brentani et al., 2013; De Filippis and Wagner, 2016). Pharmacological treatments have been used to help remedy symptoms although children and adolescents often appear to be more susceptible to adverse effects, thus requiring low dosage and titration plans (De Filippis and Wagner, 2016). The newest drug named STP1 has recently finished phase 1 clinical trials with the notoriety of being the first precision medicine drug for ASD. Observations of dose-dependent improvements of electrophysiological signals in brain regions associated with social interactions, working memory, and processing speed have been reported. These improvements have made this drug a hopeful candidate for treatment adding another promising therapeutic approach.

1.2 The genetics of ASD

Among the determinants of ASD, genetics play a key role in disease pathophysiology. As advancements in genetic testing continue, genetic diagnosis of patients has increased to 30%, with penetrance and strength of the genetic abnormality determining the genetic risk (Geschwind, 2011; Srivastava et al., 2019; Ziats et al., 2021). Folstein et al. first identified ASD as being heritable in the mid-1970s (Folstein and Rutter, 1977). Since this time, studies of ASD and other neuropsychiatric disorders have indicated heritability to reach up to 80% (Anttila et al., 2018; Geschwind and Flint, 2015; Sullivan and Geschwind, 2019). Recently, a large population-based multinational study estimated the heritability of ASD to be approximately 80% (Bai et al., 2019). Uniquely, monozygotic twin studies revealed that the heritability can reach up to 90%, however, dizygotic twins

maintain heritability up to 30% (Folstein and Rutter, 1977; Freitag et al., 2010; Hallmayer et al., 2011; Sandin et al., 2014). Although the etiology of ASD remains unknown, syndromic forms account for up to 20% of cases with partially known etiologies. Monogenic syndromes represent disorders that have been extensively studied, aiding in the understanding of the interplay between neurobehavior, etiology, and mechanisms that may contribute to idiopathic ASD (Baudouin et al., 2012; Ziats et al., 2021). Some of the most reported monogenic syndromes of ASD include Fragile X syndrome, Angelman syndrome, and Rett syndrome which are caused by mutations in *FMR1* (Richter and Zhao, 2021), *UBE3A* (Buiting et al., 2016), and *MECP2* (Good et al., 2021; Ip et al., 2018a; Pejhan and Rastegar, 2021), respectively. As this is not an exhaustive list of syndromic autism, it is worth noting that there are an estimated 115 monogenetic disorders, with additional chromosomal deletion, duplication, and aneuploidy contributing (Ziats et al., 2021).

The progression of genetic studies since the 1960s has paralleled advancements in technology development (Sullivan and Geschwind, 2019). Early successes in genetic profiling started with the identification of single-protein biomarkers. This has progressed through genome-wide panels of selected single nucleotide polymorphisms (SNPs), and now, sequencing and resequencing of whole exomes and genomes (Sullivan and Geschwind, 2019). Genome-wide association studies (GWAS) provided a platform to assay millions of SNPs within the human population that are common. As common genetic variation contributes to ~50% of genetic risk in ASD, GWAS were useful for identifying variants (Autism Spectrum Disorders Working Group of The Psychiatric Genomics

Consortium, 2017; Gaugler et al., 2014; Ma et al., 2009; Weiss et al., 2009). Gene disruption discoveries in ASD were driven by the advent of next-generation sequencing (NGS). Whole exome sequencing (WES) studies focused on genome segments that encoded human proteins (Iossifov et al., 2014; De La Torre-Ubieta et al., 2016; De Rubeis et al., 2014; Sanders et al., 2015; Satterstrom et al., 2020). These studies provided the groundwork for our current understanding of identifying risk-genes and copy number variants (CNVs) that contribute to neurodevelopmental disorders (Lim et al., 2017). One of the largest and recent WES studies analyzed over 35 000 people with approximately 12 000 ASD patients, they identified 102 ASD-risk genes with many previously being identified in other WES studies (Iossifov et al., 2014; De Rubeis et al., 2014; Satterstrom et al., 2020). Whole-genome sequencing (WGS) studies are used to identify genetic variants in the form of single nucleotide variants (SNVs) or copy number variations (CNVs) that might be enriched in ASD populations versus their neurotypical counterparts (Belkadi et al., 2015; Choi and An, 2021). As the name suggests, WGS studies examine the entire genome by fragmenting the DNA into short segments of up to approximately 150 basepairs; these short segments are then read multiple times in parallel, aligned, and matched to a reference human genome (Hayeems and Boycott, 2018). These advancements in genetic profiling have been paramount in identifying ASD risk-genes. The work in this thesis benefited greatly from our collaborators at the Hospital for Sick Children in Toronto. To date, they have performed WGS on 5,205 human samples, this includes 2,620 patients with ASD (Yuen et al., 2015, 2016, 2017). From these studies, two of the SNVs identified in patients with *de novo* mutations in *SCN2A* were characterized in this thesis. As new ASD-

risk genes are identified, a transition to functional genomics and cellular characterization continues. This is because understanding molecular and cellular convergence is critical to teasing apart the pathobiology.

As ASD is a complex disorder with high heterogeneity, the genetic architecture consists of rare inherited, *de novo*, and thousands of common polygenic variants. Discoveries through WGS and WES have been essential for identifying rare inherited and *de novo* variants. NGS studies have generated databases of millions of CNVs and SNVs for studies to use and to investigate how they converge onto common signalling pathways. Rare inherited variants are passed down from the mother or father to the child, while *de novo* variants originate only in the affected child or proband but are not present in the parents. *De novo* mutations in the human genome occur during gametogenesis, which aids in genetic diversity but can also produce deleterious effects (Belyeu et al., 2021). Many studies have determined that SNVs and indels occur in individuals approximating 70 events per individual (An et al., 2018; Belyeu et al., 2021; Jónsson et al., 2017; Kong et al., 2012; Sasani et al., 2019; Werling et al., 2018). Additionally, studies have found that parental fitness is an important determiner of genetic load on the offspring; as parental age increases so too does the frequency of *de novo* variants, increasing the likelihood of deleterious variants (Goldmann et al., 2016; Jónsson et al., 2017; Sasani et al., 2019; Shendure and Akey, 2015). This age-related enrichment on genetic load was also found to be more prominent in increasing paternal age compared to maternal age (Kong et al., 2012). Harder to detect are the larger *de novo* variants, often referred to as structural variants or CNVs.

CNVs comprise deletions, duplications, insertions, inversions, translocations, and variants that combine any of the class types listed. CNVs are alterations in sequences of the genome that contain changes in the number of copies of DNA sequences on chromosomes greater than 1 kilobase (Kb), this often affects many genes within the region (Thapar and Cooper, 2013). *De novo* CNVs are less frequently detected than their SNV counterparts, however, they contribute to many of the same neurodevelopmental disorders (Ma et al., 2017; Talkowski et al., 2012; Xu et al., 2008). Because of this confounder, detection of *de novo* CNVs requires larger cohorts to detect accurate estimates (Belyeu et al., 2021). To date, *de novo* and rare inherited CNVs are known to be harbored in sporadic and multiplex autism compared to the general population (Brandler et al., 2016; Iakoucheva et al., 2019; Krumm et al., 2015; Sebat et al., 2007; Turner et al., 2017; Wilfert et al., 2021). Taken together, SNVs and CNVS are often found enriched in children with ASD, with many of these variants categorized as gene disruptive or likely to cause disruption. Furthermore, rare variants and *de novo* variants contribute largely to the disease pathogenesis of ASD as these variants may deleteriously impact protein function.

1.2.1 Simons Foundation Autism Research Initiative

Over the years WGS, WES, and GWAS have implicated numerous genes to be associated with ASD (Iossifov et al., 2014; Sanders et al., 2012; Satterstrom et al., 2020; Yuen et al., 2015, 2016, 2017). These studies have found multiple rare-inherited, *de novo* and common variants that underlie the complex genetic landscape of ASD. As more genes are uncovered, a central repository is needed to tabulate findings. The Simons Foundation

Autism Research Initiative (SFARI) is an organization that uses its programs to improve the understanding, diagnosis, and treatment of ASD. SFARI has well-known programs within the ASD community, extending from ASD cohort recruitment and genetic rodent model generation partnering with The Jackson Laboratory to the generation of iPSC lines from probands for researchers to investigate. We have specifically used the SFARI Gene program, this program integrates data from genetic and molecular studies of ASD to create a comprehensive ASD-risk gene database. These genes are initially scored based on their recurrence and evidence in the literature linking them to ASD. The database SFARI has generated the foremost accepted database for ASD-risk genes, to date, 1,231 curated genes have been implicated in ASD. Genes are categorized into four scoring modules, syndromic, category 1 (high confidence), category 2 (strong candidate), and category 3 (suggestive evidence) (Abrahams et al., 2013). The gene scoring system was developed by geneticists, statisticians, curators, and consultants with an emphasis on evidence-based scoring to avoid over and under-representation. The syndromic category consists of genes that have been implicated in ASD, such as the previously mentioned *FMR1* and *UBE3A* in Fragile X syndrome and Angelman syndrome, respectively. Currently of the 1,231 genes, 418 are considered either high confidence or strong candidate genes for ASD risk. The high confidence category has ASD-risk genes that have been implicated in the literature typically with a minimum of three *de novo* variants, that have been classified as likely-gene disrupting. Genes in this category affect various molecular functions, many of the top published genes include functions in cell adhesion *NRXN1*, scaffolding proteins *SHANK3* and *ANK2*, ion channels *SCN2A* and *CACNA1C*, transcriptional coactivator *CREBBP*, and

transcriptional repressor *CHD8*. A step-down, category 2, or strong confidence is characterized by having two reported *de novo* likely-gene-disrupting mutations. Usually, genes in this category have been identified by GWAS or have been found to have functional effects that are consistently replicated. Finally, category 3 or suggestive evidence is described as having a single reported *de novo* likely-gene-disrupting mutation. In addition, genes in category 3 are not replicated but are a part of a significant association study. Category 3 remains the largest ASD-risk category with 477 genes, this emphasizes the lack of studies that have investigated the roles of newly identified ASD-associated genes.

1.3 The pathophysiology of ASD

1.3.1 Neuroconnectivity

During the development of the brain, complex processes are finely orchestrated that include, neurogenesis, neuronal migration, synaptogenesis, and processes like pruning that extend into adulthood (Figure 1) (Courchesne et al., 2018). Atypical neurodevelopment and altered neural communication has been associated with a prevailing hypotheses in ASD, this is the imbalanced excitation/inhibition (E/I) ratio hypothesis (Figure 2) (Culotta and Penzes, 2020; Rubenstein and Merzenich, 2003). It is important to note that the E/I ratio hypothesis overly simplifies neural circuits since there are many other factors to take into consideration. This includes developmental age where γ-Aminobutyric acid (GABA) can have an excitatory effect early in development (Ganguly et al., 2001), and different brain regions consisting of different proportions and subpopulations of excitatory and inhibitory neurons. Since they can have varying inputs and outputs in each region, this makes regional

and cellular compartment-specific E/I ratios also important (Kepecs and Fishell, 2014; Nelson and Valakh, 2015; Petreanu et al., 2009). The E/I hypothesis can also be studied using stem cell-derived human neurons and 3D organoid models to examine human neurodevelopment. These models will allow testing of the E/I hypothesis as the ability to perform electrophysiology, imaging, or circuit-based stimulations and recordings has emerged (Flaherty et al., 2019; Marro et al., 2019; Pak et al., 2015; Zhang et al., 2018). Therefore, similar to mouse studies, discrete neural circuit questions can now be investigated using human iPSC modeling.

Neurons regulate their excitatory and inhibitory inputs to maintain circuit function and stability, which is thought to be through the E/I ratio. Deviations from this ratio are thought to lead to neural dysfunction. Broadly, inhibition can mean different things, for example, subsets of inhibitory inputs, all inhibitory inputs, and inhibitory inputs over a temporal window, these classifications also apply to excitatory inputs (He and Cline, 2019). An imbalance in the E/I ratio can result from both an increase or decrease in excitatory and inhibitory neuron firing, respectively. Although an increase in the E/I ratio can occur from an increase in excitatory neuron firing, the majority of imbalances in ASD models have been associated with decreased inhibition. Additionally, when fluctuations shift the E/I ratio, neural circuits and neurons are responsible for adapting to these changes to restore the set point or to create a new set point through plasticity. Synaptic scaling, one form of plasticity, is necessary to regulate excess or absent inputs. For example, the effects of a delayed E/I developmental shift of GABA have been observed in two distinct mouse

11

models of ASD (Tyzio et al., 2014), where the depolarizing effects of abnormal GABA$_A$ receptor levels contribute to E/I imbalance in the brain.

1.3.2 Neuroconnectivity and dynamic changes at the synapse

Many ASD-risk genes and their translated proteins are regulated by neuronal activity through transcription, splicing, translation, or degradation (Ebert and Greenberg, 2013). Mutations of ASD-risk genes coding for synaptic proteins are likely to cause synaptic malfunction and disruptions in neural circuits. Activity-dependent and developmental stage-dependent transcription factors diversify transcriptional regulation using alternative promoters (Davuluri et al., 2008; Loebrich and Nedivi, 2009). Genes that have been investigated and reported to have modulatory effects on synaptic plasticity or are regulated by neural activity but are not limited to these are *Syngap1*, *Shank1-3*, *Nxrn*, *Nlgn*, *Fmrp*, and *Ube3a*. Synaptic GTPase-Activating Protein (SynGAP) is a key postsynaptic density signaling enzyme that negatively regulates small G protein signaling downstream of glutamate receptor activation (McMahon et al., 2012). SynGAP forms a signaling complex with the Ras family proteins through its physical linkage to postsynaptic scaffold proteins PSD-95 and SAP-102 which bind to N-methyl-D-aspartate (NMDA) receptors (Husi et al., 2000; Rumbaugh et al., 2006). Mice with reduced SynGAP expression show decreased hippocampal long-term potentiation (LTP) and impaired spatial learning; also, it has been reported that gain-of-function (GoF) reduced synaptic strength and loss-of-function (LoF) increased synaptic strength (McMahon et al., 2012; Muhia et al., 2010; Rumbaugh et al., 2006). SynGAP has also been implicated in altered α-amino-3-hydroxy-

5-methyl-4-isoxazole propionic acid (AMPA) receptor trafficking, where overexpression leads to decreased AMPA receptors (AMPAR) at excitatory synapses and reduced synaptic transmission (Rumbaugh et al., 2006). Furthermore, SynGAP has been shown to direct NMDA receptor-dependent modulation of synapse density and dendritic spine shape, negatively regulate ERK signalling, and stimulate p38 MAPK signaling (Kim et al., 2003; McMahon et al., 2012; Rumbaugh et al., 2006; Vazquez et al., 2004; Zhu et al., 2002). SH3 and multiple ankyrin repeat domains (SHANK) proteins are scaffolding proteins and have been shown to regulate active synapses. Knockdown of Shank1 or 2 reduces AMPAR-mediated synaptic transmission (Shi et al., 2017). In addition, Shank3 deficient mice have deficits in AMPA signaling and LTP, which are rescued by the application of insulin-like growth factor 1 (Bozdagi et al., 2013). Behaviorally, all of these mice models exhibit hallmarks of ASD or developmental delay (Bozdagi et al., 2013). Lastly, homozygous loss of Shank2 causes an imbalance of NMDA receptor function throughout development, where early development has a hyperactive state of NMDA receptor while later stages have a hypoactive state, leading to ASD-like and social deficit behaviors (Chung et al., 2019). These outcomes were ameliorated by early correction of NMDA receptor dysfunction (Chung et al., 2019). In summary, these findings highlight only some ASD-risk genes that are closely related to activity-dependent synaptic regulation (McMahon et al., 2012; Rumbaugh et al., 2006; Shi et al., 2017). Here, we discuss that scaffolding and postsynaptic density proteins can regulate excitatory synapse development and function translating to ASD, intellectual disability, and developmental delay.

1.3.3 Modeling ASD in human neurons

Although genetic mouse models of NDDs remain the gold standard for investigating human behaviour and systems biology, the field has made substantial progress in human modeling. Historically, attempts to model neuropsychiatric disorders focused on the study of human post-mortem tissue and biopsies; however, the use of these samples was limited due to the invasive nature of these procedures and the lack of expandability in culture (Gordon and Geschwind, 2020; Lee et al., 2019; Soliman et al., 2017). Additionally, as post-mortem and biopsy procedures were often performed long after the first few years of life, this itself posed a problem for understanding the molecular and cellular mechanisms that contributed to the end phenotypes. Since the discoveries of embryonic stem cells (ESC)s and induced pluripotent stem cells (iPSC)s in the late 1990s and 2007, respectively, cell culturing protocols have advanced to terminally differentiate stem cells towards the lineage of choice (Acab and Muotri, 2015; Takahashi et al., 2007). Furthermore, small chemical, growth factor, and viral transduction methods have given researchers the flexibility to target specific subpopulation cell and tissue types (Lee et al., 2019; Liu et al., 2013; Miura et al., 2022; Zhang et al., 2013). The need for robust human cellular models was further highlighted by differences in neocortical development of cortical expansion, protracted time of development, and genetics (Zhao and Bhattacharyya, 2018). Inherently, the advancement of iPSC technologies has provided unlimited access and use of stem cells that can generate end somatic cells of interest. Although these advancing cellular models create models that in part recapitulate larger mammalian development and human-specific

signatures, the limitations of 1:1 scaling of cell types and progression of fully developed cells and tissues are still present (Kim et al., 2020).

Two of the initial protocols for generating human cortical from human ESCs and iPSCs in 2D cultures used neural induction media to progress through the embryoid body (EB) formation and small molecules to inhibit bone morphogenetic protein (BMP) and transforming growth-β signalling (TGFβ) (Chambers et al., 2009; Shi et al., 2012a, 2012b). However, the caveat of these protocols and protocols built on the progress of these papers is the turnover time to generate functional synapses. Without functional synapses, human-derived neurons are not a suitable system to characterize neuronal connectivity. The time *in vitro* is prolonged and varies across protocols, with functional synapses starting to form at 7 weeks and commonly extending until 12 weeks (Espuny-Camacho et al., 2013; Hu et al., 2010; Topol et al., 2015). Secondly, the yield of neurons is often lower for many of the neural induction protocols, this also adds batch-to-batch variability as biological replicates may not produce similar proportions of neuronal subtypes.

In 2013, Zhang et al. generated a protocol that surmounted the caveats of using induction media, or small molecules (Zhang et al., 2013). The novelty of their protocol was situated in their single-step induction of iPSCs and ESCs into induced functional neurons with rapid scalability. They virally transduced their PSCs with two lentiviral vectors, one ubiquitously expressing a reverse transcriptase tetracycline activator and the other containing a TetO promoter, the transcription factor neurogenin2 (NGN2), a puromycin resistance gene, and enhanced green fluorescent protein (GFP). NGN2 is a transcription

factor that is specifically expressed in the neuroectoderm lineage, overexpression of NGN2 creates direct neuron cultures. Solely, NGN2 overexpression generates layer 2/3 cortical neurons. With the addition of doxycycline and puromycin over several days, generation of a high yielding human cortical neurons cultures is obtained. These human cortical neurons mature rapidly by co-culturing using mouse astrocytes, but within 3 weeks robust functional synapses are obtained. Although this protocol created a high-throughput protocol for generating cortical neurons, as with any protocol there are caveats. Firstly, this protocol generates only excitatory glutamatergic neurons, making this system a case-by-case use, where only prior inferences of excitatory dysfunction but not inhibitory function is hypothesized or known. More recently, Barretto et al. enhanced this protocol by finding two transcription factors Distal-less homeobox 2 (DLX2) and Achaete-Scute Family BHLH Transcription Factor 1 (ASCL1) that once over-expressed produce inhibitory neurons (Barretto et al., 2020). Furthermore, they found that co-platting both excitatory and inhibitory neurons at an 80/20 split created a more physiologically relevant model for pursuing questions about the excitation-inhibition hypothesis. Secondly, due to the nature of inducing NGN2 expression to differentiation neurons rapidly, PSCs quickly progress through the typical neurogenesis stages. EBs and NPCs are not observed, instead, PSCs' cytoarchitecture visually changes creating neurite-like projections within 3 days of doxycycline addition. Because of this confounder, using induced neurons (iNeurons) to study intermediate developmental stages and the associated gene expression profiles is unattainable. Lastly, overexpression of NGN2 can generate alternative neuron subtypes. More recently it was discovered that the NGN system has a low propensity (~1%) to

16

generate sensory neurons if the exogenous expression is prolonged; additionally, protocols producing high-yielding sensory neurons use overexpression of NGN2 in addition to small molecules (Hulme et al., 2020). The rapid single-step induction protocol continues to be examined and characterized beyond the cellular level. A single-cell RNA sequencing (scRNAseq) study investigated iNeuron subpopulations at multiple time points of the induction protocol (Lin et al., 2021). They reported 3 distinct subpopulations which expressed pan-neuronal markers Microtubule-associated protein 2 *(*MAP2) and Neural cell adhesion molecule 1 (NCAM1), and that these neurons expressed Glycoprotein M6A (GPM6A) which is expressed throughout the central nervous system (CNS). As next-generation sequencing techniques evolve, they provide more resolution of genetic profiling, highlighting that what we once thought was a homogeneous population may be more representative of a heterogeneous population. Continued advancements in iPSC technologies produced adaptations to the Zhang et al. protocol, where other groups began to virally infect NPCs with the NGN2 lentiviral vectors to produce cortical neurons (Ho et al., 2016). Many studies have continued to use the original NGN2-iNeurons protocol to screen functional deficits of genetic abnormalities in ASD modelling, and have further gone on to use iNeurons to investigate molecular and cellular phenotypes (Barretto et al., 2020; Deneault et al., 2018, 2019; Meijer et al., 2019; Nehme et al., 2018; Rhee et al., 2019; Tidball et al., 2020).

As mentioned, the complexity of human brain development differentiates itself from rodents, nonhuman primates, and other species. Highly specialized cells and regions

add to the complexity concerning cognitive function, cell diversity, and brain size and shape (Amin and Paşca, 2018; Kathuria et al., 2020; Kim et al., 2020). 2D cultures cannot recapitulate the spatiality of brain development (Geschwind and Rakic, 2013; Lu et al., 2022; Rakic, 2009). The latest efforts in generating human-derived models have focused on creating and optimizing protocols to produce 3D brain organoids that resemble the fetal human brain (Lancaster et al., 2013; Paşca, 2019; Paşca et al., 2015; Yoon et al., 2018). Similar to the 2D culture landscape, there are two main ways of generating brain organoids, unguided and guided. The unguided approach uses EBs derived from human PSCs, embedded in an extracellular matrix, and cultured in a spinning bioreactor to promote spontaneous tissue expansion and neural differentiation (Lancaster and Knoblich, 2014; Lancaster et al., 2013). This protocol allows for examination of the whole brain since cell types from the forebrain, midbrain, and hindbrain regions are made (Lancaster and Knoblich, 2014; Lancaster et al., 2013; Qian et al., 2019). Guided is the other approach generally referred to as a spheroid method, this uses small molecules and growth factors to generate region-specific tissue (Birey et al., 2017; Gordon et al., 2021; Miura et al., 2020; Paşca et al., 2015; Qian et al., 2018, 2020; Yoon et al., 2018).

As molecular and cellular characterizations continue to validate organoid models, new findings are reported. Recently, the long-term maturation of human cortical organoids was found to match key early postnatal transitions (Gordon et al., 2021). This was important because human brain development does not stop perinatally, one of the early issues for organoid cultures was extended time *in vitro*. Often organoids will stop their growth as they

are nutrient restricted, apoptosis would occur and loss of organoids followed; because of this, researchers have opted to find ways to provide additional nutrients similar to those *in vivo* (Cakir et al., 2019; Shi et al., 2020). One of the methods to provide a more nurturing environment for growth and maturation is to provide vascularization to cortical organoids. Vascularization beyond primate vascular loops of the human brain occurs after gestational week 6, initially helping with the thickening of the brain, with surface capillaries in the cerebral hemispheres growing into the ventricular zone (VZ) (Gijtenbeek et al., 2014; Raybaud, 2010). Around gestational week 25 increased vascularization of the cortical neuronal layers is increased presenting a shift from the VZ to the cortical neuronal layers (Ten Donkelaar and van der Vliet, 2006; Ten Donkelaar et al., 2014; Matsui et al., 2021; Raybaud, 2010).

Lastly, the interconnectivity between brain regions is essential for proper information processing. As the stem cell field moves towards guided methods of generating regions-specific tissue, system biologists will still question the relevance of studying an isolated brain region. To answer this, researchers have started to generate assembloids to investigate neural circuits (Bagley et al., 2017; Birey et al., 2017; Miura et al., 2022; Xiang et al., 2017). Assembloids are a fusion of two distinct spheroids, for instance, fusing a cortical organoid and a striatal organoid to study cortico-striatal circuits of the forebrain (Miura et al., 2022). Self-organization of the organoids is leveraged to cross-talk between organoids, where typical neural connections can form autonomously. As the 2D and 3D systems stated set the stage for disease modelling and brain development, the most

important aspect of human modelling comes when genetic editing is integrated into the workflow. The ability to genetically engineer isogenic lines where the genome is the same except for your gene or mutation of interest creates a powerful tool to investigate genetic contributions in an isolated system. Many studies have used CRISPR/Cas9 and other Cas enzymes to knock in (KI) and out genes, and nucleotides and alter the expression to aid in disease modelling, especially if access to patient samples is limited (Deneault et al., 2018, 2019; Hong et al., 2021; Sanjurjo-Soriano et al., 2022; Simkin et al., 2022; Xie et al., 2020).

1.3.4 Activity-dependent regulation on protein synthesis

Synaptic plasticity and activity-dependent modulation are crucial for neuronal development and are the backbone of neural network dynamics. As these phenomena require transient and long-lasting synaptic efficacy and structural changes, they are heavily dependent on protein translation. Neurons require precise control of protein synthesis for proper development and response to activity. Thus, disruptions in protein synthesis can lead to defects often found in NDDs. ASD has highly implicated aberrant protein synthesis and translation control as a major contributor to the disease pathogenesis (Kelleher and Bear, 2008). Many ASD-risk genes control different levels of neuronal development, making their timing and level of expression critically important. One protein that exerts a high degree of translational control and is highly implicated in ASD is the translational repressor FMRP. A molecular hallmark of Fragile X syndrome (FXS) is excessive protein synthesis, an observation that is considered to be a major contributor to the neural deficits associated with FXS (Bagni et al., 2012; Banerjee et al., 2018; Jacquemont et al., 2018; Richter et al.,

2015). FMRP has been shown to regulate translation initiation by its interactions with eIF4E and cytoplasmic FMRP-interacting protein 1 (CYFIP1). FMRP forms a complex with CYFIP1 to stabilize CYFIP1 on the 5' end of specific mRNAs to repress their translation. The FMRP-CYFIP1 complex also forms an interaction with eIF4E to further repress translation. Genetic reduction of FMRP or CYFIP1 results in the excessive protein synthesis phenotype observed (Jacquemont et al., 2018; Napoli et al., 2008; Richter et al., 2015). In mouse neurons lacking Fmrp, there is an elevated response of metabotropic glutamate receptor (mGluR)-dependent protein synthesis that results in impaired synaptic plasticity by reduced AMPARs in the postsynaptic membrane (Bear et al., 2004), which is reversed by reducing mGluR5 expression (Dölen et al., 2007). Another gene mutated in ASD which regulates translation is *eIF4E*, controlling translation initiation (Aitken and Lorsch, 2012; Neves-Pereira et al., 2009; Waltes et al., 2014). eIF4E has been shown to complex with CYFIP1 and FMRP (Amorim et al., 2018), and when either of these interactions is removed or reduced, there is a marked increase in protein synthesis coupled with characteristic behavioural and social deficits in ASD (Gkogkas et al., 2012; Napoli et al., 2008; Richter et al., 2015). Mutations in eIF4E in autistic patients often result in characteristic repetitive behaviour symptoms (Waltes et al., 2014). Furthermore, genetically increasing eIF4E levels in mice resulted in elevated protein synthesis as well as autistic-like behaviours (Santini et al., 2013). By pharmacologically inhibiting the eIF4E-eIF4G interaction in a FXS mouse model, the observed defects in protein synthesis and spine morphology were reversed; suggesting that targeting this pathway may potentially normalize imbalanced signalling pathways that regulate these phenotypes (Santini et al.,

2017). Furthermore, the transcriptional repressor *MECP2*, causal for Rett syndrome, affects global protein synthesis and translation of key genes regulated by neurodevelopment (Li et al., 2013; Pacheco et al., 2017; Rodrigues et al., 2020). Thus, these studies highlight the wide array of transcriptional and translational regulators disturbed in ASD and provide insight into how altered translation may contribute to the pathophysiology.

A common denominator of translational defects is the regulatory control of protein translation pathways, such as the mammalian target of rapamycin signalling pathway (mTOR) signalling pathway. Each of these signal transduction pathways has heavy involvement in synaptic function and plasticity by converging to cap-dependent protein synthesis (Costa-Mattioli et al., 2009). The targets of these pathways have been shown to play important roles in memory formation and learning. The tuberous sclerosis complex (TSC1/2) negatively regulates the mTOR pathway and has a predominant role in translation regulation (Ehninger et al., 2008; Tsai et al., 2012). In addition, the translational repressor 4E-BP, as well as downstream mTOR targets Ribosomal protein S6 kinases (S6K1) and (S6K2) are of critical importance during LTP and learning and memory (Antion et al., 2008; Banko et al., 2005, 2007; Gkogkas et al., 2012). In the FXS mouse model, genetic removal of S6K resulted in more mature dendritic spine morphology and improved behavioural outcomes, which includes improvements in social deficits and behavioural inflexibility (Bhattacharya et al., 2012). Inhibitors of S6K1 in *Fmr1* KO mice reversed translational and behavioural deficits as well as deficits in dendritic spine morphology (Bhattacharya et al., 2016). Furthermore, modulation of mGluR5 signalling has been shown

to reverse elevated protein synthesis in a *Tsc2* mouse model (Kelly et al., 2018), which is consistent with the finding that loss of the TSC results in increased mTORC1 activity and protein synthesis (Saxton and Sabatini, 2017). Taken together, these results suggest that targeted manipulation of this pathway in FXS not only can correct the molecular phenotypes, but also behavioural deficits may have applications to other NDDs that exhibit imbalanced translation. In summary, aberrant translation plays a major role in proper synaptic function and plasticity associated with NDDs.

1.3.5 The interplay between activity-dependent regulation, protein synthesis, and
mitochondrial dynamics

Mitochondria are central in the process of providing and sustaining the energetic needs of neurons and neural circuits (Bélanger et al., 2011; Magistretti and Allaman, 2015). The adenosine triphosphate (ATP) provided by mitochondria is necessary for the maintenance of neurites and synaptic transmission (Cioni et al., 2019; Li and Sheng, 2021; Rangaraju et al., 2019; Spillane et al., 2013) as these are areas of high ATP demand (Figure 3). Mitochondrial localized to a particular synaptic site, for example, provide ATP necessary for local translation during synaptic plasticity events. When these mitochondrial compartments are depleted, plasticity-induced synaptic translation is reduced (Rangaraju et al., 2019). Additionally, transporting mitochondria to these sites is mediated by the mitochondrial fission/fusion proteins, which when disrupted lead to significant alterations in the mitochondrial distribution in the neuron (Fukumitsu et al., 2016; Misko et al., 2010). The motility of mitochondria in dendritic protrusions is critical to developing spines, as

their density at these loci affects the structural plasticity of spines and synapses (Li et al., 2004). Mitochondria also perform other functions that are critical to neuronal development and synaptic function such as fission and fusion (Divakaruni et al., 2018; Rangaraju et al., 2019), compartmental trafficking (Lewis et al., 2018), and quality control mechanisms such as mitophagy (Ebrahimi-Fakhari et al., 2016; Franco-Iborra et al., 2018). When these functions go awry, several neuronal deficits may be produced, that can culminate in NDDs such as ASD. In 1985, the first report of mitochondrial dysfunction in ASD showed elevated lactate levels in the plasma of autistic children (Coleman and Blass, 1985). Since then there have been numerous reports (Haas, 2010; Palmieri and Persico, 2010; Rossignol and Frye, 2012) suggesting metabolic dysfunction may occur in ASD.

Defects in mitochondrial function in ASD can be broadly viewed as primary or secondary causations (Haas, 2010; Niyazov et al., 2016). Primary mitochondrial defects are caused by gene mutations that impair the aerobic ATP synthesis machinery, whereas secondary defects occur indirectly through other genetic or metabolic abnormalities. Mutations in mitochondrial DNA (mtDNA) are common targets in mitochondrial dysfunction in ASD (Rossignol and Frye, 2012; Zhao et al., 2019). Many patients presenting an ASD diagnosis have shown to exhibit altered mtDNA content as well as reduced electron transport chain (ETC) complex activities (Coker and Melnyk, 1991; Eeg-Olofsson et al., 1989; Großer et al., 2012; Ruch et al., 1989). Compromised mitochondrial energy output due to reduced or increased mtDNA could have detrimental consequences on neuronal function, and development contributing to the ASD pathophysiology. Further

disturbances in mitochondrial function have been identified in post-mortem brain tissues of ASD patients. Differences have been observed in brain region-specific changes in ETC complexes along with increased markers of oxidative stress (Bunton-Stasyshyn et al., 2015). Additional evidence from post-mortem brain tissue has shown that reduced ETC complex activity may be due to activity deficit in antioxidant enzymes, which may largely contribute to the impaired metabolic capacity of mitochondria in ASD patients (Ashrafi and Schwarz, 2013; Ashrafi et al., 2014; El Bekay et al., 2007; De Diego-Otero et al., 2009; Muller et al., 2004). Genetic aberrations in mitochondria, in summary, may be a contributing factor underlying the pathophysiology of a subset of ASD patients coupled with deficits in ETC activity and oxidative stress.

Mitochondrial encephalomyopathy lactic acidosis and stroke-like episodes (MELAS) is one of the best characterized mitochondrial diseases that overlap with ASD. A clinical investigation studied five patients with ASD while examining familial histories of mitochondrial DNA diseases (Pons et al., 2004). Two patients harboured the A3243G mtDNA mutation while the mothers of two other patients harboured the mutation which typically causes MELAS. In addition, this observation is further strengthened by other studies that have investigated the overlap between ASD and mtDNA mutations (Graf et al., 2000; Napoli et al., 2013; Pons et al., 2004; Weissman et al., 2008). ASD risk genes have also been implicated directly in mitochondrial dysfunction, for example, gene expression analysis on Mecp2-null mice displayed elevated respiration rates associated with increased complex III activity (Kriaucionis et al., 2006). Several previous case reports support the

notion that mitochondrial dysfunction plays a role in Rett syndrome pathophysiology (Coker and Melnyk, 1991; Eeg-Olofsson et al., 1989; Ruch et al., 1989). Other mitochondrial abnormalities, such as reduced mitochondrial membrane potential and increased ETC complex activities are observed in Mecp2-deficient mice (Großer et al., 2012; Janc and Müller, 2014). FMRP is required for the expression of SOD1 (Bechara et al., 2009), a protein responsible for destroying superoxide radicals and for preventing oxidative damage (Bunton-Stasyshyn et al., 2015). In mice lacking the gene encoding FMRP, increased oxidative stress markers are observed (El Bekay et al., 2007; De Diego-Otero et al., 2009). Recently, a Tsc mouse model was also reported to show impaired mitophagy by an accumulation of mitochondria in *Tsc1/2*-deficient neurons (Ebrahimi-Fakhari et al., 2016). It was shown that inhibiting the mTORC1 pathway or stimulating mTORC1-independent autophagy was sufficient to reduce and clear damaged and excess mitochondria and replenish mitochondria at presynaptic sites.

In human iPSC-derived neurons from patients harbouring mutations in *TSC2*, significant deficits in mitochondrial bioenergetics were identified as well (Ebrahimi-Fakhari et al., 2016). These findings were corroborated by the observation of depolarized mitochondria in the neurites of the patient neurons, indicating that those mitochondria were less effective in their oxidative phosphorylation capacity (Ebrahimi-Fakhari et al., 2016). In a CNV genetic model of ASD, patient iPSC-derived neurons harbouring the 7q11.23 copy number variant displayed mitochondrial oxidative phosphorylation complexes were unstable and resulted in reduced ATP as well as structural deficits in neuron morphology.

These observations are linked to one of the genes in the 7q11.23 deletion, *DNAJC30*, an auxiliary component of the ATP synthase complex (Tebbenkamp et al., 2018). Disrupted mitochondrial bioenergetics is a common mechanism in neuronal dysfunction. As stated above, LTP requires bursts of mitochondrial fission, however, unhealthy mitochondria are unlikely to perform the ability to elicit normal responses and thus may contribute to electrophysiological abnormalities (Bateup et al., 2013; Divakaruni et al., 2018). Further, mitochondrial deficits have been identified in other neuropsychiatric disorders such as the 22q11.2 deletion syndrome, a genetic risk factor for schizophrenia (Fernandez et al., 2019; Li et al., 2019). In 22q11.2 deletion mouse models, mitochondrial deficits are reported to affect layer-specific synaptic integrity while in patient iPSC-derived neurons ATP, and ETC complex activity levels are reduced (Li et al., 2019). The commonality of mitochondrial deficits outside of ASD suggests that the metabolic regulation of these organelles may play a larger role than expected in neuronal function and homeostasis.

It is known that disruption of ASD-risk genes impacts downstream pathways that result in metabolic disturbances within neurons. Although many studies suggest a link to metabolic disruptions, many of the therapeutic preclinical and clinical trials lag behind. Current clinical studies have broadly investigated ketogenic diets for symptomology treatment of ASD. These high-fat, low-carbohydrate diets have been successful in treating some forms of epilepsy, but have limited success in children with ASD (Mierau and Neumeyer, 2019). Other studies have suggested moderate improvements in behaviour and cognitive abilities in children who can follow the diet throughout (Cheng et al., 2017).

However, further investigation into the connection between synaptic function, mitochondrial activity, and protein translation will drastically advance our understanding of synaptic pathology associated with ASD and allow for precision-based medicine that may aid our current therapies or generate undiscovered ones.

1.4 The importance of the voltage-gated sodium channel α-subunit in neurodevelopment

The ion channel family of voltage-gated sodium channel α-subunit (*SCNxA*) genes in the human genome consist of ten genes. Within the CNS *SCN1A*, *SCN2A*, *SCN3A*, and *SCN8A* are highly expressed in neurons (Sanders et al., 2018). All ten genes are located between chromosomes 2 and 3, with the CNS-expressed channels located on chromosome 2. The homology within the family is high as it has been reported that both whole-genome and gene duplication events during early chordate and vertebrate evolution lead to the present day genes and gene clusters (Holland and Ocampo Daza, 2018; Meisler et al., 2021; Zakon, 2012). Due to the specialized nature of sodium channels, their genes are highly conserved throughout evolution, with many of the genomic regions being retained from invertebrate and prokaryotic species (Meisler et al., 2021). The voltage-gated sodium channel family has main roles in the initiation and propagation of action potentials, along with regulating backpropagation. Because these channels are so highly conserved and specialized, mutations can cause deleterious effects on the species. Pathogenic mutations in *SCN1A*, *SCN2A*, *SCN3A*, and *SCN8A* have been associated with many neurological disorders, these disorders are discussed in detail later in this section. Briefly, mutations in

the CNS-associated *SCNxA* genes most often manifest as epilepsy, seizures, ataxia, intellectual disability, and ASD (Bender et al., 2012; Echevarria-Cooper et al., 2021; Jones et al., 2016; Liao et al., 2010; Schwarz et al., 2019; Tidball et al., 2020; Yamagata et al., 2020; Zaman et al., 2018). Further, haploinsufficiency of the CNS-associated *SCNxA* genes is sufficient to induce many of the same atypical phenotypes (Deneault et al., 2018; Tai et al., 2014; Tatsukawa et al., 2019).

The subcellular localization of CNS-associated SCNxA channels is well described throughout neuron architecture. As their roles revolve around action potential initiation and propagation, high-density clustering of sodium channels has been reported at the axon initial segment (AIS), and axon or nodes of Ranvier of myelinated neurons (Bender and Trussell, 2012; Boiko et al., 2003; Huang and Rasband, 2018; Kole and Stuart, 2008). Aside from high-density clusters, SCNxA expression is found throughout the neuron including the soma, and dendrites (Kole and Stuart, 2008; Spratt et al., 2019). The channel localization has evolved across species to enhance both the response to voltage changes and conduction velocity properties. Neuron subtypes dictate the expression of the CNS-associated sodium channels along with the paralogs expressed per subtype. For example, inhibitory neurons of the medial prefrontal cortex, specifically somatostatin and parvalbumin-positive neurons predominantly express Scn1a with little to no membrane localization of Scn2a in mice (Spratt et al., 2019). However, excitatory neurons of the cortex predominantly express SCN2A during early development to generate and propagate action potentials. In excitatory neurons of the cortex SCN2A and SCN8A expression and

function are developmentally regulated, where SCN8A expression increases later to assume the primary role of action potential initiation and propagation (Bender and Trussell, 2012; Kole and Stuart, 2012; Meisler et al., 2021; Sanders et al., 2018).

1.4.1 SCN2A's role in ASD

Large-scale sequencing studies of ASD cohorts have identified SCN2A as a top 3 ASD-risk gene, harbouring an abundance of *de novo* variants (Satterstrom et al., 2020). *SCN2A* encodes the alpha subunit of the voltage-gated sodium channel Nav1.2. Nav1.2 is reported to be the only voltage-gated sodium channel that is expressed at the AIS in glutamatergic neurons of the neocortex during early development (Boiko et al., 2003; Gazina et al., 2015; Osorio et al., 2005; Sanders et al., 2018). This occurs from the late second trimester until 1-2 years of age, this means excitation in the neocortex is regulated by Nav1.2 (Sanders et al., 2018). Interestingly, this phenomenon changes later in development, and both Nav1.2's function and subcellular localization shift. After 1-2 years of age, Nav1.6 replaces much of Nav1.2 at the distal AIS and axon. Nav1.2 then becomes restricted to the proximal AIS and somatodendritic compartments aiding in boosting action potentials and in part regulating backpropagating action potentials (Hu et al., 2009; Spratt et al., 2019). *SCN8A*, a paralog of *SCN2A* encodes Nav1.6, one of the main differences is the lower voltage threshold for activation of Nav1.6. Once mature, glutamatergic neurons express Nav1.6 at the distal AIS taking over the roles of action potential initiation and propagation (Boiko et al., 2003; Kole and Stuart, 2012; Kole et al., 2008).

To simplify variants, they were historically categorized as loss-of-function (LoF) or gain-of-function (GoF). These classifications refer to the effect of the variant on the protein, in this case, does the variant enhance or decrease channel activity. One of the first studies to categorize *SCN2A* variants used overexpression of SCN2A and its variants in Human embryonic kidney (HEK) cells and computational models (Ben-Shalom et al., 2017). They found that many of the variants that contributed to an enhancement of channel activity were missense and often were from patients with epileptic syndromes, these were categorized as GoF. In opposition, variants that impaired channel activity were often protein truncating or nonsense, these variants were almost exclusively from patients with ASD (Ben-Shalom et al., 2017). This made categorizing patient mutations easier, as it seemed like variants that perturbed SCN2A function had distinct groups. However, other studies started to report a spectrum of clinical presentations associated with SCN2A perturbations. Specifically, several LoF mutations that were associated with ASD also had early and late-onset seizures, complicating the dichotomy (Wolff et al., 2017). This remains one of the mysteries in genotype to phenotype relations of SCN2A channelopathy, further, these findings emphasized the need for cellular investigation of mutations identified in the clinic. From current SCN2A reports a common theme is prevalent, an understanding that both the type of and location of the variant have a profound effect on the phenotypes observed. This was evident by clustering of missense variants, variants contributing to epileptic syndromes were often situated by the voltage sensory domain, while variants close to the pore loops were commonly associated with ASD/ID (Ben-Shalom et al., 2017).

Many of the first investigative reports of SCN2A's role in behaviour came from mouse studies. Since perturbations of SCN2A in humans are caused by point mutations, they often represent a range of expressions from haploinsufficiency to full expression of the channel. Engineered mice created to recapitulate complete loss of SCN2A or a null knockout (KO) provided early evidence of perinatal lethality (Planells-Cases et al., 2000). Since this early report, researchers have focused on heterozygous mouse models of *Scn2a*. One of the challenges that face behavioural studies with ASD-associated genes, is reproducibility. Many factors can contribute to differential outcomes between researchers, handling, seasonal changes, and most importantly differential genetic background signatures and genetic drift (Ey et al., 2012; Spencer et al., 2011). Heterozygous loss of *Scn2a* in one mouse model may not be equal in another mouse, this can be due to the perturbation method of the gene of interest. This is evident with *Scn2a* mouse models, where behaviour phenotypes can vary from report to report. In recent years, the efforts to translate the core human ASD behavioural characteristics, impaired social communication, and repetitive behaviours have accelerated in mice. Haploinsufficient *Scn2a* mouse models have assessed locomotion, anxiety, repetitive behaviour, sociability, and learning. Heterozygous male mice struggle with reversal learning tasks in parallel spatial learning (Middleton et al., 2018; Spratt et al., 2019). This meant $Scn2a^{+/-}$ had difficulties unlearning spatially dependent tasks. They have also been found to display enhanced fear conditioning, elongated fear association, social impairment, and hyperactivity in novel environments (Tatsukawa et al., 2019). Additionally, sex differences have been reported, with female $Scn2a^{+/-}$ mice having impaired social recall but lesser anxiety-like behaviours (Spratt et al.,

2019). In another study, researchers discovered that young $Scn2a^{+/-}$ mice (P22 - P44) showed reductions in ultrasonic vocalizations mimicking reduced social communication, but this was not present in adult mice (P60 - P95) (Léna and Mantegazza, 2019). This age-dependent regulation of behaviour was also seen in self-grooming and marble burring monitoring, with young $Scn2a^{+/-}$ mice spending significantly more time in both tasks. Further emphasizing that repetitive behaviours are present and that the paralog switch of Scn2a to Scn8a may underpin the age-dependent effects.

In recent years researchers have partially surmounted the consequences of perinatal lethality associated with complete loss of Scn2a. A group engineered a gene-trap mouse knockout model of Scn2a that has ~25% expression compared to wild-type mice (Eaton et al., 2021). A gene-trap knockout essentially traps upstream exons by splicing a trapping cassette that is inserted into the intron of the gene of interest, thus creating truncated transcripts (Skarnes et al., 2011; Testa et al., 2004). The trapping cassette contains the bacterial β-galactosidase (LacZ) gene reporter allowing for easy identification and validation of insertion (Testa et al., 2004). The hypothesis behind the generation of a pseudo knockout mouse model was that a 50% reduction of Scn2a is not sufficient to observe major behavioural phenotypes. Having residual Scn2a expression provides enough expression for survival but not enough to miss more complex behaviours or minute behavioural deficits. From their behavioural tests of adult mice, they concluded that Scn2a knockout mice had elevated anxiety-like behaviours, and that this was a sex specific phenotype, with females traveling longer distances in the open field test. Eaton et al. also found increased repetitive

behaviours with increased grooming with no sex differences and a lack of novelty via the marble burying test (Eaton et al., 2021). Other subtle behavioural changes included altered sensory perception of heat and slight spatial working memory impairment in male Scn2a knockout mice. The use of gene-trap of Scn2a in mice was recently used to provide insights into sleep patterns and circadian rhythms (Ma et al., 2022). Clinical studies have found sleep disorders are prevalent in children with SCN2A deficiency (Crawford et al., 2021). Briefly, their results aligned with the clinical study, Scn2a knockout mice had increased wakefulness during light and dark cycles, and reduced non-rapid-eye-movement (Ma et al., 2022). As more patients with SCN2A deficiencies are identified more comorbidities may be brought to light, providing evidence to pursue.

In an attempt to translate human genetic mutations to mouse models to better understand the behavioural outcomes, researchers have created transgenic mice with human mutations. One group engineered a mouse model that harboured a heterozygous truncating mutant in SCN2A in the last protein-coding exon (Wang et al., 2021). They found that adult mice with this Scn2a mutation displayed increased social interaction, locomotion, and reduced anxiety behaviour. To date, there is limited work on behavioural analysis of human mutations in mice. Behavioural studies are essential in providing insight between genotype and behaviour and will remain the primary way researchers study behaviour in a functional biological system where they can also tease apart molecular mechanisms.

1.4.2 SCN2A channelopathies in neurodevelopmental disorders

As NGS studies continue to identify variant enrichment in potential risk genes for NDDs, *SCN2A* remains one of the most reported genes. Variants perturbing SCN2A's function have been linked to infantile epileptic encephalopathy (IEE), benign familial infantile seizures (BFIS), ASD/intellectual disability (ASD/ID), and episodic ataxia (EA). IEE is characterized by seizures in the first six months of life, primarily it presents itself as tonic seizures leading to stiffening of body muscles (Vaher et al., 2014). Common anatomical hallmarks of IEE in infants are the underdevelopment of the cerebral hemispheres and structural abnormalities, most notably, asymmetric lesions (Yamatogi and Ohtahara, 2002). BFIS is characterized by infantile-onset seizures that resolve within the first 2 years of life often without neurodevelopmental repercussions (Sanders et al., 2018). Case studies have suggested the onset is variable ranging from 2 days to 13 months postnatal (Herlenius et al., 2007). ASD/ID, as previously mentioned is characterized by global developmental delay affecting social and language progression (Sanders et al., 2018). Less studied are the effects of pathogenic *SCN2A* variants on EA. Associated symptoms of EA range from slurred speech to involuntary muscle movements (Liao et al., 2010). There are eight 8 types of EA with type 1 and 2 being the most common and type 3-8 being very rare (Choi and Choi, 2016). However, pathogenic variants in *SCN2A* have not been linked to one specific EA type (Choi and Choi, 2016; Schwarz et al., 2019). Unlike epileptic seizures, EA episodes can result in 1-2 episodes per day lasting several weeks, with quiescent periods lasting up to years, with a much longer onset for *SC2NA* pathogenic variants (Schwarz et al., 2019). The onset of *SCN2A*-associated EA is reported to be

between 10 months and 14 years of age (Schwarz et al., 2019). Each of these SCN2A-related disorders has been monitored in the population to determine the prevalence. The last monitoring study reports were conducted in 2016, with a total estimation of 11.1% of 100 000 births linked to *SCN2A*-related causes (Baio et al., 2018; Gaily et al., 2016; Ronen et al., 1999; Sanders et al., 2018).

One notable mention of *SCN2A*'s emerging involvement with NDDs is schizophrenia (Kruth et al., 2020). Schizophrenia is highly heritable with prevalence estimates affecting 1% of individuals (Goeree et al., 2005). Schizophrenia is defined in the DSM-5 by three main symptoms, positive, negative, and cognitive symptoms. Visual and auditory hallucinations, delusions, and disorganized thoughts are included in positive symptoms, while social withdrawal, lack of motivation, flat affect, and inability to experience pleasure are included in negative symptoms. Cognitive symptoms include working memory and attention deficits. Similar to EA, the onset of Schizophrenia is typically late adolescence into early adulthood (Primavera et al., 2012). One of the first studies implicating common *SCN2A* variants in Schizophrenic patients came from analyzed postmortem brains; researchers examined the prefrontal cortex and noted that lower *SCN2A* expression was associated with poorer cognitive performance (Dickinson et al., 2014). Another group reported that SNPs in *SCN2A* were a predictor of cognitive ability in both schizophrenic and healthy individuals (Scult et al., 2015). More recently, a group functionally characterized a *de novo* missense mutation detected from NGS of a Schizophrenic cohort (Carroll et al., 2016; Fromer et al., 2014; Kohlnhofer et al., 2021).

This was the first functional characterization of an *SCN2A* mutation identified in the schizophrenic cohort, they determined the mutation was LoF after introducing the mutation into iPSC-derived cortical neurons (Kohlnhofer et al., 2021). In all, these reports suggest that SCN2A has a role in cognitive outcomes across neurological disorders. As more variants are identified cellular validation is required to understand the pathophysiology. Since all variants are not phenotypically the same due to location and type, a problem persists. Broad range therapeutic approaches to alleviate symptoms often fail. For instance, the first-line anticonvulsant medication phenytoin often used in the clinic can have no effect on variants, while other blockers can (Hackenberg et al., 2014; Zhang et al., 2021a). Further, instances of insensitivity or non-responsiveness to common pharmacological drugs have been reported in *SCN2A*-related EA (Schwarz et al., 2019). Together, this further highlights our current lack of ability to provide predictable and efficient approaches to treat or alleviate general disorders with pathogenic *SCN2A* variant underpinnings.

1.5 Summary of Intent

The overall objective of this thesis was to disseminate the effects of varying genetic perturbations of *SCN2A* on human neuron dynamics. This objective was further dissected into three main aims: functionally characterize clinically relevant variants at the cellular level, identify molecular signalling pathways that may be disrupted, and provide insights into SCN2A's expression across neuronal development. This was done to guide a detailed investigation of *SCN2A*'s pathogenic variant effects on human neurons and to in part elucidate the pathobiology of SCN2A channelopathies.

Aim1: This aim was to functionally characterize three different genetic perturbations of *SCN2A* in human neurons. At the onset of this project, we had two human isogenic *SCN2A* knockout lines that we were interested in functionally characterizing and comparing to understand the cellular deficits. Previously, one *SCN2A* line was partially characterized along with other ASD-risk genes highlighting their neuronal network and synaptic communication dynamics (Deneault et al., 2018). However, this project evolved into a larger characterization venture when we obtained patient samples from two *SCN2A* deficient families through our collaboration with Dr. Stephen Scherer. Previous studies had not yet ventured into human modelling and characterizing mutations of *SCN2A*. There was a need for such studies and this was emphasized when researchers began to model channel and cell dynamics complemented with HEK cell transfections of mutated channels to obtain preliminary insights (Ben-Shalom et al., 2017). The need to characterize mutations stems from *SCN2A* harbouring an abundance of *de novo* variants paired with a lack of understanding of how they contribute to clinical phenotypes. This understanding is critical for treatments where binning mutations based on either their channel dysfunction or clinical presentation could be important for simplifying treatment regimens. From this, we began to see that a small fraction of mutations were studied and characterized and that recurrent mutations were observed at a low rate. Further, many mutations are often clustered in similar regions of the channel contributing to a global phenotype of ASD or EE but rarely ever the same predicted or experimental mechanistic features. From this and our understanding of neuronal activity and its importance in the regulation of transcription, translation, and neurodevelopment we explored dendrite growth, and single cell and

neuronal network activity. Using techniques such as immunocytochemistry, patch-clamp, and multi-electrode arrays we were able to uncover the importance of variant location and penetrance on neuronal activity and morphology. Specifically, the R607* LoF mutation behaved similarly to the *SCN2A* KO neurons, where the G1744* LoF mutation did not. Our results indicated that the G1744* mutation was less severe and that neurons were able to recover their excitability and enhance key intrinsic properties. The results of this work are currently in a preprint published on BioRxiv in September 2021, where I am the first author of this study.

Aim 2: My second aim was to identify cellular or molecular signalling pathways that were disrupted in human neurons with *SCN2A* deficiency. To date, reports on *SCN2A* deficiency have focused on the initial pathophysiology of the neuronal excitability, varying rescue techniques, and mouse behaviour (Begemann et al., 2019; Léna and Mantegazza, 2019; Ogiwara et al., 2018; Que et al., 2021a; Spratt et al., 2019; Wolff et al., 2017; Zhang et al., 2021a). However, studies still lack mechanistic answers that provide insights into how *SCN2A* deficiency affects molecular biology. This understanding is important as it provides targetable signalling pathways that could help to ameliorate the phenotypes observed, and further provides another classification to group mutations if they converge or diverge on specific signalling pathways. We used the R607* mutation to validate our aim since it had the most severe neuronal phenotypes. Through a collaboration with Dr. Yu Lu, we were able to perform proteomic and bioinformatic analyses to determine the downstream effects of *SCN2A* deficiency. From these experiments, we discovered that R607* induced neurons

(iNeurons) had differentially expressed proteins (DEPs) compared to their familial control iNeurons, and that these DEPs clustered into specific cellular or molecular pathways. The results of this work revealed *SCN2A* haploinsufficiency is sufficient to disrupt the cellular processes in human iNeurons. The results of this work are currently in a preprint published on Biorxiv in September 2021, where I am the first author of this study.

Aim 3: Lastly, in this aim, we wanted to take advantage of having readily available human iPSC lines and our knowledge of genetic engineering to delineate the findings from the p.G1744* variant. Since the findings were unexpected for a traditional LoF variant, we wanted to further characterize the *de novo* point mutation in a clean background. For this, we wanted to create an isogenic model that differed by only a single basepair, the variant. This would prove useful in elucidating the cellular findings of general enhancement or no differences between control and proband from the first chapter. Using these combined tools, we can separate the question of causality between solely the variant contributing to the phenotype or differences in genetic background. Even though all our samples are sex-matched with familial controls, a difference of approximately 50% of the DNA still exists. Obtaining familial controls is rare in human disease modelling, but to provide more targeted findings, this was a necessary venture. Secondly, reproducing findings observed in iPSC-derived neuronal modelling can be difficult as many factors can differ between facilities such as culturing and freezing techniques, the timing of media changes, and more (Volpato et al., 2018). Because of this, we wanted to confirm that our findings followed a similar trend in a completely different genetic background, so we performed these experiments

isolated from the patient lines used in Chapter 1. Once the isogenic line was made, our patch-clamp and morphology data indicated that the p.G1744* variant did not impair neuronal dynamics but it also did not enhance neuronal characteristics as with the proband and familial control.
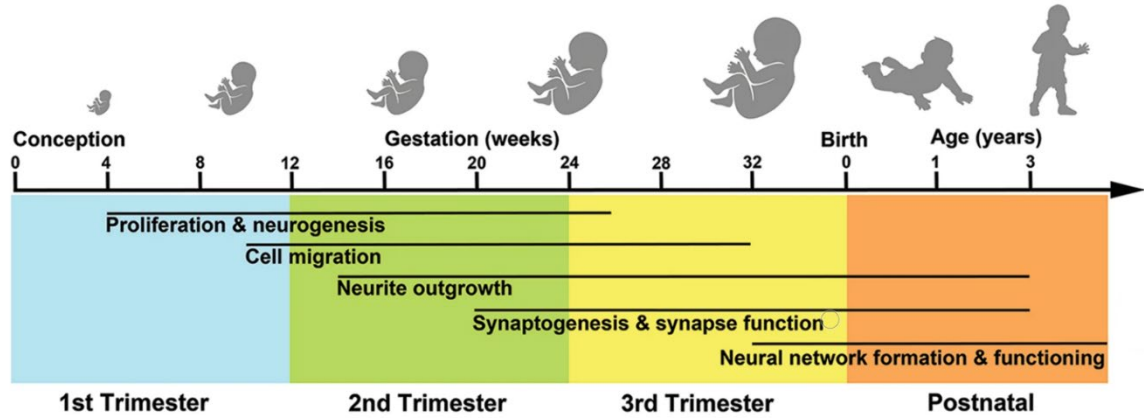
Figure 1. Schematic of human development.

Developmental timeline of major overlapping events that start at conception and continue in early adulthood. SCN2A is solely expressed in developing cortical neurons starting at the 2nd trimester until 2 years postnatal. Figure adapted from Courchesne et al., 2018.
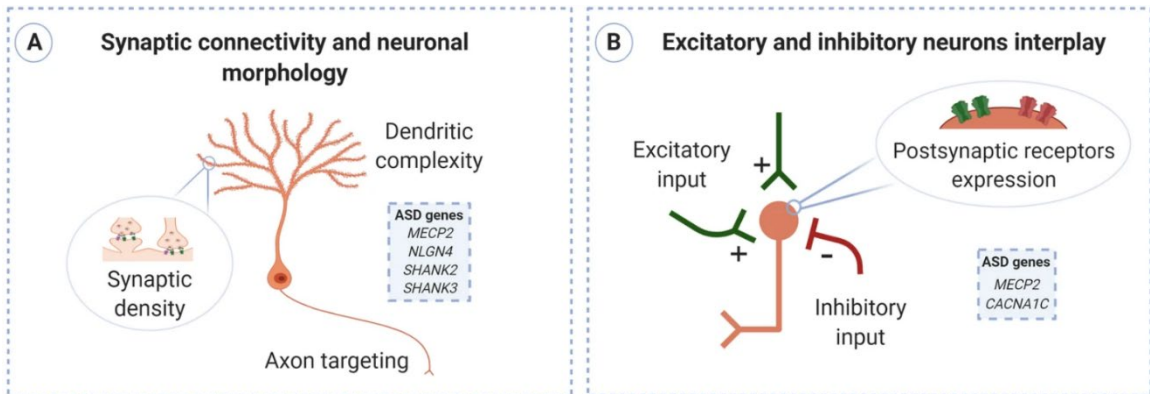
Figure 2. Excitation-inhibition mechanisms that are altered in neurodevelopmental disorders.

A) The development and maintenance of neuronal connectivity is dependent on typical function and maturation of synapses, dendrites and axons.

B) Maintenance of excitatory-inhibitory inputs is regulated by feedback loops that aid in regulating single neuron and network activity. Cellular models of ASD-risk genes have implicated them in altering the processes shown in (A) and (B). Figure adapted from Culotta and Penzes, 2020.
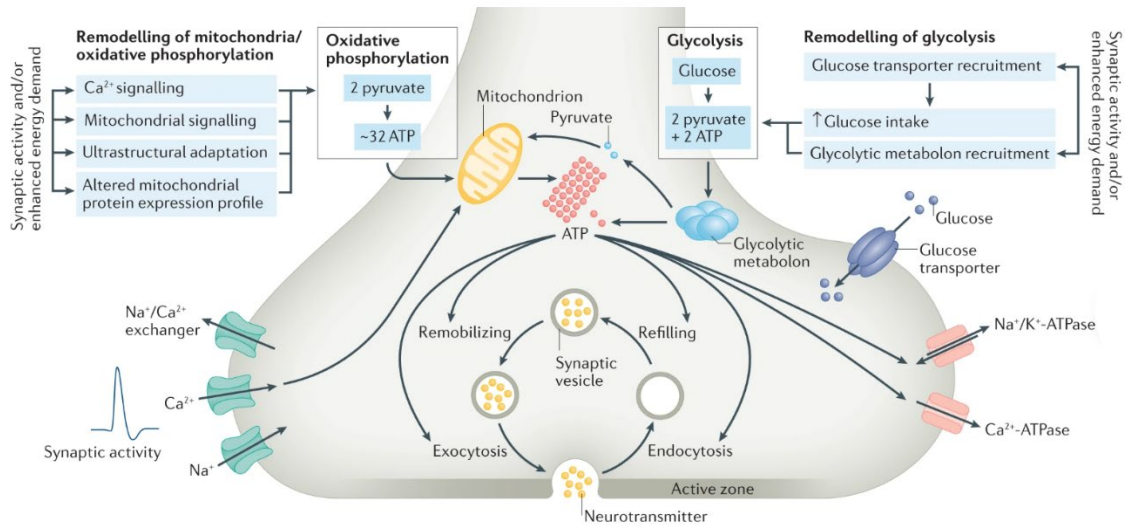
Figure 3. Presynaptic neuronal mechanisms that are mitochondrial dependent.

Mitochondria produce approximately 90% of the ATP required for neuronal function.
ATP is then distributed throughout the membrane producing energy for mechanisms
involved in exo- and endocytosis, ion concentration maintenance, and synaptic
transmission. Mitochondria are constantly remodeled from the transient and long-term
energy demands of the neuron. Figure adapted from Li and Sheng, 2021.

CHAPTER 2: SCN2A DISRUPTION BY KNOCKOUT OR *DE NOVO* VARIANTS IMPACTS HUMAN NEURON FUNCTION AND MORPHOLOGY

Brown, C.O, Uy, J.A Murtaza, N, Rosa, E, Alfonso, A, Xing, S, Dave, B.M., Kilpatrick, S, Cheng, A.A, White, S.H, Howe, J, Scherer, S.W, Lu, Y, and Singh, K.K. (2021). Disruption of the autism-associated gene *SCN2A* differentially alters synaptic development and bioenergetic signaling in patient iPSC-glutamatergic neurons. BioRxiv.

This article is open source.

2.1 Preface

This manuscript was published as a preprint in BioRxiv, on September 17, 2021. This chapter will exclusively focus on cellular phenotyping of the genetic perturbations of SCN2A in iNeurons. Experimental conception and planning were done by Chad Brown and Dr. Karun K. Singh. The majority of the cellular experimentation including, electrophysiology was performed by Chad Brown. Electrophysiological recordings were analyzed by Chad Brown. Images from immunocytochemistry were a shared responsibility between Chad Brown and Jarryll Uy; the analysis of images was performed by Chad Brown. The majority of the manuscript was written by Chad Brown, with Jarryll Uy contributing in part. Dr. Karun K. Singh reviewed the manuscript writing.

We would like to thank Dr. Stephen W. Scherer for providing access to the patient samples that were used throughout this study and Dr. Yu Lu for performing mass

2.2 Abstract

SCN2A is an autism spectrum disorder (ASD) risk gene and encodes a voltage-gated sodium channel. Autism-associated *SCN2A* variants are thought to be pathogenic by reducing channel function; however, the impacts of autism-associated *SCN2A de novo* variants on human neuron development are unknown. We studied SCN2A using isogenic $SCN2A^{-/-}$ induced pluripotent stem cells (iPSCs), and patient-derived iPSCs harbouring a p.R607* or a C-terminal p.G1744* *de novo* truncating variant. We generated excitatory glutamatergic neurons and found that $SCN2A^{+/p.R607*}$ and $SCN2A^{-/-}$ neurons displayed a reduction in synapse formation and excitatory synaptic activity, suggesting LoF phenotypes. However, the C-terminal p.G1744* variant, which leads to early-onset seizures in addition to ASD, altered action-potential dynamics but not synaptic activity. Further,

proteomic analysis and functional validation of *SCN2A*^{+/p.R607*} neurons revealed defects in bioenergetic signalling pathways, which were not present in *SCN2A*^{+/p.G1744*} neurons. Our study reveals that autism-associated *SCN2A de novo* variants are not all LoF, and differentially impact synaptic function and bioenergetic signalling.

2.3 Introduction

Autism spectrum disorder (ASD) is a childhood-onset, heterogeneous group of neurodevelopmental disorders characterized by deficits in social communication, and restricted and repetitive patterns of behaviour, or interests (Ofner et al., 2018). Genetic studies have identified hundreds of genes to the underlying etiology, including rare-inherited and *de novo* variants (Bai et al., 2019; Grove et al., 2019; Iossifov et al., 2014; Ruzzo et al., 2019; Sanders et al., 2015; Satterstrom et al., 2020; Yuen et al., 2017). One of the leading candidate autism risk genes is *SCN2A*, which encodes the neuronal α-subunit of the voltage-gated sodium channel Nav1.2 (Crawford et al., 2021; Sanders et al., 2012; Satterstrom et al., 2019, 2020; Wang et al., 2016). SCN2A is primarily expressed in glutamatergic neurons, and the function of SCN2A and its location changes throughout development. Early expression at the distal AIS is essential for the initiation and propagation of action potentials, while later in development, expression is clustered at the proximal AIS to regulate action potential backpropagation (Bender and Trussell, 2012; Hu et al., 2009; Kole and Stuart, 2012; Spratt et al., 2019). *SCN2A* is thought to predominantly regulate excitatory neuron function, while inhibitory neuron characteristics remain largely unchanged (Ogiwara et al., 2018; Spratt et al., 2019; Wang et al., 2021).

Understanding how variants in *SCN2A* contribute to neurological disorders can inform potential therapies or long-term clinical outcomes. Cell line and computational studies have identified the potential impact of the *SCN2A* variants (Begemann et al., 2019; Ben-Shalom et al., 2017; Echevarria-Cooper et al., 2021; Que et al., 2021b). These studies indicated that *SCN2A* GoF variants are likely associated with an enhancement of channel function and EE. LoF variants in *SCN2A* including those that result in protein truncations are associated with reduced channel function, leading to ASD and intellectual disability (Begemann et al., 2019; Ben-Shalom et al., 2017; Sanders et al., 2018). The majority of studies on SCN2A have been done on mouse models and suggest heterozygous loss of Scn2a function results in reduced channel function and developmental excitatory circuit abnormalities (Ogiwara et al., 2018; Shin et al., 2019; Spratt et al., 2019; Tatsukawa et al., 2019). While mouse models provide important insights, it does not possess the human and/or patient's genetic background, which can influence disease phenotypes (Mis et al., 2019). Further, patient iPSC-neurons modelling missense SCN8A-associated epilepsy encephalopathy variants revealed defects in sodium channel currents and action potential dynamics (Tidball et al., 2020). However, *SCN2A* has not been modelled using a patient-specific neuronal system (Deneault et al., 2018; Kohlnhofer et al., 2021; Lu et al., 2019). We and others previously showed that $SCN2A^{-/-}$ glutamatergic neurons display reduced synaptic activity. However, computational, cell line, mouse and iPSC-derived neuron models have yet to show whether they reflect phenotypes from patient-derived neurons, and the signalling mechanisms involved (Begemann et al., 2019; Ben-Shalom et al., 2017; Deneault et al., 2018; Ogiwara et al., 2018; Shin et al., 2019; Spratt et al., 2021, 2019;

Tatsukawa et al., 2019; Wolff et al., 2017; Zhang et al., 2021a). Further, since SCN2A is a large channel with multiple domains, it remains unknown whether protein-truncating variants at different locations in the gene have the same functional effect. Potential differences could impact how SCN2A variants are clinically classified, or determine which pharmacological intervention can be used.

To address this gap, we generated iPSCs from two ASD probands with sex-matched parental controls, as well as a new isogenic $SCN2A^{-/-}$ iPSC line. We used the Neurogenin2 (NGN2) protocol (Zhang et al., 2013) to generate excitatory glutamatergic neurons (iNeurons) for electrophysiological and proteomic studies (Figure 1A). This included an ASD patient with the $SCN2A^{+/p.R607*}$ variant, and an ASD individual with early-onset seizures with a $SCN2A^{+/p.G1744*}$ variant. These variants are located near opposite ends of the channel, providing a comparison of different protein domains. We found that electrophysiological analysis of isogenic $SCN2A^{-/-}$ and $SCN2A^{+/p.R607*}$ iNeurons revealed a similar reduction in synapse development, synaptic transmission, and neuronal network activity. However, $SCN2A^{+/p.G1744*}$ iNeurons displayed no changes in synaptic transmission, but instead possessed enhanced action potential characteristics. Taken together, our characterization of neuronal activity and morphology showcase that the type and location of genetic perturbations within SCN2A produce a spectrum of cellular phenotypes across development, and that this further manifests into varying clinical presentations.

2.4 Materials and Methods

2.4.1 Approval and generation of iPSCs

All pluripotent stem cell work was approved by the Canadian Institutes of Health Research Stem Cell Oversight Committee. Blood was taken from individuals with the approval from SickKids Research Ethics Board after informed consent was obtained, REB approval file 1000050639. This study was also approved by the Hamilton Integrated Research Ethics Board, REB approval file #2707. CD34+ blood cells were verified using flow cytometry and collected for iPSC reprogramming. All iPSCs were generated by Sendai virus reprogramming and clonal expansion using the CytoTune – iPSC 2.0 kit (ThermoFisher) to deliver the reprogramming factors. Once colonies were large enough (approximately 15-17 days post-Sendai transduction), each colony was transferred to 1 well of a 12-well plate coated with irradiated MEFs and plated in iPSC media (DMEM/F12 supplemented with 10% KO serum, 1x non-essential amino acids, 1x GlutaMAX, 1mM β-mercaptoethanol, and 16ng/mL basic fibroblast growth factor (bFGF)). Once iPSCs were expanded and established they were transitioned to matrigel coated plates and grown in mTeSR1 (STEMCELL Technologies) and subsequent passaging continued to use ReLeSR (STEMCELL Technologies). iPSC lines without karyotypic abnormalities were used and this was verified by G-band karyotyping performed by the Centre for Applied Genomics (Hospital for Sick Children). To verify the expression of pluripotent markers OCT4 and NANOG, immunocytochemistry was performed.

2.4.2 Generation of SCN2A KO cells

A 3x stop premature termination codon (StopTag) was designed similarly to our previously described method for introducing a StopTag into the DNA to knock out the expression of genes of interest (Deneault et al., 2018). This 3x StopTag was delivered by a synthesized single-stranded oligodeoxynucleotide (ssODN) containing two 50-nucleotide-long homology arms with the StopTag, V5 epitope, and EcoRI restriction site sequences coding 59 nucleotides. The knock-in site was selected to situate the StopTag 80 bp upstream of the exon 5-6 junction, to increase the likelihood of transcript knockout by the nonsense-mediated decay pathway (Neu-Yilik et al., 2011). A normal iPSC line named "50B" previously described was used to insert the StopTag and generate an isogenic *SCN2A* KO line (Deneault et al., 2018). The StopTag ssODN template, a pSpCas9(BB)-2A-GFP plasmid (Addgene, catalog no. 48138), and paired gRNAs targeting exon 5 of *SCN2A* were nucleofected into the 50B iPSCs using the Amaxa 4D-nucleofector with code CA137. GFP expressed cells were isolated 48h after nucleofection and clonally grown. Digital droplet PCR and dilution culture steps previously described were used to enrich for *SCN2A* KO populations (Deneault et al., 2018; Miyaoka et al., 2014). The purified *SCN2A* KO wells were expanded and assayed for pluripotency, karyotypic abnormalities, and sequencing validation of StopTag insertion. (Figure S1).

2.4.3 Induction of iPSCs into glutamatergic neurons

We sought to explore functional differences between the 3 genetic models of *SCN2A* deficiency. For this, we needed to differentiate the newly generated iPSCs into excitatory neurons. Since previous findings showed inhibitory neurons were unaffected by

SCN2A deficiency, we required an established system to explore excitatory neuron-driven differences (Ogiwara et al., 2018; Spratt et al., 2019; Wang et al., 2021). To rapidly upscale experiments and focus on excitatory neurons, we used the previously published constitutive expression protocol of NGN2 to generate homogeneous populations of glutamatergic neurons (Zhang et al., 2013). These iNeurons displayed stable membrane, firing, and synaptic properties when co-cultured with mouse glial cells by day *in vitro* (DIV) 21 (Zhang et al., 2013, 2018). Importantly as we previously described, this protocol provided consistent differentiation levels between cell lines derived from different participants (Deneault et al., 2018, 2019). We modified this protocol by inducing NGN2 for 3 days starting at DIV 1 and puromycin selecting for 2 days starting at DIV 2 and adding mouse glial cells at DIV 5. Half-iNeuron media (iNI) (Neurobasal media, 1x SM1, 1x GlutaMAX 1x pen/strep, 1µg/mL laminin, 10 ng/uL brain-derived neurotrophic factor (BDNF) and 10 ng/uL glial-cell derived neurotrophic factor (GDNF)) changes were performed every other day. Patch-clamp recordings were generated between DIV 24 and 27 post-NGN2-induction. Comparable bioelectric properties were previously reported (Deneault et al., 2018, 2019; Yi et al., 2016; Zhang et al., 2013, 2018).

2.4.4 Immunocytochemistry

iPSCs were washed gently 2 times with phosphate-buffered saline (PBS) and fixed in 4% paraformaldehyde in PBS for 8 min at room temperature. The cells were then washed 2 times with PBS and left overnight at 4°C. The next day, the cells were permeabilized at -30°C with ice cold methanol for 10 min. The cells were then washed 2 times with PBS for 8 min and incubated with primary antibodies overnight at 4°C. The following day, the cells

were washed 3 times with PBS for 8 min. Secondary antibodies were incubated for 1 hr at room temperature covered with aluminum foil, followed by 3 washes in PBS for 8 min. After the washes, 300 mM 4′,6-diamidino-2-phenylindole (DAPI) in PBS was incubated for 8 min, followed by 2 washes with PBS. Coverslips were then quickly dried with a Kimwipe and mounted on VistaVision glass microscope slides (VWR) with 10 μL of Prolong Gold Anti-Fade mounting medium (Life Technologies). Mounted coverslips were allowed to cure overnight in a dark slide box at room temperature. Images were acquired using a Zeiss LSM700 confocal microscope.

On DIV 25, iNeurons were fixed at room temperature in 4% paraformaldehyde in PBS for 15 min. The cells were then washed 3 times for 10 min with PBS, then blocked and permeabilized (B/P) with a B/P solution containing (0.3% Triton-X, 10% Donkey Serum, and PBS) for 1 hr. The cells were then incubated overnight at 4°C with primary Microtubule-associated protein 2 and Synapsin 1 antibodies in B/P solution. The next day, cells were washed 3 times for 10 min in PBS and incubated with secondary antibodies in B/P solution for 1.5 hours at room temperature and covered with aluminum foil. The cells were then washed 3 times for 10 min and incubated with 300mM DAPI for 8 min. The cells were then washed 1 time with PBS for 10 min. Coverslips were then quickly dried with a Kimwipe and mounted on VistaVision glass microscope slides (VWR) with 10 μL of Prolong Gold Anti-Fade mounting medium (Life Technologies). Mounted coverslips were allowed to cure overnight in a dark slide box at room temperature. Images were acquired using a Zeiss LSM700 confocal microscope.

2.4.5 Analysis of presynaptic puncta and primary dendrites

Synaptic morphology was processed and analyzed with ImageJ software. The Synapsin1 (SYN1) antibody was co-immunostained with MAP2 to determine dendrites with presynaptic puncta. Three biological replicates were used for each line with the data generated from five iNeurons per replicate per condition. A total of 15 iNeurons per condition per line were used with two dendrites of equal dimensions used per iNeuron. Data represent the number of synaptic puncta averaged by two dendrites per iNeuron within 30 μm segments. The same images were used to calculate dendrite complexity. This was determined by counting the number of MAP2-positive primary dendrites branching from the soma.

2.4.6 Multielectrode array

All recordings were performed using 48-well clear bottom MEA plates (Axion Biosystems), consisting of 16 electrodes per well. Plates were coated with filter-sterilized 0.1% polyethyleneimine solution in borate buffer pH 8.4 for 2 hr at 37°C, washed with water four times and dried overnight. 40 000 DIV 4 doxycycline iNeurons were seeded in a 20 μL drop of iNI media at the centre of each well for 1.5 hr, then an additional 150 μL of iNI media was added. The day after, 20 000 mouse astrocytes per well were seeded on top of iNeurons in 150 μL per well of iNI media. Mouse astrocytes were prepared from postnatal day 1 CD-1 mice as described (Kim and Magrané, 2011). Half media changes were performed every other day with iNI media until the endpoint of the experiments. The electrical activity of neurons was measured a minimum of once-a-week post-seeding onto MEA plates using the Axion Maestro MEA reader (Axion Biosystems). On the day of

recording, MEA plates were equilibrated for 5 min on the pre-warmed reader at 37°C. Real-time spontaneous neural activity was recorded for 10 min to use for offline processing. Recordings were sampled at 10 kHz and filtered with a bandpass filter from 200 Hz to 3 kHz. A threshold of greater than 6 standard deviations was used to detect spikes and separate noise. Electrodes were considered active if a minimum of 5 spikes were detected per minute. Wells that were unable to generate 10 active electrodes of the 16 by DIV 42 were not used for analysis. Bursts were defined as a minimum of 5 spikes with a maximum of 100-millisecond inter-spike interval (ISI). Network bursts were defined as a minimum of 10 spikes with a maximum of 100 milliseconds ISI and at least 35% of electrodes in synchrony. Offline processing was performed using Axion Biosystems Neural Metric Tool.

2.4.7 In vitro electrophysiology

iNeurons were replated on DIV 4 onto polyornithine/laminin-coated coverslips in a 24-well plate at a density of 100 000/well with 0.5 mL of iNI media. On DIV 5, primary mouse astrocytes were added at a density of 50 000/well to support iNeurons' viability and maturation. Half media changes were performed every other day and wells were maintained until DIV 24 – 26 for recordings. At DIV 9, iNI was supplemented with 2.5% FBS which was adapted from (Zhang et al., 2013). Whole-cell patch-clamp recordings were performed at room temperature using Multiclamp 700B amplifier (Molecular Devices) from borosilicate patch electrodes (P-97 puller and P-1000 puller; Sutter Instruments) containing a potassium-based intracellular solution (in mM): 123 K-gluconate, 10 KCl, 10 HEPES; 1 EGTA, 1 MgCl2, 0.1 CaCl2, 1 Mg-ATP, and 0.2 Na4GTP (pH 7.2). 0.06% sulpharhodamine dye was added to the intracellular solution to confirm the selection of

multipolar neurons. The extracellular solution consisted of (in mM): 140 NaCl, 5 KCl, 1.25 NaH_2PO_4, 1 $MgCl_2$, 2 $CaCl_2$, 10 glucose, and 10 HEPES (pH 7.4). Data were digitized at 10 – 20 kHz and low-pass filtered at 1 - 2 kHz. Recordings were omitted if access resistance was >30 MΩ. Whole-cell recordings were clamped at -70 mV and corrected for a calculated -10mV junction potential. Rheobase was determined by a step protocol with 5 pA increments, where the injected current had a 25 ms duration. Action potential waveform parameters were all analyzed in reference to the threshold. Repetitive firing step protocols ranged from -20 pA to +50 pA with 5 pA increments for the isogenic KO line. This was adapted for the patient-derived iNeurons as it took more current to elicit their rheobase. The repetitive firing step protocol ranged from -40 pA to +90 pA with 10 pA increments. No more than two iNeurons per coverslip were used to reduce the variability. Data were analyzed using the Clampfit software (Molecular Devices), while phase-plane plots were generated in the OriginPro software (Origin Lab).

2.4.8 Statistical analysis

Data are expressed as mean ± SEM. Three viral NGN2 transductions were used as biological replicates for statistical analysis, except for CTRL-F2 and G1744* MEA data, where two biological replicates were used. We used the Student's unpaired t-test, two-way ANOVA, and post hoc Sidak tests in GraphPad Prism 8 statistical software for statistical analyses. Sidak was used to correct for multiple comparisons. Grubbs' test was used to remove outliers. The p-values in the figure legends are from the specified tests, and $p < 0.05$ was considered statistically significant.

2.5 Results

2.5.1 Generation and characterization of isogenic SCN2A knockout and two patient-derived truncating de novo variants in human iPSCs and iNeurons

We recruited two unrelated families with *de novo* protein-truncating variants in *SCN2A* in the proband and sex-matched parental controls that did not have the variant (Figure 1B). The variants were identified by whole-genome sequencing (Yuen et al., 2017). Both probands were male; one had ASD and a *de novo* truncating variant at amino acid position 607 (*SCN2A$^{+/p.R607*}$)*, while the other proband had ASD and early-onset seizures with a C-terminal truncating variant at position 1744 (*SCN2A$^{+/p.G1744*}$*) (Figure 1B). iPSCs were generated as previously described (Deneault et al., 2018, 2019), with all lines having a normal karyotype, expressing pluripotency markers, and were mycoplasma free (Figure S1A and C). We confirmed that the iPSCs from the probands carried the *SCN2A* variant (Figure S1D). In addition to the patient-derived and parental control iPSCs, we generated a new *SCN2A$^{-/-}$* iPSC line using CRISPR/Cas9 to insert a STOP-tag into exon 5 of an iPSC line we previously used (named 50B) (Deneault et al., 2018), which was confirmed by sequencing (Figure S1D) (referred to as CTRL-iso and KO respective to wild-type and knockout neurons). The first family, or *SCN2A$^{+/p.R607*}$* variant and familial control are referred to as CTRL-F1 and R607*, while the second family or *SCN2A$^{+/p.G1744*}$* variant and familial control are referred to as CTRL-F2 and G1744* (Figure 1D).

2.5.2 SCN2A expression in cortical neurons

We validated *SCN2A* expression in iNeurons using digital droplet PCR (ddPCR). Compared to controls, we found that probes targeting exon 4-5 had minimal detectable

SCN2A transcript in isogenic KO neurons, demonstrating that the CRISPR-Cas9-inserted 3x stop-tag single-stranded oligodeoxynucleotides donor (ssODN) disrupted *SCN2A* expression (Figure 1E). Using R607* iNeurons, ddPCR detected a small quantity of *SCN2A* mRNA, which is likely derived from the remaining allele (Figure 1F). We also examined iNeurons from the G1744* variant located in exon 27, which is beyond the predicted non-sense mediated decay breakpoint (Nagy and Maquat, 1998; Sanders et al., 2018). We quantified *SCN2A* expression at exon 4-5 and found that the G1744* variant produces a small reduction in expression of *SCN2A* (Figure 1G), suggesting a lesser impact on mRNA levels.

2.5.3 SCN2A perturbation in human cortical neurons reduces synapse formation but not dendritic growth

To study the morphological effects of *SCN2A* perturbation on human glutamatergic neurons, we used iNeuron that were co-cultured with mouse glia from our varying models of *SCN2A* deficiency. To assess the differences between the deficiency severity, and synaptic and dendritic morphology, we fixed our iNeuron co-cultures between DIV 26-28. This coincided with the onset of our electrophysiological recordings. Previous studies have shown that $Scn2a^{+/-}$ animal studies have immature spine development in cortical excitatory neurons (Spratt et al., 2019). We immunostained with the Microtubule-associated protein 2 (MAP2) commonly used in dendrite identification of mature neurons, and Synapsin 1 (SYN1) which is used in identifying presynaptic vesicles often near the active zones. Co-cultures were also stained with DAPI to identify DNA in the nuclei of either glia or iNeurons. From this, we determined that there was no change in the number of MAP2-

positive primary dendrites that originated from the soma in all genetic models of *SCN2A* deficiency, suggesting that SCN2A may not regulate dendrite formation (Figure 2A-C). However, this finding did not rule out the possibility of dendrite arborization and spine growth being altered.

Next, we examined synapse formation in the context of *SCN2A* deficiency. Since the iNeuron co-cultures were previously stained with SYN1 we were able to perform a synaptic analysis on the same samples used for the dendrite inquiry, thus providing a stronger correlation between any findings of dendrite and synapse morphology. The synapse examination was divided into two categories, density, and puncta size. Each of which would describe a distinctive characteristic of the synapse. We examined synaptic density to provide insight into synaptic connectivity, this was done by analyzing the number of axonal boutons that were close to a postsynaptic neurons' dendrite. Differences in synapse size can be attributed to many biological reasons, in our use case, SYN1 is associated with the membrane of presynaptic vesicles, and any differences would be crudely referenced to changes in vesicle numbers or size. From our analysis, we found gross decreases in synapse density for all neuron models of *SCN2A* deficiency (Figure 2D-F). This data suggests that two fully functional alleles of *SCN2A* are necessary for an appropriate number of synaptic connections to form. When examining the presynaptic size, we found increases in our KO and G1744* iNeurons respective to their controls (Figure 2F). However, no differences were seen in size for R607* iNeurons (Figure 2E). Together, these data indicate that *SCN2A* deficiency is not sufficient to impair primary dendrite growth, but does reduce synaptic connectivity and may alter synapse size.

2.5.4 SCN2A deficiency differentially impacts passive and active membrane properties of iNeurons

Neurons are dynamic and are capable to regulating one's self-activity to environmental stimuli. One aspect that helps to define the dynamic nature of neurons are membrane properties. Neuron membranes innately define two core characteristics, this being capacitance, and resistance. From this, we can crudely determine properties including size, resting membrane potential, and leakiness. Additionally, it is well documented how membrane properties can shape synaptic integration. We first inquired how *SCN2A* deficiency may impact membrane properties. Using a whole-cell patch clamp we determined that R607* iNeurons had reduced capacitance compared to CTRL-F1 iNeurons (Figure 2I), however, the other two deficient *SCN2A* lines did not (Figure S2). Further, the input resistance of KO iNeurons was significantly increased compared to CTRL-iso iNeurons (Figure 2G), implicating *SCN2A* deficiency in differential membrane properties. All other membrane properties remained unchanged (Figure S2).

To better understand the intrinsic properties of our iNeurons under *SCN2A* deficiency, we analyzed the action potential waveform. Throughout, we found that the R607* and KO iNeurons behaved similarly, but G1744* iNeurons diverged from the other genetic manipulations. R607* and KO iNeurons had reduced action potential amplitude respective to their controls (Figure 2I), suggesting that fewer sodium channels are present. Additionally, KO iNeurons showed a significant reduction in the maximum rise rate of the depolarization phase (Figure 2G), where R607* iNeurons trended towards a decreased rate but were not statistically significant (Figure 2I). This suggests that the maximal sodium

conductance was impaired through the ion channels. This was more evident when generating the phase-plane plot to visually represent the kinetic differences of the action potential waveforms (Figure 2I). All other parameters of action potential waveform were not statistically significant between R607* and KO iNeurons (Figure S2). When examining the G1744* iNeurons' action potential waveform we observed a stark contrast to the R607* and KO iNeurons. First, we found that the threshold of G1744* iNeurons was more hyperpolarized compared to CTRL-F2 iNeurons (Figure 2L). This suggests that the site of which the all or none response of the iNeuron was closer to the resting membrane potential as the resting membrane potential was not changed (Figure 2K). Second, we found that this change in threshold coincided with increased action potential amplitude, half-width, and the maximum rise and decay rates (Figure 2M-P). Together, this indicates that G1744* iNeurons have a more robust action potential that is generated at more negative voltages. Further, since they have an increased maximal amplitude, and rate of depolarization and repolarization phase, they generate narrower action potentials compared to CTRL-F2 iNeurons (Figure 2Q). We also generated a phase-plane plot to better visually represent the kinetics of the action potential waveform (Figure 2Q).

To supplement the action potential waveform data, we also questioned the repetitive firing capabilities of our iNeurons. Glutamatergic neurons have been characterized with the ability to fire a train of action potentials in a short time, we questioned if *SCN2A* deficiency would also affect action potential trains. We discovered that when KO iNeurons were injected with positive current, there was a transient hyperexcitable phenotype, this was evident by an increased number of action potentials observed at small positive current

injections (Figure 2H). The R607* iNeurons which represent *SCN2A* haploinsufficiency did not show this transient effect and persisted to show no statistically significant difference to CTRL-F1 iNeurons (Figure 2J). Finally, the G1744* iNeurons did not differ from the CTRL-F2 iNeurons (Figure 2R). Taken together, this data suggests that there is a paradoxical phenomenon of hyperexcitability that is present only with homozygous loss of SCN2A expression. Further, heterozygous expression of SCN2A is sufficient to support action potential train firing.

Lastly, in an attempt to inquire if synaptic connectivity was altered in our *SCN2A* deficient iNeurons, we examined synaptic transmission. SCN2A is an essential regulator of excitability in glutamatergic neurons. For this, we looked at excitatory postsynaptic currents and characterized both the frequency and the magnitude of the currents. For this analysis, a 60 s segment was analyzed taken from the 180 s of recording until the start of the 240s. We determined that during this recording period KO iNeurons displayed a reduction in the number of currents that were detected, but the magnitude of the currents was unaffected compared to CTRL-iso iNeurons (Figure 3A). Additionally, R607* iNeurons followed suit with a significant decrease in the frequency of the currents but not the amplitude of the events (Figure 3B). However, G1744* iNeurons showed no impairment in synaptic connectivity for both frequency and magnitude (Figure 3C). This suggests that there is an impairment in the frequency of synaptic connectivity with KO and R607* iNeurons interacting less through chemical synapses.

2.5.5 Severity of SCN2A deficiency differentially impairs neuronal network activity and development

We previously determined that KO, R607* G1744* iNeurons showed decreases in presynaptic density but only KO and R607* iNeurons displayed decreases with their synaptic transmission on a single cell level. This caused us to question if the impairments in synaptic morphology and the frequency of synaptic communication would persist and disrupt neuronal network dynamics. We separated and analyzed our network data into three distinct parameter categories, these being activity, connectivity, and oscillations or major network bursting patterns. All data was extrapolated from the raster plots generated from the MEA system (Figure 4A, H, and O). From our analysis, we discovered an interesting phenomenon of decreased number of active electrodes across our KO and R607* iNeurons (Figure 4B and D). This was not evident in the G1744* iNeurons, suggesting that heterozygous or more severe loss of SCN2A is sufficient to impair a subset of neuron firing in a network (Figure 4P). We further found that the weighted mean firing rate was impacted. KO and R607* iNeurons displayed a reduction in the number of spikes that were generated across time, this was corrected for the number of active electrodes since CTRL-iso and CTRL-F1 iNeurons had more active electrodes throughout development (Figure 4C and J). The weighted mean firing rate remained unchanged for G1744* iNeurons (Figure 4Q). Because of the differences in the active electrodes for KO and R607* iNeurons, we were unable to use the meaning firing rate as an accurate indicator of general activity.

Next, to determine the bursting characteristics of our genetic models of *SCN2A* deficiency, we analyzed clustered spikes that we defined as bursts if there was a minimum

of 5 spikes within 100 milliseconds. KO iNeurons displayed a decrease in bursting and the number of spikes per burst (Figure 4D, E). When examining the bursting of patient iNeurons, unlike the KO iNeurons, R607* iNeurons exhibited a small increase in bursting early in development (Figure 4K), which became reduced compared to CTRL-F1 iNeurons. Furthermore, R607* iNeurons displayed a decrease in the number of spikes per burst for a transient window between DIV 39 – 46 (Figure 4E vs. L). Secondary burst parameters were also examined to further characterize bursting patterns (Figure S3A-B and E-F). Interestingly, G1744* iNeurons did not show any difference in burst frequency but had a stark reduction in the number of spikes per burst during early development (Figure 4R and S, Figure S3I and J).

Network bursting and synchronization occurs in later stages of neuronal development, which is crucial for the organization and regulation of excitation (Kim et al., 2019; Kirwan et al., 2015; Masquelier and Deco, 2013; Stegenga et al., 2008). We found that the number of spikes per network burst was reduced in KO and R607* iNeurons at approximately 4 weeks (Figure 3F and M). Network burst frequency and network burst duration were also recorded and corroborated impaired network capacity (Figure S3C-D and G-H,). Interestingly, we found that early on within network bursts, G1744* iNeurons had reduced spikes, similar to KO and R607* iNeurons; however, after DIV 49, there was a reversal and G1744* iNeurons had more spikes (Figure 4T). This was also reflected in the large increase in the burst and network burst duration (Figure S3K and L), which is opposite to the KO and R607* iNeurons. This is noteworthy because this proband has early-onset seizure activity; therefore, the increased spikes per network burst and their duration,

which may occur due to the abnormal action potential characteristics, may contribute to epilepsy. An alternative explanation is that the G1744* iNeurons have an elongated early maturation phase where normal developing burst sequences are altered initially but compensate for the decreased number of spikes in bursts allowing for a rebound in mid to late development.

Lastly, we examined synchronization, which is a parameter defined as the probability for neighbouring electrodes to detect activity in quick succession based on prior electrode activity. This is measured as an index ranging from $0 - 1$, where 1 represents neighbouring electrodes detecting activity based on a prior active electrode, 100% of the time. Interestingly, we found that all iNeurons displayed deviation from their respected control lines, suggesting that synchronization of neurons in the network was impaired by any type of SCN2A disruption (Figure 4G, N, and U). However, this measurement does not take into account the probability of random spikes contributing to the synchrony of the neuronal network.

2.5.6 Excitatory-inhibitory co-culture ratios regulate the magnitude of electrical events but does not alter the patterns

Outside the scope of the manuscript but that was paramount to our understanding of our model, was our investigation of how inhibitory neurons modulate excitatory cultures. We decided to test this concept on CTRL-F2 iNeurons in the MEA format with varying densities of iNeurons. GABAergic iNeuron generation followed previously published reports of exogenous expression of ASCL1 and DLX2 to directly differentiate iPSCs and NPCs into iNeurons (Barretto et al., 2020; Yang et al., 2017) (Figure S4A). We used ratios

of 100, 90/10, 70/30, and 50/50 excitatory to inhibitory iNeurons to examine biological and non-biologically relevant ratios that were used in our initial screen. These ratios were changed based on a total of 50 000 iNeurons. Further, we longitudinally monitored our cultures to better understand the developmental trajectory. We followed a similar analysis pipeline outlined in our MEA section by looking at activity, connectivity, and oscillations or major network bursting patterns.

We first examined the activity parameters of our excitatory-inhibitory co-cultures. We found that all 4 ratios followed a similar trajectory with the number of active electrodes, however, this started to deviate at DIV 39 with the 70/30 and 50/50 ratios decreasing their active electrodes, while 100 and 90/10 ratios did not (Figure S4B). Weighted mean firing rate did not differ significantly until DIV 53 and 56 for these cultures with ratios of 100 and 90/10 having high firing rates (Figure S4C). This suggests that the introduction of GABAergic iNeurons reduces glutamatergic iNeurons firing in a linear graduate response. Bursting characteristics were less affected by the introduction of GABAergic iNeurons. We discovered that burst frequency had no differences across the ratios (Figure S4D). However, trajectories started to differ for the number of spikes per burst at DIV 56 for 100, and 90/10 ratios (Figure S4E). This suggests that around DIV 56 glutamatergic iNeurons with less GABAergic iNeuron inputs increase the number of spikes associated with bursting. Lastly, analysis of network bursting dynamics resulted in no differences observed in network burst frequency across development (Figure S4F). When inspecting the synchronization index, the results mirrored our predicted outcomes, the amount of synchrony decreased with the increasing GABAergic iNeurons population, however, this

plateaued with 30% GABAergic iNeurons (Figure S4G). This suggests that a negative feedback mechanism exists where an excess of 30% GABAergic iNeurons does not further reduce the network activity and communication to help maintain a baseline.

2.6 Discussion

The cellular phenotypes underlaid by the severity and location of *de novo SCN2A* mutations remains poorly understood. As more variants are curated, clinicians and researchers continue to falter when it comes to expansive human neuronal characterization studies. Reports have indicated that clinical diagnosis of ASD or EE of the SCN2A channelopathy tend to have variants associated with clusters in specific regions within the protein. Clustering of missense variants contributing to epileptic syndromes is often localized proximally to the voltage sensory domain, while variants close to the pore loops are commonly associated with ASD/ID (Ben-Shalom et al., 2017). However, our study expands on previous human and mouse work by further modelling patient mutations in human neurons and reporting findings on two previously unpublished variants. Further, we took great interest in functionally validating the G1744* mutation in our iNeurons as there are no reports investigating an *SCN2A* loss of function variant that produces both ASD and seizure phenotypes. We discovered the gross cytoarchitecture of primary dendrites was unaltered in our iNeurons, however, synaptic morphology differed, and this was likely due to changes in neuronal activity. Further, we reveal that both *SCN2A* mutations behave dissimilarly in both intrinsic and extrinsic neuronal parameters, highlighting a dichotomy for LoF mutations. Finally, we demonstrate that neuronal network activity is differentially

impacted by the type and location of the mutations, with the R607* mutation producing more severe phenotypes.

2.6.1 Cytoskeletal dynamics are regulated by neuronal activity via loss of SCN2A

Literature has long reported that long-term memory formation creates lasting changes to neuronal morphology. Specifically, the increased presence of dendritic spines is often observed in learning-induced events (Lamprecht, 2021). These spines can also undergo elimination under depressive states of neural circuits. Since dendritic spines are primary sites of excitatory input, changes in their shape, presence and density can significantly alter synaptic connectivity which underlies neuronal networks. Spine dynamics are also proportionally related to synaptic currents observed on the postsynaptic neuron, with AMPAR-mediated currents the most affected (Matsuzaki et al., 2001). Scn2a heterozygous mouse studies have reported a maturation-dependent regulation of dendritic spines (Spratt et al., 2019). Throughout development dendritic arbour structure remains unchanged with Scn2a haploinsufficiency; cortical neurons examined between P5 – 6 maintained similar morphology in filopodial spines between control and Scn2a heterozygous neurons (Spratt et al., 2019). Mature neurons (>P23) expressed no changes in spine density, but *Scn2a*$^{+/-}$ neurons did present with spines that were longer, and with smaller head volume compared to the total head and neck volume (Spratt et al., 2019). These findings highlighted that *Scn2a*$^{+/-}$ mature neurons tend to have similar features to immature neurons. When examining dendrites in our *SCN2A* deficient iNeurons, we noticed similar trends to the above results mentioned in mouse tissue sections. In all three of our *SCN2A* deficient genetic models, primary dendrites remained unchanged. From our

analysis, primary dendrites are similar to the basal dendrites, unlike tissue sections, we are unable to obtain data from apical dendrites since our neurons are grown as a monolayer. This suggests that SCN2A does not regulate apical or basal dendrite arborization in mouse and human neuronal models. Given that we did not analyze dendritic spines, we instead examined synapse morphology by immunostaining the presynaptic terminals and microtubule structure of our iNeurons. At DIV 25 – 28, all *SCN2A* deficient iNeurons expressed decreases in the density of terminals synapsing onto a postsynaptic neuron's dendrite. This indicated that there could be fewer functional synapses formed which would impair synaptic connectivity. Since we did not examine this phenomenon at earlier time points, we cannot state that it is developmentally regulated as with reports of dendritic spines. However, we can state that the developmental stage of our iNeurons was sufficient to produce synaptic deficits, and that impairments of synaptic morphology are a hallmark of *SCN2A* deficiency in mouse and human neurons.

2.6.2 Differential SCN2A expression regulates neuronal activity by altering intrinsic and extrinsic neuron characteristics

Using patch-clamp electrophysiology to investigate single neuron characteristics, we observed three main themes. First, human iPSC-derived KO iNeurons displayed a paradoxical hyperexcitability phenotype, similar to mouse *Scn2a$^{-/-}$* neurons (Spratt et al., 2021; Zhang et al., 2021a), but not in patient iNeurons as they have a heterozygous loss of SCN2A function. This reduction in synaptic transmission in KO iNeurons could be due to the localization of SCN2A during early development predominately being expressed at the AIS and secondarily in the somatodendritic compartments (Bender and Trussell, 2012;

Gazina et al., 2015; Hu and Bean, 2018; Hu et al., 2009; Spratt et al., 2019). An alternative explanation is that SCN2A regulates neuronal activity-dependent transcriptional activity that drives synaptic gene expression, and protein translation which was disrupted in our proteomics analysis discussed in the following chapter (Deneault et al., 2018; Ip et al., 2018b; Madabhushi and Kim, 2018; Nelson and Valakh, 2015; Zhang et al., 2018).

Our second main observation highlighted that R607* iNeurons had a decrease in synaptic transmission, however, it is unknown if this is a direct or indirect impact. Extrapolating and comparing to mouse Scn2a haploinsufficiency, the reduction in excitatory synaptic transmission in human R607* iNeurons could be driven by changes in the AMPA:NMDA ratio, inferring an abundance of silent synapses due to an abundance of AMPA-lacking spines (Hanse et al., 2013; Kerchner and Nicoll, 2008; Spratt et al., 2019). We also noted that both KO and R607* iNeurons generated less spontaneous electrical activity, which could suggest *SCN2A* deficiency, without seizures, dampens neural networks, and produces small quiescent pockets within the network (Deneault et al., 2018). Future studies can examine how other *SCN2A* missense variants impact human neuron synaptic function, as these variants do not cause protein truncation, but only amino acid changes, leading to effects on channel function (Ben-Shalom et al., 2017; Echevarria-Cooper et al., 2021).

The third major observation pointed towards a mixed neuronal phenotype in our late truncating mutation. The G1744* variant is characterized as a LoF mutation. However, the individual presents with early-onset seizures, and the variant is past the predicted non-sense mediated decay breakpoint (Nagy and Maquat, 1998; Sanders et al., 2018). The major

finding from this line was an enhancement of the action potential waveform, similar to a human neuronal model of the SCN2A-L1342P variant (Que et al., 2021b). However, the L1342P variant is characterized as a gain-of-function mutation from computational modelling and its association with epilepsy, but it has mixed GoF and LoF phenotypes (Begemann et al., 2019; Que et al., 2021b). Even with action potential waveform enhancements, we did not observe increases in neuronal excitability, dissimilar to the L1342P variant. Unlike previous SCN2A mouse and human studies, we did not observe a difference in synaptic transmission of G1744* iNeurons (Deneault et al., 2018; Spratt et al., 2019; Wang et al., 2021), suggesting there is compensation for the reduction in synapse formation. The differences between R607* and G1744* underscore the importance of studying multiple variants in sodium channels to ascertain the impact on function, as this was shown for *SCN8A* (Lopez-Santiago et al., 2017).

2.6.3 Differential SCN2A expression alters spontaneous neuronal network activity in iPSC-derived neurons

Information processing and communication between neurons and groups of neurons are driven by clustered activity in neuronal networks. Clustering patterns known as bursts are known to underly neural coding, whether increasing overall network activity based on synaptic transmission feedback or modulating the synchronization of networks. In cultured neurons, we can use MEA's to record spontaneous firing activity across time extending until months. This platform has proven useful when investigating neurodevelopment using iPSC-derived neurons. We can now track the trajectory of spiking activity from no spiking to bursting and integration into functional networks, whereas in disease states, this

development may not be as linear (Massobrio et al., 2015; Mccready et al., 2022). Moreover, MEA's provide the flexibility to measure varying metrics that capture differing information about activity that may be relevant to the disease state. Inferences drawn from the readouts have the goal of helping to tease apart some of the complexity of spatiotemporal organization (Engle et al., 2018; Mccready et al., 2022). Knowing this, we observed two major takeaways from our data.

First, KO iNeurons were unable to generate an even distribution of spontaneous activity throughout their networks, this was evident with the decrease in active electrodes. We hypothesized that this was due to silent synapses that were present throughout the network. Synapses are an essential site for the transfer of information between pre and postsynaptic neurons. Synapses that are deemed "silent" often lack AMPARs on the postsynaptic neuron, suggesting that any currents conducted by the neuron require depolarization and are N-Methyl-D-aspartate receptor (NMDAR) mediated (Hanse et al., 2013; Isaac, 2003; Isaac et al., 1995, 1997; Kanold et al., 2019; Kerchner and Nicoll, 2008). Silent synapses are common in the early development of many glutamatergic synapses of several brain regions (Isaac et al., 1997; Kanold et al., 2019; Rumpel et al., 1998, 2004). However, unsilencing of silent synapses occurs across development aiding in the development of maturing networks (Hanse et al., 2013). Based on our results of KO iNeurons, maturation of these silent synapses seems to be delayed affecting the generation of random spikes and synchronization within the network. Further, since elevated activity in early development is a mechanism that is correlated to converting silent synapses to AMPAR and NMDAR-containing (Anastasiades and Butt, 2012), this may additionally

suggest that KO iNeurons are impaired when developing their networks and adapting. Interestingly, this phenomenon was also present in the early truncating mutation. This suggested that silent synapses may be more abundant in iNeurons that are SCN2A haploinsufficient or more severe.

Lastly, in G1744* iNeurons we did not observe a decrease in active electrodes, suggesting that the cellular phenotypes here were not associated with our above hypothesis. Instead, we speculated that the reduction of spikes during early development was compensated by the early onset seizures. This could explain why at later timepoints the only difference was the synchronization of the network with no bursting (Que et al., 2021b; Tidball et al., 2020). Additionally, G1744* iNeurons may have compensatory activity early in development that aids in the recovery, which may be due to a truncated protein being produced that avoids non-sense mediated decay. Given that the G1744 position is near the calmodulin-binding domain of SCN2A, variants near the C-terminus may impact local calcium signalling, which has yet to be examined. A recent paper investigated $Na_V1.5$ channel function and the functional consequences of impaired calmodulin regulation in cardiomyocytes (Kang et al., 2021). Since the homology across the family of voltage-gated sodium channels (Na_Vs) is high, we may be able to assimilate the truncation of the calmodulin-binding domain to their calmodulin disruption model. Disruptions in calmodulin binding to the C-terminal of $Na_V1.5$ is associated with arrhythmias that are associated with GoF and LoF syndromes such as long QT and Brugada, respectively (Kang et al., 2021). One explanation that may explain the increase in neuronal activity observed with the G1744* iNeurons is what was observed in $Na_V1.5$ channels of the cardiomyocytes.

An increase in persistent sodium currents can occur with the disruption of calmodulin regulation, this current fails to inactive even during prolonged depolarization; thus, enhancing the response of the neuron to synaptic input and action potential waveform (Stafstrom, 2007). Further, an abundance of the literature suggests that abnormally large persistent sodium currents are associated with epilepsy (Stafstrom, 2007; Wengert and Patel, 2020). Reports of patient variants causing EE have shown increased persistent sodium currents too (Begemann et al., 2019; Liao et al., 2010; Wolff et al., 2017). This may also explain why there is an enhancement of the action potential waveforms described in the previous subsection for iNeurons containing the G1744* variant.

Taken together, these data reveal the complexity of variant location and type in the context of Navs. Perturbation of the channel expression has deleterious effects on individual and networks of neurons. Furthermore, there seems to be a high gene-dosage association with the severity of phenotypes observed, KO iNeurons have the most severe phenotypes, and haploinsufficient R607* iNeurons follow closely, with G1744* iNeurons functioning closets to control levels. This characterization of patient variants and a KO model underscores the need for more advanced investigations into patient variants. The goal of this is to better understand how each variant contributes to the cellular phenotypes and the regulation of neuronal activity. Once there is a clearer picture of the intricacies, manipulating cellular mechanisms that may ameliorate abnormal activity could be a viable next step in correcting abnormal brain development.

2.7 Conclusion

In conclusion, we used iPSC-derived patient neurons expressing differing variants to cellularly characterize neuronal dysfunction. Additionally, as a way to isolate the function of *SCN2A,* we created an isogenic KO. In an attempt to categorize the association between variant location and cellular outcome, we found novel enhancements in neurons attributed to a late truncating loss of function variant. These findings reiterate that categorizing variants as LoF or GoF may be too general, and a deeper look is needed to delineate the effects these variants have on the channel and neuron. As *SCN2A* human cellular model studies begin to focus on patient variant characterization, novel neuronal outcomes will be identified. From this, common characteristics among variants in a relevant context could provide useful grouping parameters.

A

B

Chr2, *SCN2A*, c.1819C>T, p.R607*, dn

Chr2, *SCN2A*, c.5230G>T, p.G1744*, dn

↗ ASD iPSC line
★ Control iPSC line

C

SCN2A/Na$_v$1.2

Extracellular

Intracellular

G1744*

R607*

● Protein truncating mutation
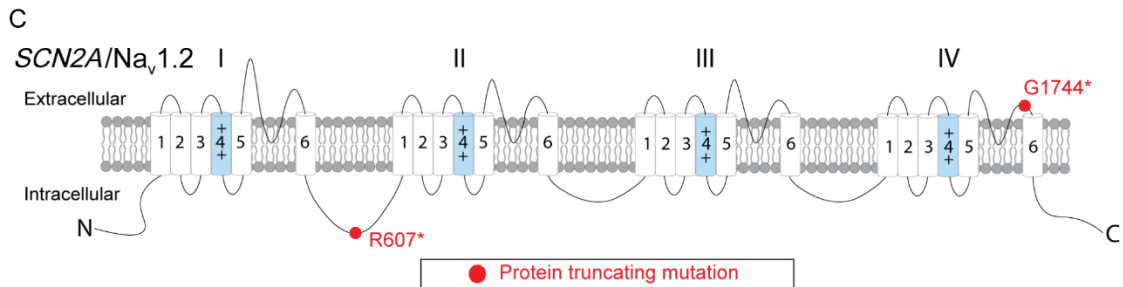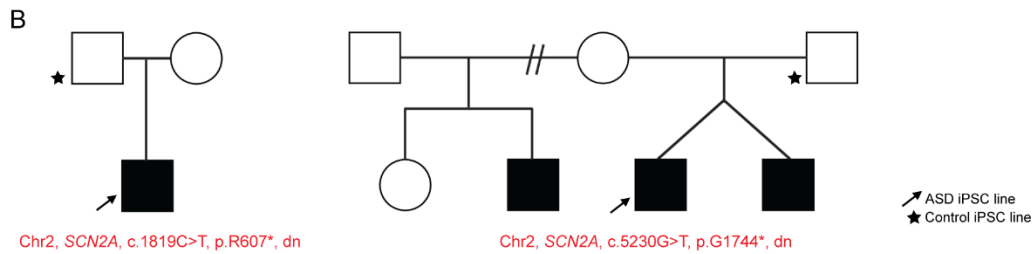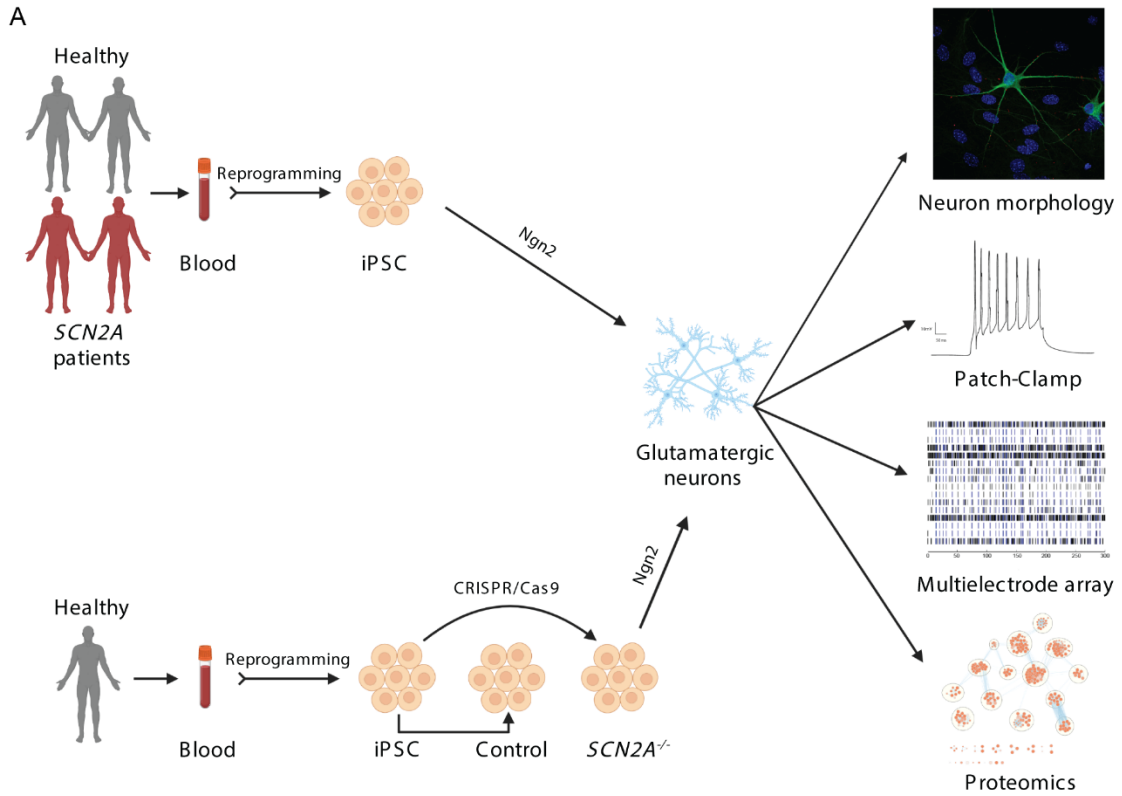
D

iPSC line	Genotype	Variant	Label
50B	Wildtype	*SCN2A$^{+/+}$*	CTRL-iso
50B	Knockout	*SCN2A$^{-/-}$*	KO
0611	Wildtype	*SCN2A$^{+/+}$*	CTRL-F1
0611	Heterozygous	*SCN2A$^{+/p.R607*}$*	R607*
0264	Wildtype	*SCN2A$^{+/+}$*	CTRL-F2
0264	Heterozygous	*SCN2A$^{+/p.G1744*}$*	G1744*

E

Exon 4-5 ddPCR

F

Exon 4-5 ddPCR

G

Exon 4-5 ddPCR
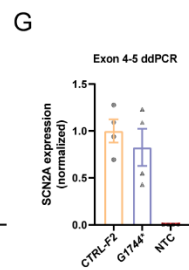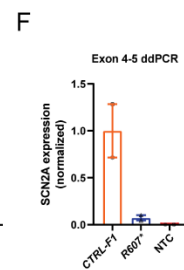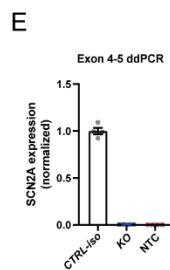
Figure 1. Experimental pipeline to probe cellular and molecular consequences of *SCN2A* deficiency in iPSC-derived iNeurons. See also figure S1.

A) Experimental pipeline to test cellular and signalling function.

B) *SCN2A* patient and family pedigrees.

C) Schematic of *SCN2A* structure with the associated location of the de novo variants.

D) Classification of iPSC lines used and their associated naming convention.

E-G) Digital droplet PCR normalized *SCN2A* expression probed at exon 4 – 5. (E) CTRL-iso (n=4) and KO (n=4) iNeurons. (F) CTRL-F1 (n=2) and R607* (n=2) iNeurons. (G) CTRL-F2 (n=4) and G1744* (n=4) iNeurons.
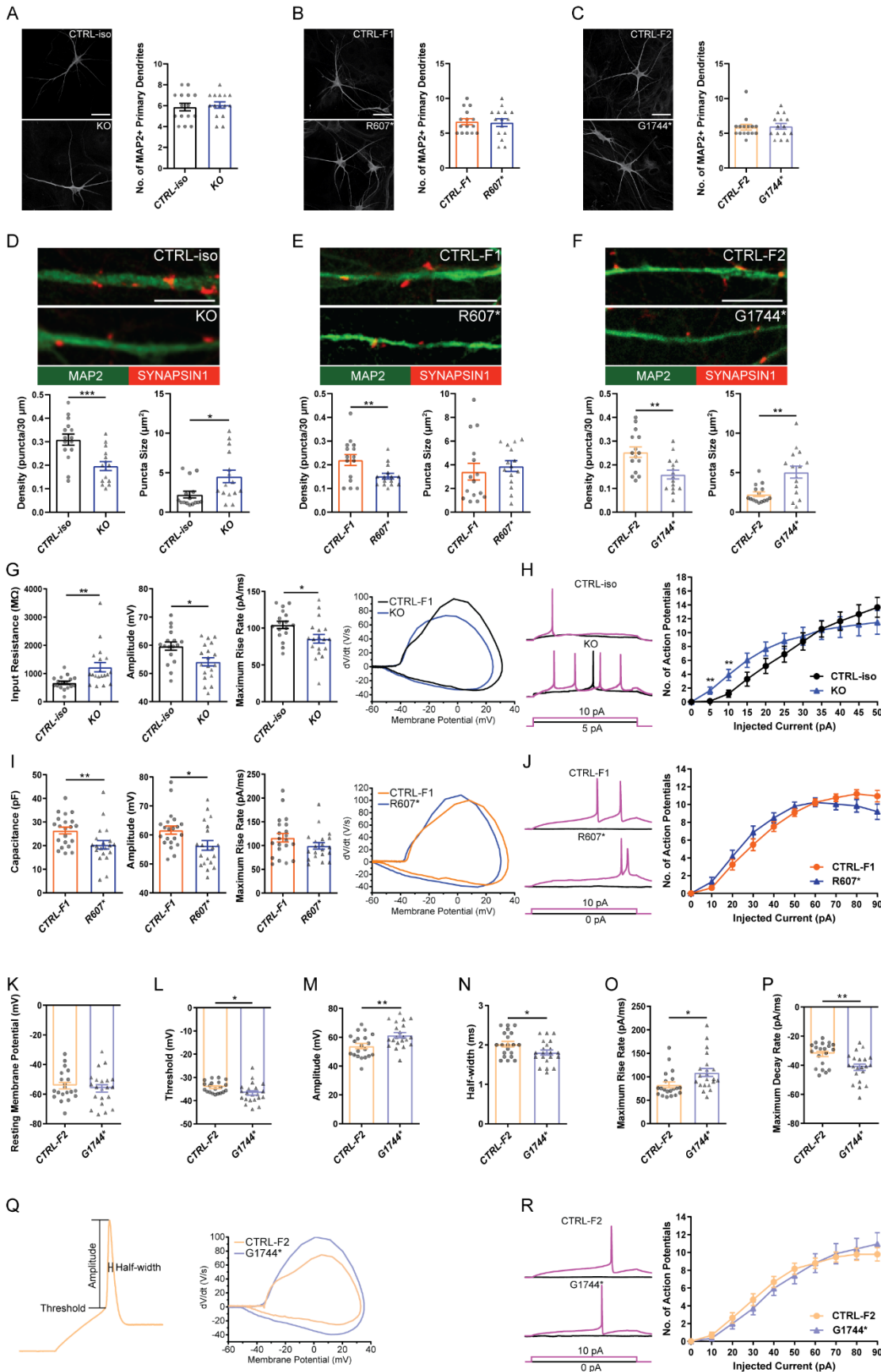
Figure 2. Effects of *SCN2A de novo* variants and CRISPR knockout on iNeuron morphology and synaptic function. See also figure S2.

A-C) Representative images of immunocytochemistry for dendrite complexity and analysis of MAP2-positive primary dendrites. (A) CTRL-iso (n=15) and KO (n=15) iNeurons. (B) CTRL-F1 (n=15) and R607* (n=15) iNeurons. (C) CTRL-F2 (n=15) and G1744* (n=15) iNeurons. 3 viral transductions. Scale bar, 40 μm.

D-F) Representative images and quantification of synaptic puncta density and size. (D) CTRL-iso (n=15) and KO (n=15) iNeurons. (E) CTRL-F1 (n=15) and R607* (n=15) iNeurons. (F) CTRL-F2 (n=15) and G1744* (n=15) iNeurons. 3 viral transductions. Scale bar, 10 μm.

G) Membrane and action potential properties of CTRL-iso and *SCN2A* KO iNeurons (n=17 and 19, respectively), 3 viral transductions. Left: bar graph of recorded input resistance. Middle: bar graph of measured action potential amplitude. Right: bar graph of the maximum rise rate and the associated phase plane plot of action potential kinetics. Data represent means ± SEM. *$p < 0.05$, **$p < 0.01$, Student's t-test.

H) Repetitive firing properties of CTRL-iso and KO iNeurons. CTRL-iso (n=17) and KO (n=19) iNeurons, 3 viral transductions. Data represent means ± SEM. *$p < 0.05$, **$p < 0.01$, Student's t-test.

I) Membrane and action potential properties of CTRL-F1 and R607* iNeurons (n=21 and 20, respectively), 3 viral transductions. Left: bar graph of recorded capacitance. Middle: bar graph of measured action potential amplitude. Right: bar graph of the maximum rise rate and the associated phase plane plot of action potential kinetics. Data represent means

± SEM. *p < 0.05, **p < 0.01, Student's t-test.

J) Repetitive firing properties of CTRL-F1 and R607* iNeurons. CTRL-F1 (n=21) and R607* (n=20) iNeurons, 3 viral transductions. Data represent means ± SEM. *p < 0.05, Student's t-test.

K-Q) Membrane and action potential properties of CTRL-F2 and G1744* iNeurons (n=20 and 21, respectively), 3 viral transductions. (K) resting membrane potential, (L) threshold of the action potential, (M) amplitude of the action potential relative to threshold, (N) half-width of the action potential, (O) maximum rise rate from action potential threshold to amplitude, (P) maximum decay rate from action potential amplitude to threshold, (Q) representative action potential depicting measurements for analysis and the associated phase-plane plot of the respective action potential kinetics.

R) Repetitive firing properties of CTRL-F2 and G1744* iNeurons. CTRL-F2 (n=20) and G1744* (n=21) iNeurons, 3 viral transductions. Data represent means ± SEM. *p < 0.05, Student's t-test.
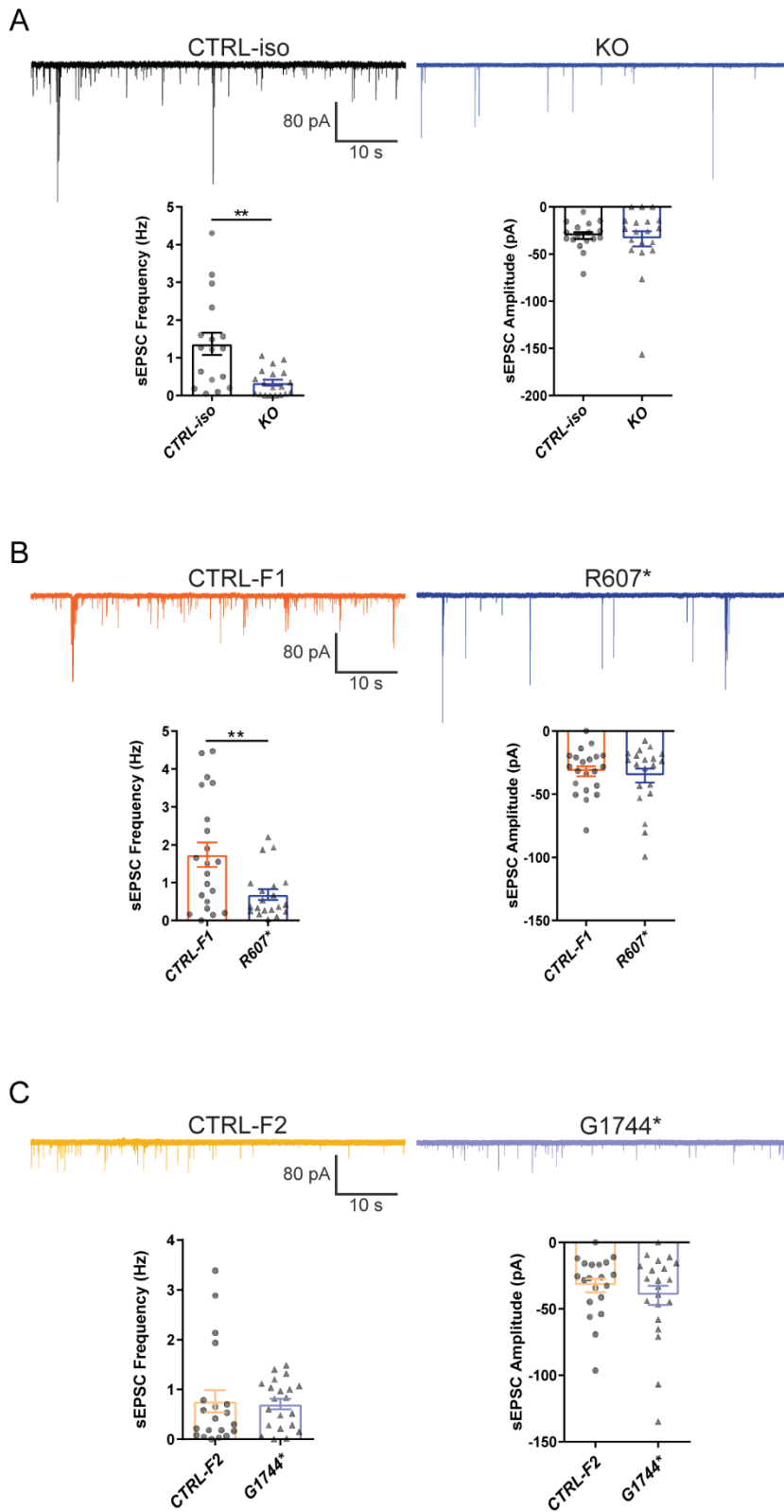
Figure 3. Complete and partial loss of *SCN2A* has differential effects on synaptic transmission.

A-C) Synaptic transmission representative traces and analysis of *SCN2A* deficient iNeurons. (A) Left: sEPSC frequency of synaptic transmission. Right: sEPSC amplitude of synaptic transmission. CTRL-iso (n=17) and KO (n=19) iNeurons. (B) Left: sEPSC frequency of synaptic transmission. Right: sEPSC amplitude of synaptic transmission. CTRL-F1 (n=21) and R607* (n=20) iNeurons. (C) Left: sEPSC frequency of synaptic transmission. Right: sEPSC amplitude of synaptic transmission. CTRL-F2 (n=20) and G1744* (n=21) iNeurons. 3 viral transductions. Data represent means ± SEM. *p < 0.05, **p < 0.01, Student's t-test.
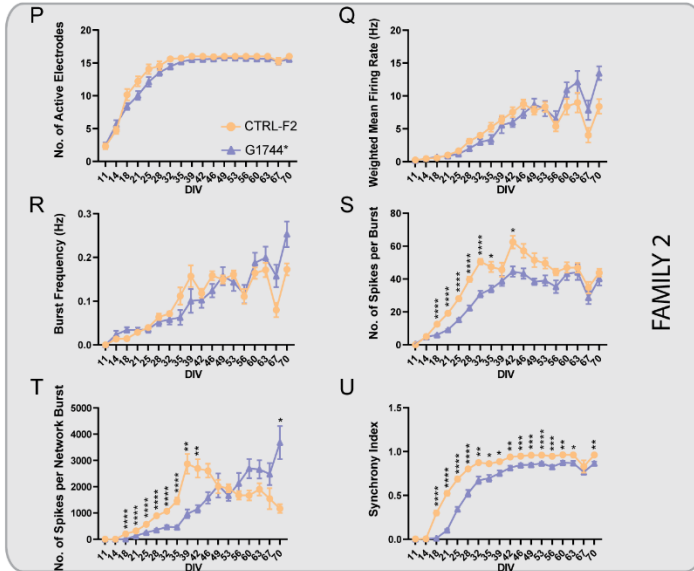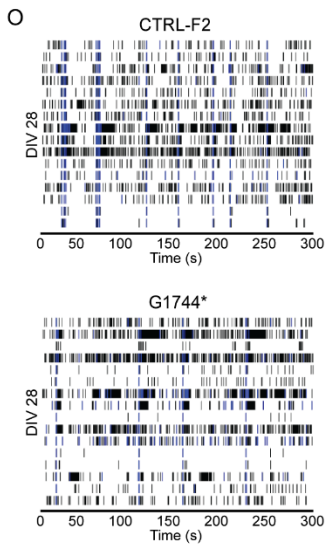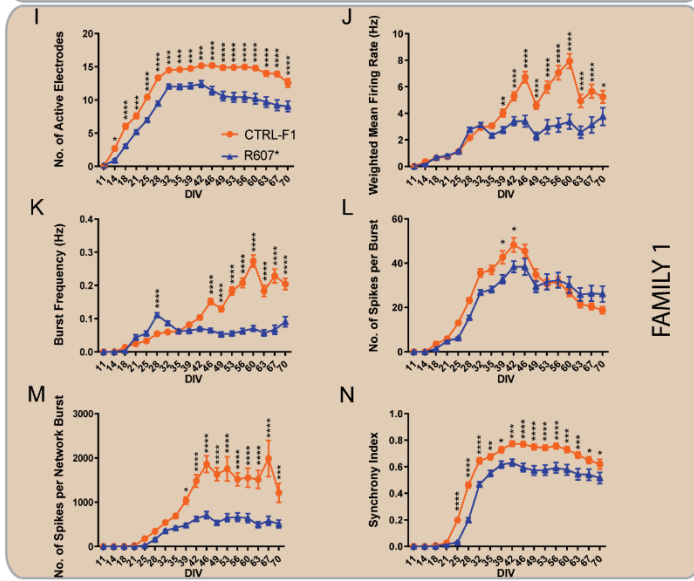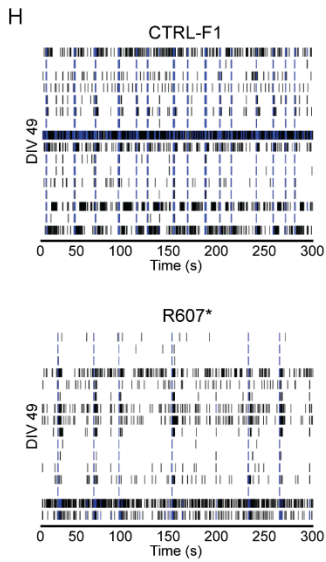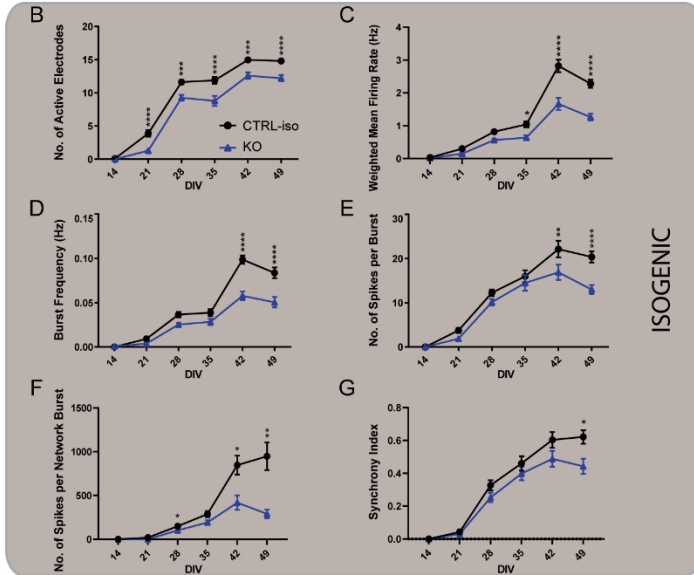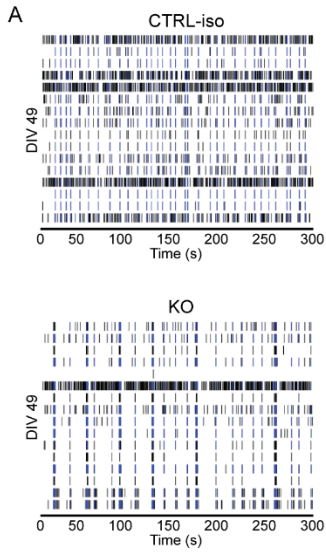
Figure 4. Effects of *SCN2A de novo* variants and knockout on the development of spontaneous network activity in iPSC-derived iNeurons. See also figure S3.

A) Example raster plots of recordings of neuronal network activity at DIV 49 for CTRL-iso and *SCN2A* KO iNeurons.

B-G) Quantification of MEA parameters for CTRL-iso and KO iNeurons. (B) number of active electrodes, (C) weighted mean firing rate, (D) burst frequency, (E) number of spikes per burst, (F) number of spikes per network burst, (G) synchrony index. CTRL-iso (n=47 wells) and KO (n=43 wells) iNeurons, 3 viral transductions. Data represent means ± SEM. *p < 0.05, **p < 0.01, ***p < 0.001, ****p < 0.0001, two-way ANOVA with post hoc Sidak correction.

H) Example raster plots of recordings of neuronal network activity at DIV 49 for CTRL-F1 and R607* iNeurons.

I-N) Quantification of MEA parameters for CTRL-F1 and R607* iNeurons. (I) number of active electrodes, (J) weighted mean firing rate, (K) burst frequency, (L) number of spikes per burst, (M) number of spikes per network burst, (N) synchrony index. CTRL-F1 (n=48 wells) and R607* (n=46 wells) iNeurons, 3 viral transductions. Data represent means ± SEM. *p < 0.05, **p < 0.01, ***p < 0.001, ****p < 0.0001, two-way ANOVA with post hoc Sidak correction.

O) Example raster plots of recordings of neural network activity at DIV 28 for G1744* and CTRL-F2 iNeurons.

P-U) Quantification of MEA parameters for CTRL-F2 and G1744* iNeurons. (P) number of active electrodes, (Q) weighted mean firing rate, (R) burst frequency, (S) number of

spikes per burst, (T) number of spikes per network burst, (U) synchrony index. CTRL-F2 (n=20 wells) and G1744* (n=19 wells), 2 viral transductions. Data represent means ± SEM. *p < 0.05, **p < 0.01, ***p < 0.001, ****p < 0.0001, two-way ANOVA with post hoc Sidak correction.

A

	OCT4	NANOG	DAPI	Merged	Karyotype
CTRL-iso					
KO					
CTRL-F1					
R607*					
CTRL-F2					
G1744*					

B

CTRL-iso   CTRL-F1   R607*   CTRL-F2   G1744*

TRA160 / SSEA4

C

100 bp Ladder CTRL-iso KO CTRL-F1 R607* CTRL-F2 G1744* Negative Control Positive Control

D

R607*, 1819C>T
A G C C/T G A A G A

G1744*, 5230G>T
A A G G/T G A G A C

KO
G G G A A A C C C A T T C C C A A T C C C C T T C T T G G G C T T G A T T C A A G A A T T C G C T A A C T A G C T G A

V5 epitope   3x Stop-tag
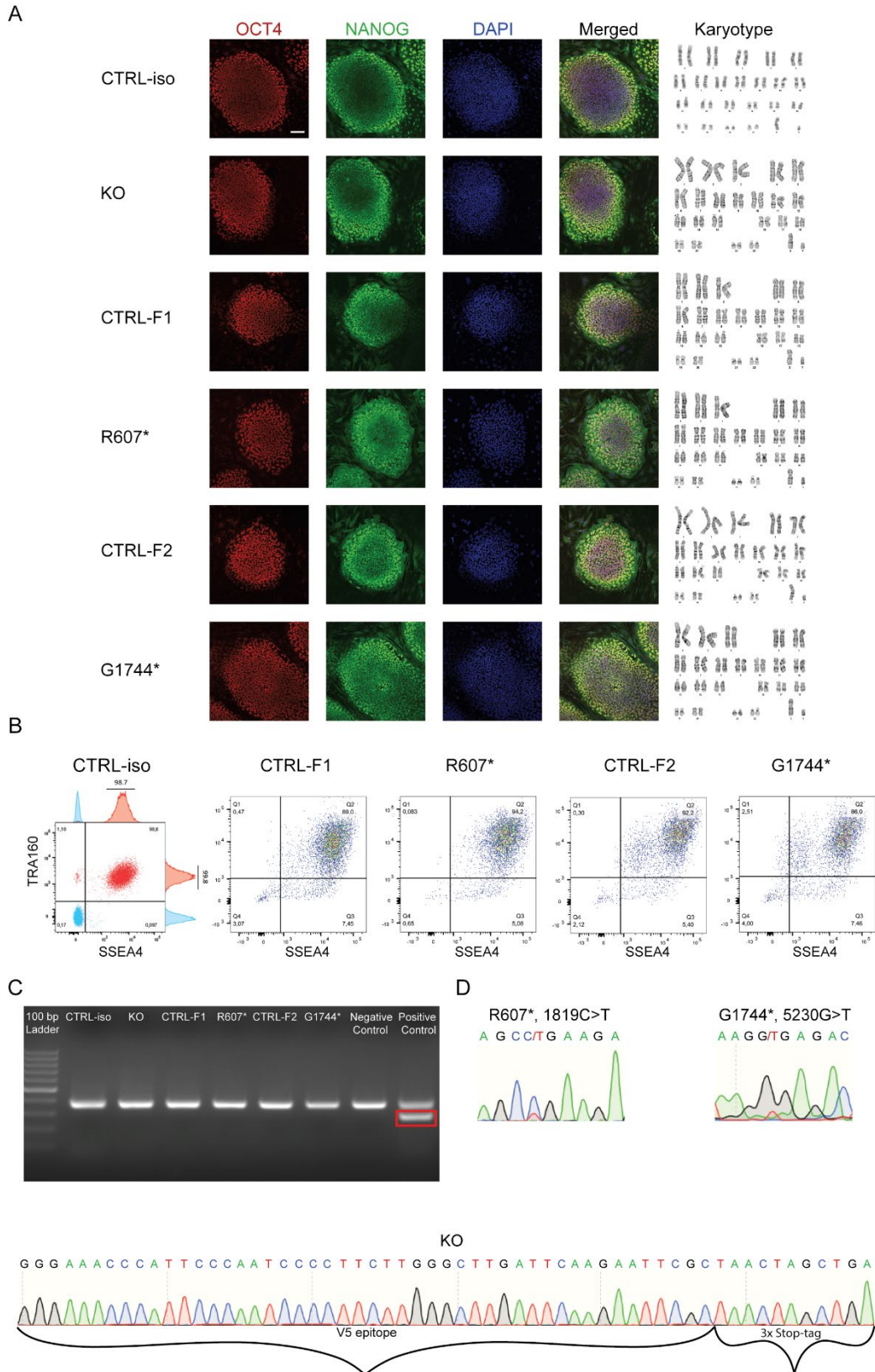
Figure S1. iPSC validation of *SCN2A* deficient genetic models.

A) Left: Representative immunocytochemistry of *SCN2A* iPSC lines for OCT4, NANOG and DAPI. Right: Chromosomal images from G-banding karyotyping. Scale bar, 100 μm.

B) Flow cytometry plots for pluripotency markers TRA160 and SSEA4.

C) Mycoplasma validation of *SCN2A* iPSC lines.

D) Sanger sequencing validation. Left: R607* variant validation. Right: G1744* variant validation. Bottom: isogenic KO V5 epitope and 3x StopTag insertion validation.
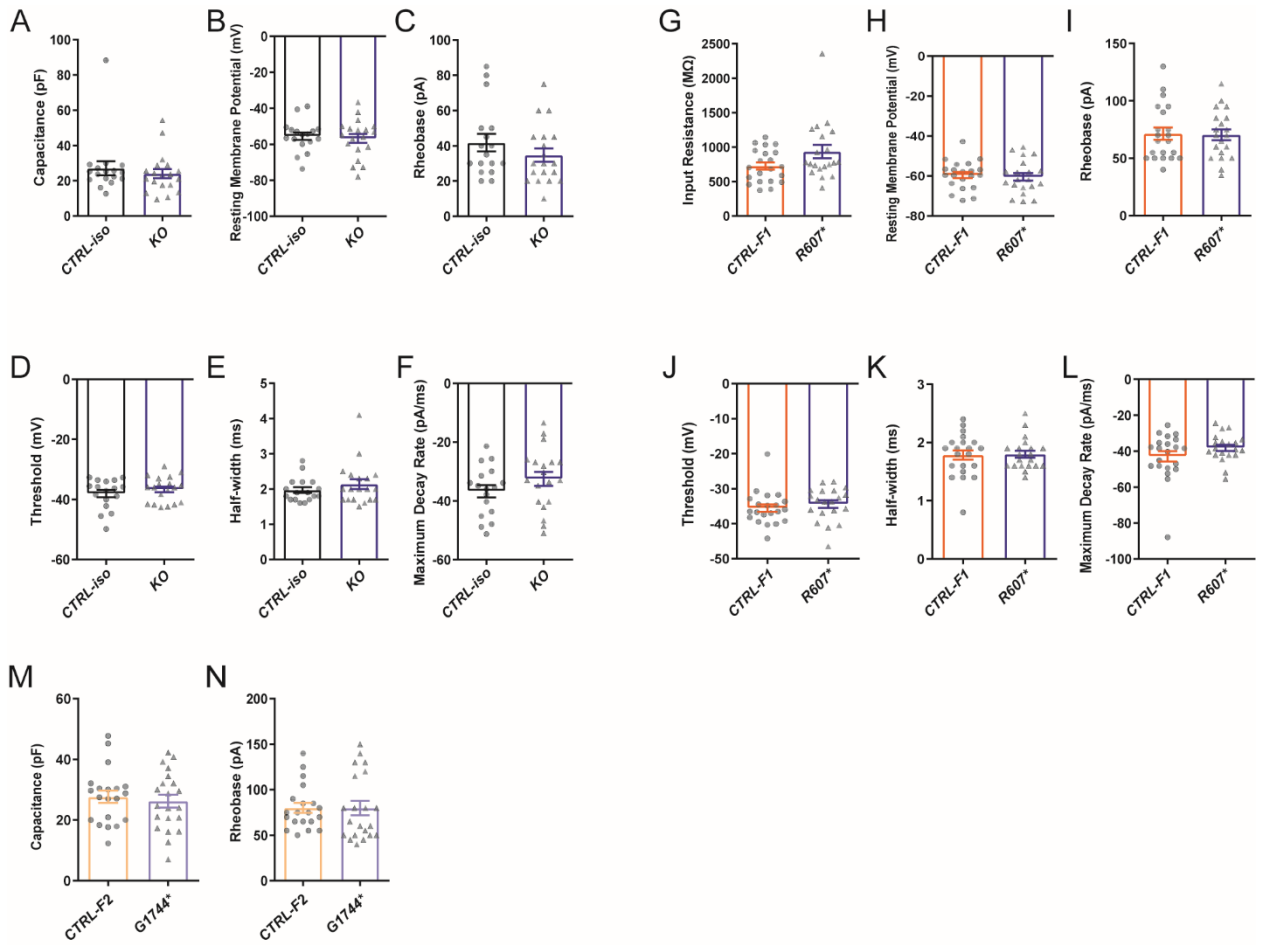
Figure S2. Intrinsic properties of *SCN2A* deficient iNeurons.

A-F) Patch-clamp electrophysiology of CTRL-iso and KO iNeurons (n=17 and 19, respectively), 3 viral transductions. (A) capacitance, (B) resting membrane potential, (C) rheobase, (D) threshold of action potential, (E) half-width of action potential, (F) maximum decay rate.

G-L) Patch-clamp electrophysiology of CTRL-F1 and R607* iNeurons (n=21 and n=20, respectively), 3 viral transductions. (G) input resistance, (H) resting membrane potential, (I) rheobase, (J) threshold of action potential, (K) half-width of action potential, (L) maximum decay rate.

M-N) Patch-clamp electrophysiology of CTRL-F2 and G1744* iNeurons (n=20 and n=21), 3 viral transductions. (A) capacitance, (B) rheobase. Data represent means ± SEM. *$p < 0.05$, Student's t-test.
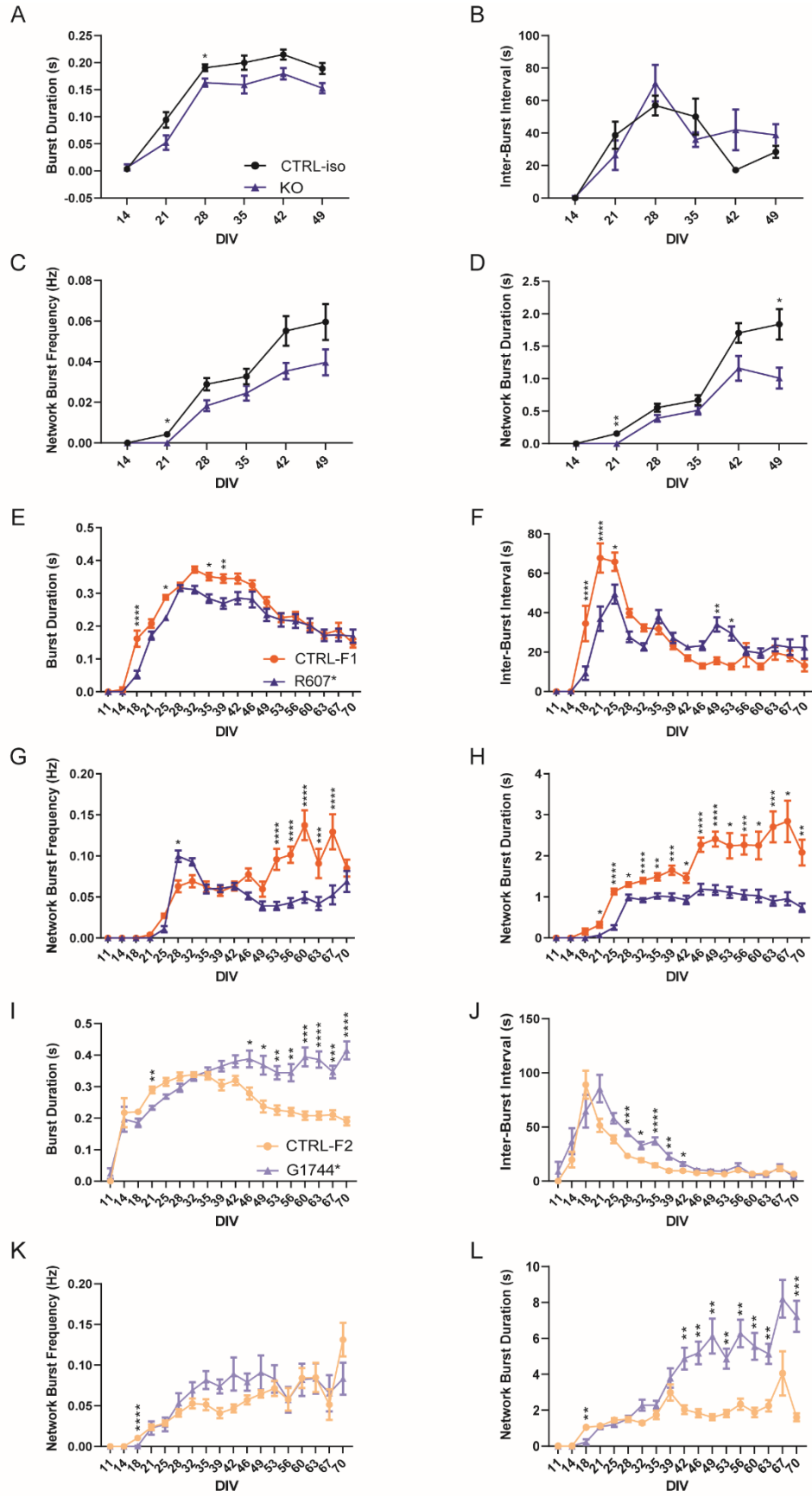
Figure S3. Spontaneous network activity of *SCN2A* deficiency via multi-electrode array.

A-D) Analysis of additional isogenic KO iNeuron spontaneous network parameters. CTRL-iso (n=47 wells) and KO (n=43 wells), 3 viral transductions. (A) burst duration, (B) inter-burst interval, (C) network burst frequency, (D) network burst duration.

E-H) Analysis of additional R607* iNeuron spontaneous network parameters. CTRL-F1 (n=48 wells) and R607* (n=46 wells), 3 viral transductions. (E) burst duration, (F) inter-burst interval, (G) network burst frequency, (H) network burst duration.

I-J) Analysis of additional G1744* iNeuron spontaneous network parameters. CTRL-F2 (n=20 wells) and G1744* (n=19 wells), 2 viral transductions. (I) burst duration, (J) inter-burst interval, (K) network burst frequency, (L) network burst duration. Data represent means ± SEM. *$p < 0.05$, **$p < 0.01$, ***$p < 0.001$, ****$p < 0.0001$, two-way ANOVA with post hoc Sidak correction.
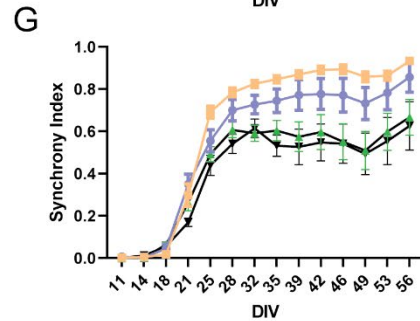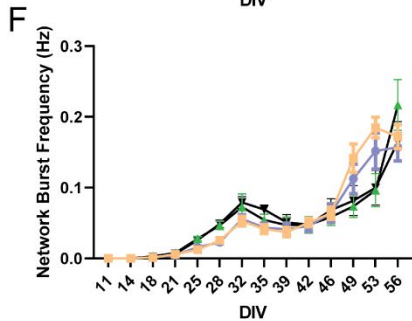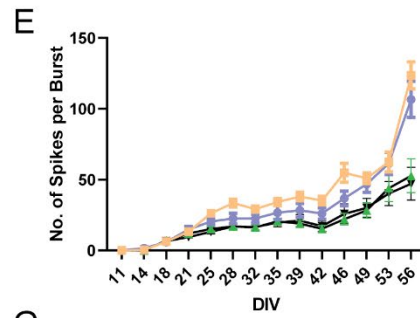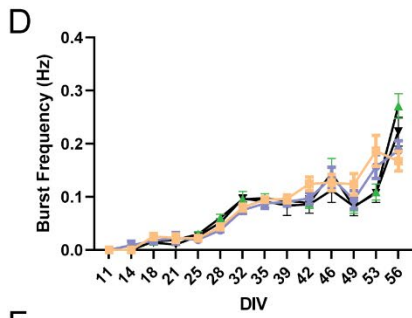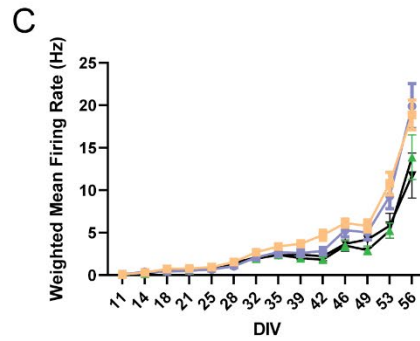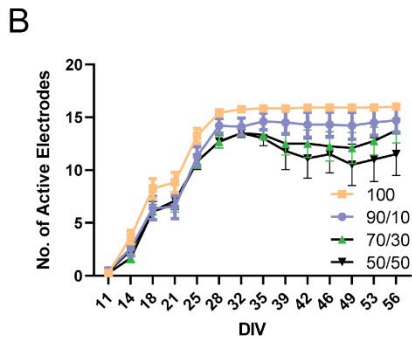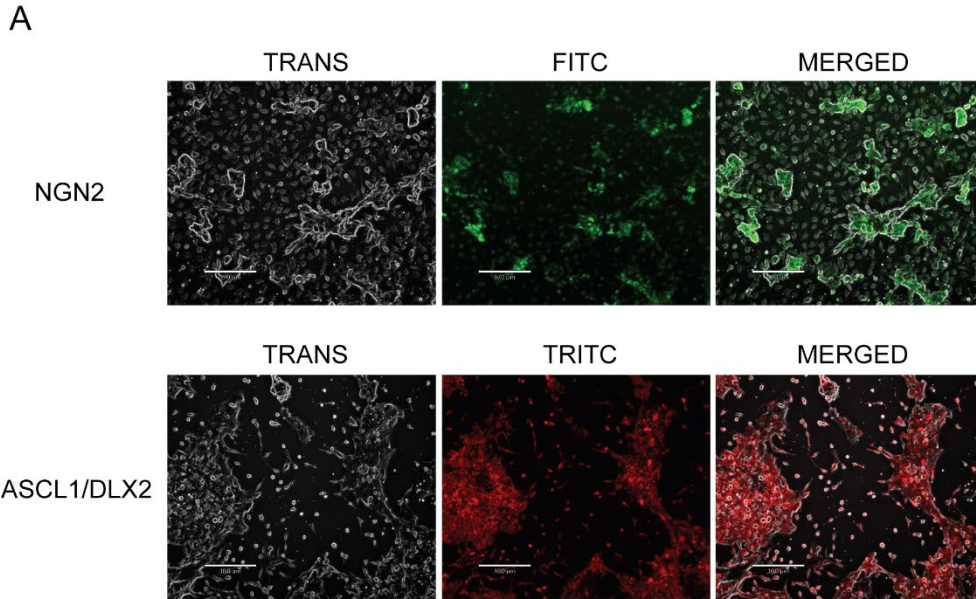
Figure S4. Validation of co-culture iNeurons and characterization of spontaneous network activity development.

A) Representative epifluorescence images of iPSC induction into neurons. Top: 3 days post doxycycline induction of iPSCs transduced with lentivirus vectors containing NGN2, Bottom: 3 days post doxycycline induction of iPSCs transduced with lentivirus vectors containing ASCL1/DLX2.

B-G) Quantification of MEA parameters at varying co-culture ratios for CTRL-F2 iNeurons. (B) number of active electrodes, (C) weighted mean firing rate, (D) burst frequency, (E) number of spikes per burst, (F) network burst frequency, (G) synchrony index. 100 (n=12 wells), 90/10 (n=10 wells), 70/30 (n=12 wells), 50/50 (n=10 wells) iNeurons, 1 viral transduction. Data represent means ± SEM. No analysis was performed.

2.8 References

Anastasiades, P.G., and Butt, S.J.B. (2012). A Role for Silent Synapses in the Development of the Pathway from Layer 2/3 to 5 Pyramidal Cells in the Neocortex. J. Neurosci. *32*, 13085–13099.

Bai, D., Yip, B.H.K., Windham, G.C., Sourander, A., Francis, R., Yoffe, R., Glasson, E., Mahjani, B., Suominen, A., Leonard, H., et al. (2019). Association of Genetic and Environmental Factors With Autism in a 5-Country Cohort. JAMA Psychiatry.

Barretto, N., Zhang, H., Powell, S.K., Fernando, M.B., Zhang, S., Flaherty, E.K., Ho, S.-M., Slesinger, P.A., Duan, J., and Brennand, K.J. (2020). ASCL1- and DLX2-induced GABAergic neurons from hiPSC-derived NPCs. J. Neurosci. Methods *334*, 108548.

Begemann, A., Acuña, M.A., Zweier, M., Vincent, M., Steindl, K., Bachmann-Gagescu, R., Hackenberg, A., Abela, L., Plecko, B., Kroell-Seger, J., et al. (2019). Further corroboration of distinct functional features in SCN2A variants causing intellectual disability or epileptic phenotypes. Mol. Med. *25*, 6.

Ben-Shalom, R., Keeshen, C.M., Berrios, K.N., An, J.Y., Sanders, S.J., and Bender, K.J. (2017). Opposing Effects on NaV1.2 Function Underlie Differences Between SCN2A Variants Observed in Individuals With Autism Spectrum Disorder or Infantile Seizures. Biol. Psychiatry *82*, 224–232.

Bender, K.J., and Trussell, L.O. (2012). The Physiology of the Axon Initial Segment. Annu. Rev. Neurosci. *35*, 249–265.

Crawford, K., Xian, J., Helbig, K.L., Galer, P.D., Parthasarathy, S., Lewis-Smith, D., Kaufman, M.C., Fitch, E., Ganesan, S., O'Brien, M., et al. (2021). Computational analysis of 10,860 phenotypic annotations in individuals with SCN2A-related disorders. Genet. Med. 2021 237 *23*, 1263–1272.

Deneault, E., White, S.H., Rodrigues, D.C., Ross, P.J., Faheem, M., Zaslavsky, K., Wang, Z., Alexandrova, R., Pellecchia, G., Wei, W., et al. (2018). Complete Disruption of Autism-Susceptibility Genes by Gene Editing Predominantly Reduces Functional Connectivity of Isogenic Human Neurons. Stem Cell Reports *11*, 1211–1225.

Deneault, E., Faheem, M., White, S.H., Rodrigues, D.C., Sun, S., Wei, W., Piekna, A., Thompson, T., Howe, J.L., Chalil, L., et al. (2019). CNTN5-/+or EHMT2-/+human iPSC-derived neurons from individuals with autism develop hyperactive neuronal networks. Elife *8*, 1–26.

Echevarria-Cooper, D.M., Hawkins, N.A., Misra, S.N., Huffman, A., Thaxton, T., Thompson, C.H., Ben-Shalom, R., Nelson, A.D., Lipkin, A.M., George, A.L., et al. (2021). Cellular and behavioral effects of altered NaV1.2 sodium channel ion permeability in Scn2aK1422E mice. BioRxiv 2021.07.19.452930.

Engle, S.J., Blaha, L., and Kleiman, R.J. (2018). Best Practices for Translational Disease Modeling Using Human iPSC-Derived Neurons. Neuron *100*, 783–797.

Gazina, E. V., Leaw, B.T.W., Richards, K.L., Wimmer, V.C., Kim, T.H., Aumann, T.D., Featherby, T.J., Churilov, L., Hammond, V.E., Reid, C.A., et al. (2015). 'Neonatal' Nav1.2 reduces neuronal excitability and affects seizure susceptibility and behaviour.

Hum. Mol. Genet. *24*, 1457–1468.

Grove, J., Ripke, S., Als, T.D., Mattheisen, M., Walters, R.K., Won, H., Pallesen, J., Agerbo, E., Andreassen, O.A., Anney, R., et al. (2019). Identification of common genetic risk variants for autism spectrum disorder. Nat. Genet. *51*, 431–444.

Hanse, E., Seth, H., and Riebe, I. (2013). AMPA-silent synapses in brain development and pathology. Nat. Rev. Neurosci. 2013 1412 *14*, 839–850.

Hu, W., and Bean, B.P. (2018). Differential Control of Axonal and Somatic Resting Potential by Voltage-Dependent Conductances in Cortical Layer 5 Pyramidal Neurons. Neuron *97*, 1315-1326.e3.

Hu, W., Tian, C., Li, T., Yang, M., Hou, H., and Shu, Y. (2009). Distinct contributions of Nav1.6 and Nav1.2 in action potential initiation and backpropagation. Nat. Neurosci. *12*, 996–1002.

Iossifov, I., O'Roak, B.J., Sanders, S.J., Ronemus, M., Krumm, N., Levy, D., Stessman, H.A., Witherspoon, K.T., Vives, L., Patterson, K.E., et al. (2014). The contribution of de novo coding mutations to autism spectrum disorder. Nature *515*, 216–221.

Ip, J.P.K., Nagakura, I., Petravicz, J., Li, K., Wiemer, E.A.C., and Sur, M. (2018). Major Vault Protein, a Candidate Gene in 16p11.2 Microdeletion Syndrome, Is Required for the Homeostatic Regulation of Visual Cortical Plasticity. J. Neurosci. *38*, 3890–3900.

Isaac, J.T.R. (2003). Postsynaptic silent synapses: evidence and mechanisms. Neuropharmacology *45*, 450–460.

Isaac, J.T.R., Nicoll, R.A., and Malenka, R.C. (1995). Evidence for silent synapses: Implications for the expression of LTP. Neuron *15*, 427–434.

Isaac, J.T.R., Crair, M.C., Nicoll, R.A., and Malenka, R.C. (1997). Silent Synapses during Development of Thalamocortical Inputs. Neuron *18*, 269–280.

Kang, P.W., Chakouri, N., Diaz, J., Tomaselli, G.F., Yue, D.T., and Ben-Johny, M. (2021). Elementary mechanisms of calmodulin regulation of NaV1.5 producing divergent arrhythmogenic phenotypes. Proc. Natl. Acad. Sci. U. S. A. *118*.

Kanold, P.O., Deng, R., and Meng, X. (2019). The integrative function of silent synapses on subplate neurons in cortical development and dysfunction. Front. Neuroanat. *13*, 41.

Kerchner, G.A., and Nicoll, R.A. (2008). Silent synapses and the emergence of a postsynaptic mechanism for LTP. Nat. Rev. Neurosci. 2008 911 *9*, 813–825.

Kim, H.J., and Magrané, J. (2011). Isolation and culture of neurons and astrocytes from the mouse brain cortex. Methods Mol. Biol. *793*, 63–75.

Kim, J.H., Lee, H.J., Choi, W., and Lee, K.J. (2019). Encoding information into autonomously bursting neural network with pairs of time-delayed pulses. Sci. Rep. *9*, 1–11.

Kirwan, P., Turner-Bridger, B., Peter, M., Momoh, A., Arambepola, D., Robinson, H.P.C., and Livesey, F.J. (2015). Development and function of human cerebral cortex neural networks from pluripotent stem cells in vitro. Dev. *142*, 3178–3187.

Kohlnhofer, B., Liu, Y., Woodruff, G., Lovenberg, T., Bonaventure, P., and Harrington,

A.. (2021). The Schizophrenia Variant V1282F in SCN2A Causes Functional Impairment of NaV1.2. J. Schizophr. Res.

Kole, M.H.P., and Stuart, G.J. (2012). Signal Processing in the Axon Initial Segment. Neuron *73*, 235–247.

Lamprecht, R. (2021). Actin Cytoskeleton Role in the Maintenance of Neuronal Morphology and Long-Term Memory. Cells *10*.

Liao, Y., Anttonen, A.K., Liukkonen, E., Gaily, E., Maljevic, S., Schubert, S., Bellan-Koch, A., Petrou, S., Ahonen, V.E., Lerche, H., et al. (2010). SCN2A mutation associated with neonatal epilepsy, late-onset episodic ataxia, myoclonus, and pain. Neurology *75*, 1454–1458.

Lopez-Santiago, L.F., Yuan, Y., Wagnon, J.L., Hull, J.M., Frasier, C.R., O'Malley, H.A., Meisler, M.H., and Isom, L.L. (2017). Neuronal hyperexcitability in a mouse model of SCN8A epileptic encephalopathy. Proc. Natl. Acad. Sci. *114*, 2383–2388.

Lu, C., Shi, X., Allen, A., Baez-Nieto, D., Nikish, A., Sanjana, N.E., and Pan, J.Q. (2019). Overexpression of NEUROG2 and NEUROG1 in human embryonic stem cells produces a network of excitatory and inhibitory neurons. FASEB J. *33*, 5287–5299.

Madabhushi, R., and Kim, T.-K. (2018). Emerging themes in neuronal activity-dependent gene expression. Mol. Cell. Neurosci. *87*, 27–34.

Masquelier, T., and Deco, G. (2013). Correction: Network Bursting Dynamics in Excitatory Cortical Neuron Cultures Results from the Combination of Different Adaptive

Mechanism. PLoS One *8*, e75824.

Massobrio, P., Tessadori, J., Chiappalone, M., and Ghirardi, M. (2015). In Vitro Studies of Neuronal Networks and Synaptic Plasticity in Invertebrates and in Mammals Using Multielectrode Arrays. Neural Plast. *2015*.

Matsuzaki, M., Ellis-Davies, G.C.R., Nemoto, T., Miyashita, Y., Iino, M., and Kasai, H. (2001). Dendritic spine geometry is critical for AMPA receptor expression in hippocampal CA1 pyramidal neurons. Nat. Neurosci. *4*, 1086.

Mccready, F.P.;, Gordillo-Sampedro, S.;, Pradeepan, K.;, Martinez-Trujillo, J.;, Ellis, J., Kim, J., Kim, D.-S., Mccready, F.P., Gordillo-Sampedro, S., Pradeepan, K., et al. (2022). Multielectrode Arrays for Functional Phenotyping of Neurons from Induced Pluripotent Stem Cell Models of Neurodevelopmental Disorders. Biol. 2022, Vol. 11, Page 316 *11*, 316.

Mis, M.A., Yang, Y., Tanaka, B.S., Gomis-Perez, C., Liu, S., Dib-Hajj, F., Adi, T., Garcia-Milian, R., Schulman, B.R., Dib-Hajj, S.D., et al. (2019). Resilience to pain: A peripheral component identified using induced pluripotent stem cells and dynamic clamp. J. Neurosci. *39*, 382–392.

Miyaoka, Y., Chan, A.H., Judge, L.M., Yoo, J., Huang, M., Nguyen, T.D., Lizarraga, P.P., So, P.-L., and Conklin, B.R. (2014). Isolation of single-base genome-edited human iPS cells without antibiotic selection. Nat. Methods 2014 113 *11*, 291–293.

Nagy, E., and Maquat, L.E. (1998). A rule for termination-codon position within intron-

containing genes: When nonsense affects RNA abundance. Trends Biochem. Sci. *23*, 198–199.

Nelson, S.B., and Valakh, V. (2015). Excitatory/Inhibitory Balance and Circuit Homeostasis in Autism Spectrum Disorders. Neuron *87*, 684–698.

Neu-Yilik, G., Amthor, B., Gehring, N.H., Bahri, S., Paidassi, H., Hentze, M.W., and Kulozik, A.E. (2011). Mechanism of escape from nonsense-mediated mRNA decay of human β-globin transcripts with nonsense mutations in the first exon. RNA *17*, 843–854.

Ofner, Marianna, Coles, Anthony, Decou, Mary Lou, Do, Minh T, Bienek, Asako, Snider, Judy and Ugnat, A.-M. (2018). Autism Spectrum Disorder among Children and Youth in Canada 2018 - Canada.ca.

Ogiwara, I., Miyamoto, H., Tatsukawa, T., Yamagata, T., Nakayama, T., Atapour, N., Miura, E., Mazaki, E., Ernst, S.J., Cao, D., et al. (2018). Nav1.2 haplodeficiency in excitatory neurons causes absence-like seizures in mice. Commun. Biol. *1*, 96.

Que, Z., Olivero-Acosta, M.I., Zhang, J., Eaton, M., Skarnes, W.C., and Yang, Y. (2021). Sodium channel Nav1.2-L1342P variant displaying complex biophysical properties renders hyperexcitability of cortical neurons derived from human iPSCs. BioRxiv 2021.01.18.427192.

Rumpel, S., Hatt, H., and Gottmann, K. (1998). Silent Synapses in the Developing Rat Visual Cortex: Evidence for Postsynaptic Expression of Synaptic Plasticity. J. Neurosci. *18*, 8863–8874.

Rumpel, S., Kattenstroth, G., and Gottmann, K. (2004). Silent Synapses in the Immature Visual Cortex: Layer-Specific Development Regulation. J. Neurophysiol. *91*, 1097–1101.

Ruzzo, E.K., Pérez-Cano, L., Jung, J.Y., Wang, L. kai, Kashef-Haghighi, D., Hartl, C., Singh, C., Xu, J., Hoekstra, J.N., Leventhal, O., et al. (2019). Inherited and De Novo Genetic Risk for Autism Impacts Shared Networks. Cell *178*, 850-866.e26.

Sanders, S.J., Murtha, M.T., Gupta, A.R., Murdoch, J.D., Raubeson, M.J., Willsey, A.J., Ercan-Sencicek, A.G., DiLullo, N.M., Parikshak, N.N., Stein, J.L., et al. (2012). De novo mutations revealed by whole-exome sequencing are strongly associated with autism. Nature *485*, 237–241.

Sanders, S.J., He, X., Willsey, A.J., Ercan-Sencicek, A.G., Samocha, K.E., Cicek, A.E., Murtha, M.T., Bal, V.H., Bishop, S.L., Dong, S., et al. (2015). Insights into Autism Spectrum Disorder Genomic Architecture and Biology from 71 Risk Loci. Neuron *87*, 1215–1233.

Sanders, S.J., Campbell, A.J., Cottrell, J.R., Moller, R.S., Wagner, F.F., Auldridge, A.L., Bernier, R.A., Catterall, W.A., Chung, W.K., Empfield, J.R., et al. (2018). Progress in Understanding and Treating SCN2A-Mediated Disorders. Trends Neurosci. *41*, 442–456.

Satterstrom, F.K., Walters, R.K., Singh, T., Wigdor, E.M., Lescai, F., Demontis, D., Kosmicki, J.A., Grove, J., Stevens, C., Bybjerg-Grauholm, J., et al. (2019). Autism spectrum disorder and attention deficit hyperactivity disorder have a similar burden of rare protein-truncating variants. Nat. Neurosci. *22*, 1961–1965.

Satterstrom, F.K., Kosmicki, J.A., Wang, J., Breen, M.S., De Rubeis, S., An, J.-Y., Peng, M., Collins, R., Grove, J., Klei, L., et al. (2020). Large-Scale Exome Sequencing Study Implicates Both Developmental and Functional Changes in the Neurobiology of Autism. Cell.

Shin, W., Kweon, H., Kang, R., Kim, D., Kim, K., Kang, M., Kim, S.Y., Hwang, S.N., Kim, J.Y., Yang, E., et al. (2019). Scn2a haploinsufficiency in mice suppresses hippocampal neuronal excitability, excitatory synaptic drive, and long-term potentiation, and spatial learning and memory. Front. Mol. Neurosci. *12*, 145.

Spratt, P.A.W., Alexander, R.P., Ben-Shalom, R., Keeshen, C.M., Sanders, S.J., Bender Correspondence, K.J., Spratt, P.W., Sahagun, A., Kyoung, H., and Bender, K.J. (2021). Paradoxical hyperexcitability from NaV1.2 sodium channel loss in neocortical pyramidal cells. Cell Rep. *36*, 109483.

Spratt, P.W.E., Ben-Shalom, R., Keeshen, C.M., Burke, K.J., Clarkson, R.L., Sanders, S.J., and Bender, K.J. (2019). The Autism-Associated Gene Scn2a Contributes to Dendritic Excitability and Synaptic Function in the Prefrontal Cortex. Neuron *103*, 673-685.e5.

Stafstrom, C.E. (2007). Persistent Sodium Current and Its Role in Epilepsy. Epilepsy Curr. *7*, 15.

Stegenga, J., Le Feber, J., Marani, E., and Rutten, W.L.C. (2008). Analysis of cultured neuronal networks using intraburst firing characteristics. IEEE Trans. Biomed. Eng. *55*, 1382–1390.

Tatsukawa, T., Raveau, M., Ogiwara, I., Hattori, S., Miyamoto, H., Mazaki, E., Itohara, S., Miyakawa, T., Montal, M., and Yamakawa, K. (2019). Scn2a haploinsufficient mice display a spectrum of phenotypes affecting anxiety, sociability, memory flexibility and ampakine CX516 rescues their hyperactivity. Mol. Autism *10*, 15.

Tidball, A.M., Lopez-Santiago, L.F., Yuan, Y., Glenn, T.W., Margolis, J.L., Clayton Walker, J., Kilbane, E.G., Miller, C.A., Martina Bebin, E., Scott Perry, M., et al. (2020). Variant-specific changes in persistent or resurgent sodium current in SCN8A-related epilepsy patient-derived neurons. Brain *143*, 3025–3040.

Wang, H.-G., Bavley, C.C., Li, A., Jones, R.M., Hackett, J.E., Bayleyen, Y., Lee, F.S., Rajadhyaksha, A.M., and Pitt, G.S. (2021). Scn2a severe hypomorphic mutation decreases excitatory synaptic input and causes autism-associated behaviors. JCI Insight.

Wang, T., Guo, H., Xiong, B., Stessman, H.A.F., Wu, H., Coe, B.P., Turner, T.N., Liu, Y., Zhao, W., Hoekzema, K., et al. (2016). De novo genic mutations among a Chinese autism spectrum disorder cohort. Nat. Commun. *7*, 1–10.

Wengert, E.R., and Patel, M.K. (2020). The Role of the Persistent Sodium Current in Epilepsy: Https://Doi.Org/10.1177/1535759720973978 *21*, 40–47.

Wolff, M., Johannesen, K.M., Hedrich, U.B.S., Masnada, S., Rubboli, G., Gardella, E., Lesca, G., Ville, D., Milh, M., Villard, L., et al. (2017). Genetic and phenotypic heterogeneity suggest therapeutic implications in SCN2A-related disorders. Brain *140*, 1316–1336.

Yang, N., Chanda, S., Marro, S., Ng, Y.-H., Janas, J.A., Haag, D., Ang, C.E., Tang, Y., Flores, Q., Mall, M., et al. (2017). Generation of pure GABAergic neurons by transcription factor programming. Nat. Methods *14*, 621–628.

Yi, F., Danko, T., Botelho, S.C., Patzke, C., Pak, C., Wernig, M., and Südhof, T.C. (2016). Autism-associated SHANK3 haploinsufficiency causes Ih channelopathy in human neurons. Science (80-.). *352*, aaf2669.

Yuen, R.K.C., Merico, D., Bookman, M., Howe, J.L., Thiruvahindrapuram, B., Patel, R. V., Whitney, J., Deflaux, N., Bingham, J., Wang, Z., et al. (2017). Whole genome sequencing resource identifies 18 new candidate genes for autism spectrum disorder. Nat. Neurosci. *20*, 602–611.

Zhang, J., Chen, X., Lanman, N.A., Skarnes, W.C., Correspondence, Y.Y., Eaton, M., Wu, J., Ma, Z., Lai, S., Park, A., et al. (2021). Severe deficiency of the voltage-gated sodium channel Na V 1.2 elevates neuronal excitability in adult mice ll Severe deficiency of the voltage-gated sodium channel Na V 1.2 elevates neuronal excitability in adult mice. Cell Rep. *36*, 109495.

Zhang, Y., Pak, C., Han, Y., Ahlenius, H., Zhang, Z., Chanda, S., Marro, S., Patzke, C., Acuna, C., Covy, J., et al. (2013). Rapid Single-Step Induction of Functional Neurons from Human Pluripotent Stem Cells. Neuron *78*, 785–798.

Zhang, Z., Marro, S.G., Zhang, Y., Arendt, K.L., Patzke, C., Zhou, B., Fair, T., Yang, N., Südhof, T.C., Wernig, M., et al. (2018). The fragile X mutation impairs homeostatic plasticity in human neurons by blocking synaptic retinoic acid signaling. *4338*, 1–16.

CHAPTER 3: PROTEOMIC ANALYSIS OF REDUCED SCN2A EXPRESSION IN A HUMAN NEURON MODEL REVEALS NOVEL ALTERED SIGNALLING PATHWAYS

3.1 Preface

This chapter was designed by Chad Brown, Jarryll Uy, and Dr. Karun Singh. The proteomics experiments were performed by Dr. Yu Lu, with assistance from Chad Brown, Jarryll Uy, and Dr. Sansi Xing. Analysis of proteomics data was done in major part by Jarryll Uy, and Chad Brown assisted throughout. Metabolism experiments were performed by Chad Brown. Data were analyzed and figures were prepared by Chad Brown. This section is included in the manuscript published as a preprint on BioRxiv. This work was supported by Grants from the Canadian Institutes of Health Research (CIHR), Ontario Brain Institute-POND study, and the Natural Sciences and Engineering Research Council (NSERC) to K.K.S. Y.L received funding from NSERC and ERA-NET NEURON, and S.W.S received funding from OBI-POND, Autism Speaks and CIHR. J.U was awarded a fellowship from CIHR (CGS-M) and the University of Toronto Vision Science Research Program, and C.O.B was awarded a fellowship from the McMaster University Michael G. DeGroote Institute for Pain Research and Care. We also acknowledge the resources of MSSNG (www.mss.ng), Autism Speaks and The Centre for Applied Genomics at The Hospital for Sick Children, Toronto, Canada. We also thank the participating families for their time and contributions to this database.

3.2 Introduction

Mass spectrometry (MS) proteomics has become an ever more useful tool when investigating the end cellular messaging products in NDDs. Initially, mass spectrometry was used to generate high-resolution protein abundance and post-translational modifications, more recently, analysis of protein interactions has been obtainable. We pursued a quantitative proteomics approach that would allow for label-based identification. This would provide us with a bottom-up approach used to generate enhanced precision of quantification and identification through mass spectrometry. This bottom-up approach digests proteins into peptides with the identification of multiple peptides determining the protein call. Additionally, samples are labelled using isobaric tags known as tandem mass tags (TMT) (Dayon et al., 2008). TMT-labeling the samples decreases the variability in an experiment since biological replicates and conditions are mixed into a single sample. Thus, the TMT-labelling approach makes multiplexing of samples obtainable, unlike other label-free systems.

We used proteomics to investigate previously unknown signalling pathways in our SCN2A cellular models. In essence, this was done to capture the complete proteomic profile of our cellular models of SCN2A. The central dogma of genetics, specifically, the interplay between DNA, RNA and protein is not a 1:1:1 ratio (Liu et al., 2016). Further, the relationship between RNA and proteins is not simply based on the abundance or concentration of one another. Expression levels of proteins are regulated beyond the transcript by upstream open reading frames, binding of non-coding RNAs, ubiquitin-proteasome pathways, protein translation delay via ribosomes and protein localization; as

these can contribute to altered protein concentration and abundance, we are aware that steady-state translation and post-translational modifications are additional variables, suggesting, sole RNA-seq may not fully capture the end molecular signalling pathways that are at play.

Previous reports of SCN2A's role in NDDs, in particular, ASD, have focused solely on the primary effects of the ion channel on neuron function (Begemann et al., 2019; Ben-Shalom et al., 2017; Echevarria-Cooper et al., 2021; Que et al., 2021b; Spratt et al., 2019; Zhang et al., 2021b). These studies indicated that *SCN2A* GoF variants are likely associated with an enhancement of channel function and EE; while LoF variants in *SCN2A* including those that result in protein truncations are associated with reduced channel function, leading to ASD and intellectual disability. However, current studies have not progressed past the immediate pathophysiology of the ion channel. To better understand the molecular impact of *SCN2A* variants in iNeurons, we performed quantitative TMT-tagged shotgun proteomics on DIV 14 iNeurons. We focused on the R607* variant since it had the more severe electrophysiological phenotypes. Proteomic analysis identified 17 enriched clusters that contained significant differentially expressed proteins. Since synaptic plasticity, translation and mitochondrial function are tightly correlated and contribute to typical neuron function we decided to investigate two of the most physiologically relevant clusters, these were mitochondrial function and neuron projection development.

Mitochondria are central in the process of providing and sustaining the energetic needs of neurons and neural circuits (Bélanger et al., 2011; Magistretti and Allaman, 2015). The ATP provided by mitochondria is necessary for the maintenance of neurites and

synaptic transmission (Cioni et al., 2019; Rangaraju et al., 2019; Spillane et al., 2013) as these are areas of high ATP demand. Mitochondrial localized to a particular synaptic site, for example, provide ATP necessary for local translation during synaptic plasticity events. When these mitochondrial compartments are depleted, plasticity-induced synaptic translation is reduced (Rangaraju et al., 2019). Additionally, transporting mitochondria to these sites is mediated by the mitochondrial fission/fusion proteins, which when disrupted lead to significant alterations in mitochondrial distribution in the neuron (Fukumitsu et al., 2016; Misko et al., 2010). The motility of mitochondria in dendritic protrusions is critical to developing spines, as their density at these loci affects the structural plasticity of spines and synapses (Li et al., 2004). Mitochondria also perform other functions that are critical to neuronal development and synaptic function such as fission and fusion (Divakaruni et al., 2018; Rangaraju et al., 2019), compartmental trafficking (Lewis et al., 2018), and quality control mechanisms such as mitophagy (Ebrahimi-Fakhari et al., 2016; Franco-Iborra et al., 2018). When these functions go awry, several neuronal deficits may be produced, that can culminate in NDDs such as ASD. In 1985, the first report of mitochondrial dysfunction in ASD showed elevated lactate levels in the plasma of autistic children (Coleman and Blass, 1985). Since then there have been numerous reports (Haas, 2010; Palmieri and Persico, 2010; Rossignol and Frye, 2012) suggesting metabolic dysfunction may occur in ASD.

In this chapter, we attempted to uncover downstream signalling networks that were dysregulated by activity-dependent mechanisms using proteomics on the more severe SCN2A truncating patient mutation (p.R607*). From this, we performed initial functional

validations on the enriched mitochondrial function pathway cluster that were able to confirm our proteomic findings. This reiterated how powerful proteomics is when identifying unknown protein signalling networks that are altered due to impaired neuron function.

3.3 Materials and Methods

3.3.1 Human samples

All pluripotent stem cell work was approved by the Canadian Institutes of Health Research Stem Cell Oversight Committee. Blood was taken from individuals with the approval from SickKids Research Ethics Board, after informed consent was obtained, REB approval file 1000050639. This study was also approved by the Hamilton Integrated Research Ethics Board, REB approval file #2707. To rapidly upscale experiments, we used the previously published constitutive expression protocol of NGN2 to generate homogeneous populations of glutamatergic neurons. (Zhang et al., 2013). These iNeurons displayed stable membrane, firing and synaptic properties when co-cultured with mouse glial cells by DIV 21 (Zhang et al., 2013, 2018). Importantly as we previously described, this protocol provided consistent differentiation levels between cell lines derived from different participants (Deneault et al., 2018, 2019). We modified this protocol by inducing NGN2 for 3 days starting at DIV 1 and puromycin selecting for 2 days starting at DIV 2 and adding mouse glial cells at DIV 5. Half-iNeuron media (iNI) (Neurobasal media, 1x SM1, 1x GlutaMAX 1x pen/strep, 1µg/mL laminin, 10 ng/uL BDNF and 10 ng/uL GDNF) changes were performed every other day. These neurons were then enzymatically lifted

with Accutase (STEMCELL Technologies) for 6 mins and subsequently centrifugated and pelleted for lysis.

3.3.2 Proteomic profiling by Tandem-Mass-Tag-based Mass Spectrometry

Approximately 150 μg of total protein was extracted from 3 independent NGN2 transductions at DIV14 for the patient-derived CTRL-F1 and R607* iNeurons (total of 6 samples per patient family) using 8 M urea and 100 mM ammonium bicarbonate. These protein samples were reduced with 10 mM tris(2-carboxyethyl)phosphine for 45 min at 37 °C, alkylated with 20 mM iodoacetamide for 45 min at room temperature, and digested by trypsin (Promega) (1:50 (w/w) enzyme-to- protein ratio) overnight at 37 °C. The resulting peptides were desalted with the 10 mg SOLA C18 Plates (ThermoFisher), dried, and labelled with 16-plex tandem mass tag reagents (ThermoFisher) in 100 mM triethylammonium bicarbonate, and quenched with 5% hydroxylamine before being pooled together. 40 μg of the pooled sample was separated into 36 fractions by high-pH reverse-phase liquid chromatography (RPLC) using a homemade C18 column (200 μm × 30 cm bed volume, Waters BEH 130 5 μm resin) running a 70 min gradient from 11 to 32% acetonitrile− 20 mM ammonium formate (pH 10) at a flow rate of 5 μL/min. Each fraction was then loaded onto a homemade trap column (200 μm × 5 cm bed volume) packed with POROS 10R2 10 μm resin (Applied Biosystems), followed by a homemade analytical column (50 μm × 50 cm bed volume) packed with Reprosil-Pur 120 C18-AQ 5 μm particles (Dr. Maisch) with an integrated Picofrit nanospray emitter (New Objective). LC-MS experiments were performed on a Thermo Fisher Ultimate 3000 RSLCNano UPLC system that ran a 3 hr gradient (11− 38% acetonitrile−0.1% formic acid) at 70 nL/min coupled to

a Thermo QExactive HF quadrupole-Orbitrap mass spectrometer. A parent ion scan was performed using a resolving power of 120 000; then, up to 30 of the most intense peaks were selected for MS/MS (minimum ion counts of 1000 for activation) using higher energy collision-induced dissociation (HCD) fragmentation. Dynamic exclusion was activated such that MS/MS of the same m/z (within a range of 10 ppm; exclusion list size = 500) detected twice within 5 s was excluded from the analysis for 30 s.

3.3.3 Proteomic data and pathway enrichment analysis

LC-MS data were searched against a UniProt human protein database (ver 2017-06, 25020 entries) for protein identification and quantification by Protein Discover software (ThermoFisher). Only proteins with 2 or more unique peptides were used for downstream analysis. Protein abundance quantification was normalized by taking the sum of each TMT channel and normalizing it to a control sample. Protein quantities were log2 transformed to calculate fold changes and p-values were calculated using Student's t-test. Post UniProt accessions were converted to official Gene Symbols using UniProt's Retrieve/ID mapping tool. The resulting data were subjected to the Benjamini-Hochberg procedure for correcting multiple hypothesis testing. We selected arbitrary cutoffs of adjusted $P < 0.05$ and a log2FC ± 20% for "differentially expressed proteins". The differentially expressed protein dataset was used for principal component analysis and pathway enrichment analysis.

To gain further insight into the molecular perturbations, we used g:Profiler for over-representation analysis using the default parameters except for excluding electronic GO annotations with our differentially expressed proteins dataset (Reimand et al., 2016, 2019). We used GO terms from Biological Process categories with FDR < 0.05 in this analysis.

The following data tables containing enriched GO terms were used to generate an enrichment map using the Cytoscape plugin Enrichment Map with an FDR cutoff of 0.05 (Merico et al., 2010; Shannon et al., 2003). The resulting network was first automatically annotated using the AutoAnnotate plugin to aid in the discovery of biological themes of interest (Kucera et al., 2016). The labels for closely clustered GO terms were edited for readability and comprehension using Adobe Illustrator. Clusters of interest were further examined by selecting GO terms belonging to the respective cluster and plotting the most differentially expressed proteins.

3.3.4 Mitochondrial respiration analysis

iNeurons were replated on DIV 4 onto polyornithine/laminin-coated in the Seahorse XF96 Cell Culture Microplate (Agilent Technologies) at a density of 50 000/well, with the four corner wells left empty for the Seahorse XFe96 analyzer calibration. On DIV 5, primary mouse astrocytes were added at a density of 25 000/well to support iNeurons' viability and maturation. Half media changes were performed every other day and wells were maintained until DIV 14 for recordings. At DIV 9, iNI was supplemented with 2.5% FBS which was adapted from (Zhang et al., 2013). On DIV 13, the XF extracellular flux sensory cartridge was hydrated with Ultrapure water and incubated overnight at 37°C in a CO_2 free incubator. On DIV 14, mitochondrial stress test media was made (XF base media, 0.5 mM sodium pyruvate, 1.35 mM GlutaMAX, and 8.75mM filtered glucose) and warmed to 37°C. iNeurons were then washed twice with 200 μL of the MST media, after the second wash 180 μL of the MST media was added to the wells and left to incubate at 37°C for 1 hr in a CO_2 free incubator. The XF extracellular flux sensory cartridge was removed and

the MST assay compounds were added to final concentrations of (3 μM Oligomycin, 1 μM FCCP, and 1 μM Rotenone/Antimycin A). The XF extracellular flux sensory cartridge was then put into the Seahorse XFe96 analyzer to calibrate compounds and sensors. After, the XF96 Cell Culture Microplate was then inserted into the XF extracellular flux sensory cartridge and both plates were taken up into the Seahorse XFe96 analyzer. Measurements for each respiration phase were taken over 21-minute windows with measurements every 7 minutes, drugs were injected one after another with rotenone and antimycin A injected together. A CyQUANT cell proliferation assay was performed after recordings to normalize the oxygen consumption rate. Analysis was performed in the Wave software (Agilent Technologies).

3.3.5 CyQUANT cell proliferation assay

Immediately after 96-well plates containing iNeurons were done in the XF96 analyzer, media in the 96-well plates was removed and the iNeuron plate was frozen at -80°C and stored. Once the data obtained from the XF96 analyzer, 96-well plates were thawed at room temperature. Once thawed wells containing iNeurons were resuspended with 1x cell lysis buffer supplemented with (180 mM NaCl, 1 mM $CaCl_2$, and 1 mM $MgCl_2$). iNeurons were then left to incubate at room temperature for 1 hr. After the hour, an equal volume of 2x CyQUANT GR dye was added that was diluted in cell lysis buffer. The 96-well plate was then transferred to a spectrophotometer to determine the relative intensity. This intensity reading was then used to normalize the oxygen consumption rate per well.

3.4 Results

3.4.1 Altered biological processes in p.R607 iNeurons*

We used DIV 14 CTRL-F1 and R607* iNeurons that were cultured without mouse glia to eliminate the cross-species peptide identification. From the raw data, a principal component analysis was done to examine the variance in our data set. We found that each transduction of CTRL-F1 iNeurons clustered closely, where R607* iNeurons had a larger spread (Figure 1A). Genotypes clustered separately, more than intragroup variance, suggesting that there were more differences between genotypes than within genotypes. To depict the 2337 significantly differentially expressed proteins (p-adjusted < 0.05, FC > 1.2 or FC < 0.8) a volcano plot was generated (Figure 1B). We used g:Profiler for functional enrichment analysis (Figure 5C) using both increased and decreased differentially expressed proteins (Reimand et al., 2016, 2019). Among the enrichment clusters were Mitochondrial Function, Neuron Projection Development, Translation, and Cytoskeletal Organization (Figure 2A and S1). Further examination of the enriched clusters for the GO:Biological process terms revealed changes in Mitochondrial function: organization and translation, and Neuron projection development: neuron development and differentiation (Figure 2B). The differentially expressed proteins, both upregulated and downregulated belonging to each of the 2 clusters of interest are shown (Figure 2C). Of note, we found a reduction in expression of key mitochondrial proteins such as TOMM20 (p-adj = 0.00489, Log2FC = -1.05) and the mitochondrial fusion regulators Mitofusin 1 (MFN1) (p-adj = 0.002, Log2FC = -0.34) and Mitofusin 2 (MFN2) (p-adj = 0.004, Log2FC = -0.487). These

data suggest R607* iNeurons may have altered mitochondrial function (Chen et al., 2003; Filadi et al., 2015, 2018; Pecorelli et al., 2020).

3.4.2 Mitochondrial function is impaired in p.R607 iNeurons*

To functionally validate the findings from the proteomic profiling, we used a live-cell metabolic assay to investigate R607* iNeuron defects. We used the Seahorse assay that reported real-time metabolic rates. This was useful since iNeurons were temperature and oxygen-controlled aiding in the detection sensitivity for metabolic changes. Our analysis of mitochondrial respiration from iNeurons was supportive of the proteomic findings. First, R607* iNeurons consumed less oxygen throughout the experiment relative to CTRL-F1 iNeurons (Figure 3A). This suggests that R607* iNeurons may have a disrupted equilibrium between oxidative phosphorylation and glycolysis. Further, when we analyzed the major components of mitochondrial respiration, we noticed significant decreases in basal respiration, ATP production, and proton leak (Figure 3C-E). This indicates that mitochondria of R607* iNeurons could not generate enough energy or maintain an appropriate separation of protons to support the ETC. Additionally, maximal respiration, non-mitochondrial respiration and spare respiratory capacity were all decreased, hinting that mitochondria could not meet maximal bioenergetic demands compared to CTRL-F1 (Figure 3F-H).

To supplement the R607* iNeuron findings, we performed the same live-cell assay on the iNeurons harbouring the less severe p.G1744* variant. Our results indicate that the oxygen consumption rate was unchanged across CTRL-F2 and G1744* iNeurons (Figure 3B). A deeper analysis of the raw data indicated that most mitochondrial respiration

parameters were unchanged except for non-mitochondrial consumption (Figure 3I-N). A decrease in non-mitochondrial oxygen consumption is convoluted with many outcomes that can be affected, however, a common conclusion is a decrease in using glycolysis. Together, these data suggest that R607* iNeurons cannot meet the metabolic demands, and may require more use of glycolysis as opposed to oxidative phosphorylation. Additionally, a lack of phenotypes in the G1744* iNeurons points towards a severity-dependent phenotype with more severe variants having a greater impact on energy demands.

3.5 Discussion

3.5.1 Delineation of cellular signalling defects in p.R607*iNeurons

The proteomic profiling revealed that the R607* patient iNeurons had significantly impaired neuronal development, synaptic signalling and mitochondrial networks. The validation that mitochondrial and metabolic function is defective in R607* neurons suggests a link between SCN2A, neuronal activity and mitochondrial activity. Mitochondrial dysfunction has previously been associated with ASD and NDDs (Frye, 2020; Rossignol and Frye, 2012) and up to 80% of ASD cases have biomarkers of mitochondrial and ETC activity dysfunction (Rossignol and Frye, 2012). Recent reports have also linked mitochondrial dynamics to altered neuronal activity (Divakaruni et al., 2018; Lee et al., 2018; Rangaraju et al., 2019; Sung et al., 2008). This could link how the reduction in the synaptic activity of the R607* variant leads to impaired mitochondrial function, which impacts ATP and energy stores, the reduced mitochondrial respiration could also be a key driver of synaptic deficits. Mitochondrial function has also been implicated in specific genetic forms of ASD or NDDs (Cicaloni et al., 2020; Crivellari et

al., 2021; Ebrahimi-Fakhari et al., 2016; Gebara et al., 2021; Klein Gunnewiek et al., 2020; Kwan et al., 2020; Mithal and Chandel, 2020), suggesting convergence on this pathway is a risk factor.

Other pathway clusters were enriched but not focused as heavily on as mitochondrial function. The cytoskeletal organization and neuron projection development were of secondary interest. The cytoskeleton aids cells in maintaining their shape and internal organization. This is of interest as SCN2A is trafficked, and has transient localization. As with most transmembrane proteins, SCNxA's are trafficked to the surface of neurons through vesicular transport (Catterall et al., 1986; Schmidt and Catterall, 1986; Solé and Tamkun, 2020). The specific mechanism of how SCNxA's are distributed throughout a neuron is unknown, however, there are three main proposed mechanisms. 1) preferential somatic delivery and lateral diffusion into the AIS followed by ANKG immobilization; 2) random delivery to both AIS and the rest of the neuron; and 3) directed delivery into each compartment with AIS having the preference due to the need for high channel concentration (Solé and Tamkun, 2020). Whichever one or combination of these mechanisms is used to deliver SCNxA's channels throughout the neuron relies heavily on the cytoskeleton. Additionally, MAP1B binding to SCN8A is reported to prevent compartment-specific endocytosis, emphasizing the relationship between SCNxA's and the cytoskeleton (Solé and Tamkun, 2020). Recently, two reports reemphasized the importance of Ank2 to Scn2a localization (Gupta and Jenkins, 2022; Nelson et al., 2022). Ank2 undergoes a posttranslational modification known as S-palmitoylation to associate with epithelial cells and localize to the AIS of neurons (Gupta and Jenkins, 2022; He et al.,

2012). Gupta et al. used floxed Ank2 mouse cortical neurons and transfected them with a Nav1.2-3x FLAG construct, their data suggested that Nav1.2 could not localize correctly to the dendritic membrane (Gupta and Jenkins, 2022). In addition to Ank2 and Scn2a colocalizing on dendrites and the dendritic membrane, Ank2 haploinsufficiency was found to impair dendritic but not somatic excitability (Nelson et al., 2022). This suggested that Ank2 is necessary for typical Nav1.2 function in the dendrites. Together, these reports and our findings hint at a need for more in-depth proteomic profiling of SCN2A variants to determine if multiple variants converge on common pathways.

3.5.2 Regulation of mitochondrial dynamics in altered neuronal activity states

Neuronal development requires an immense amount of energy that mitochondria need to produce. This is usually in the form of ATP production. Further, the requirements to maintain and extend dendrites, and generate new synapses for synaptic transmission puts on a strain on mitochondria. Throughout the development process and into maturity neurons are actively communicating through synaptic transmission, this also has high energy demands (Silva et al., 2021). When examining mitochondrial respiration data for R607* iNeurons we cannot know if the phenotypes we observe are a direct impact of the variant or indirect. Because metabolism and neuronal activity are tightly intertwined, we cannot predict whether metabolic defects were present first leading to decreased neuronal activity or neuronal activity was decreased due to the variant that led to fewer energy demands. Further experimentation would be needed to tease this mechanistic question apart. One way to aid in answering the direct or indirect question would be to use imaging experiments of neuronal mitochondria during early development. Mitochondria motility is

a key determinant of the cells' ability to meet high energy demand states, like during synaptogenesis or learning (Li et al., 2004; Silva et al., 2021; Sung et al., 2008). Additionally, neurogenesis and cell fate transitions are driven by metabolism and mitochondria (Iwata et al., 2020; Knobloch and Jessberger, 2017). Both of these milestone events occur in early in the development timeline to capture differences between genotypes. The G1744* iNeurons did not produce a strong phenotype, but this was suspected from the patch-clamp data (Chapter 2, Figure 2). This reinforced the idea that some *SCN2A* variants may cause unique disruptions in signalling clusters.
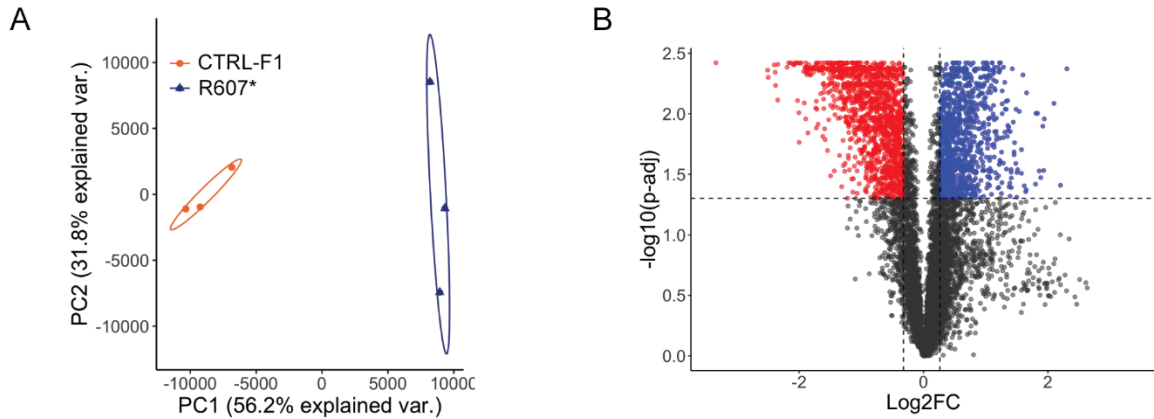
Figure 1. Proteomic analysis of SCN2A$^{+/p.R607*}$ iNeurons reveals differentially expressed proteins.

A) PCA plot showing clustering of the 3 biological replicates for each genotype used in proteomics.

B) Volcano plot showing differentially expressed proteins. Downregulated proteins are shown in red and upregulated proteins are shown in blue. Gray points are non-differentially expressed proteins. The horizontal dashed line represents the p-adjusted threshold of 0.05 and the vertical dashed lines represent the threshold of ± 20% foldchange on a log$_2$ scale.
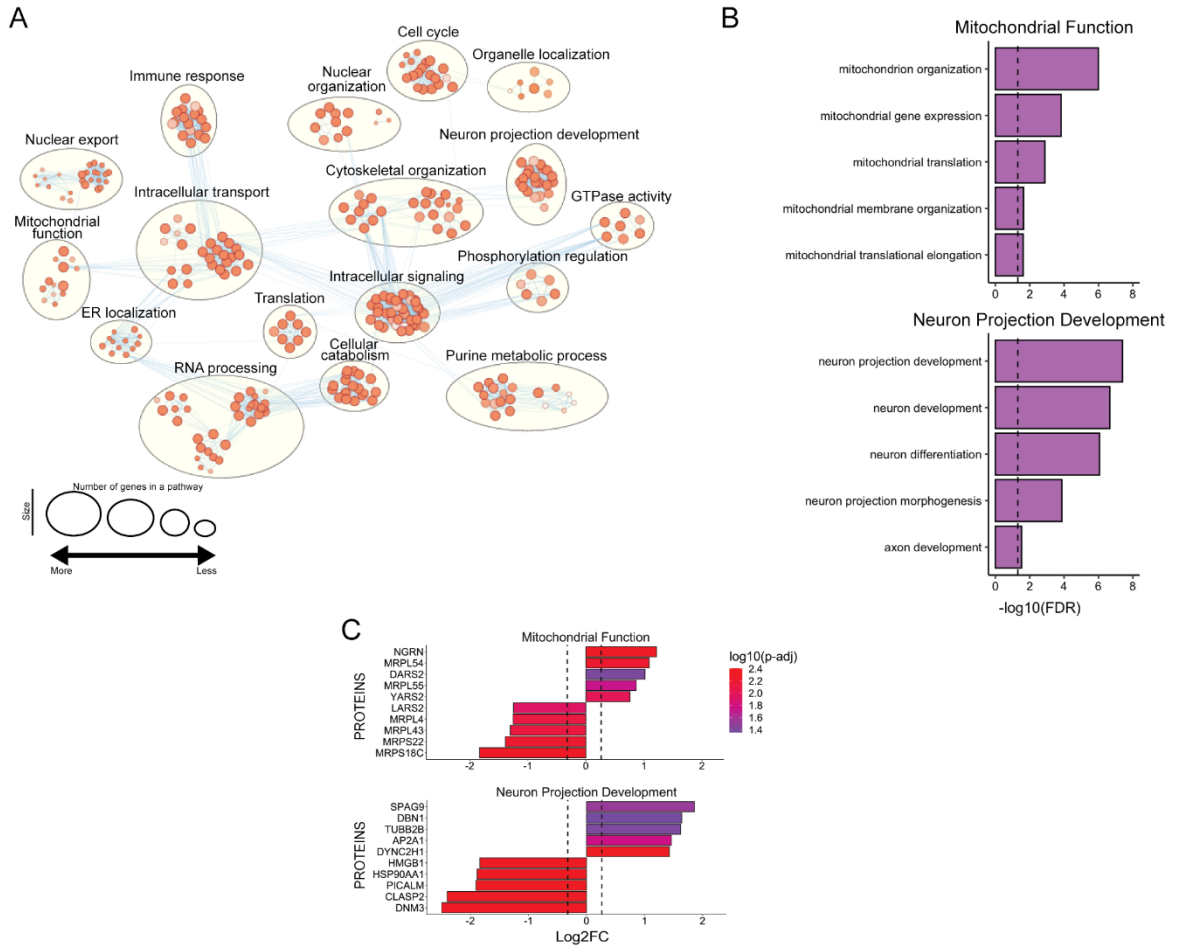
Figure 2. Protein enrichment and ontology analysis of SCN2A$^{+/p.R607*}$ iNeurons reveals defects in neuronal development and bioenergetic pathways. See also figure S1.

A) Network visualization of g:Profiler enrichment of GO:Biological Processes (BP) of both increased and decreased DEPs. Orange dots represent over-represented GO:BP terms. A large circle indicates the number of genes within a term and darker shades represent a higher degree of significance found during enrichment. Clusters indicate biological pathways with common proteins and functions.

B) GO analysis of clusters from A) showing selected GO:BP terms.

C) Top differentially expressed proteins from clusters identified in A).
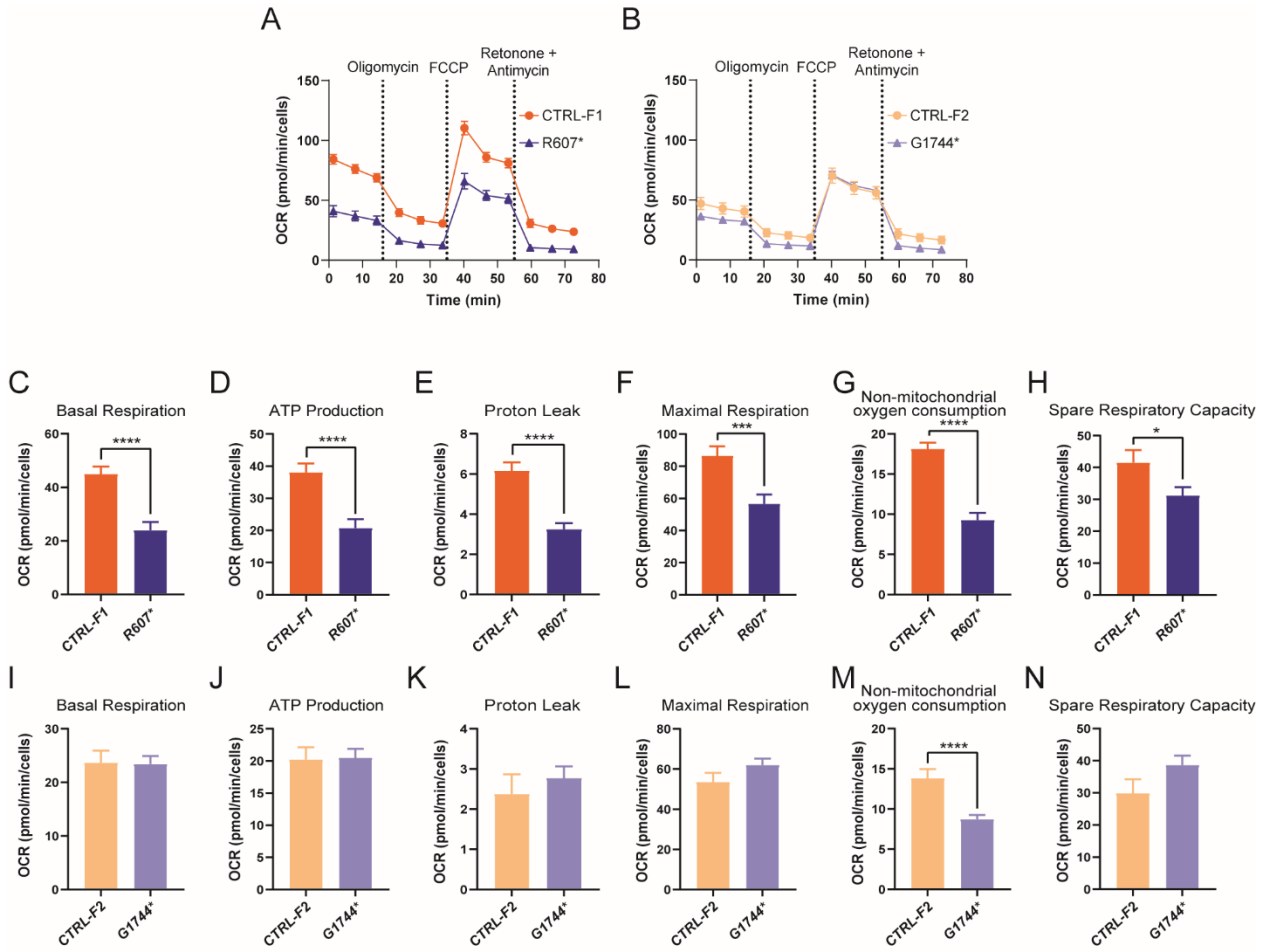
Figure 3. Mitochondrial respiration analysis of SCN2A$^{+/p.R607*}$ and SCN2A$^{+/p.G1744*}$ iNeurons reveals differential defects in bioenergetics.

A-B) Live-cell metabolic assay for validation studies of R607* iNeuron proteomics. (A) Line graph depicting changes in R607* and CTRL-F1 iNeurons in Seahorse assay. (B) Line graph depicting G1744* and CTRL-F2 iNeurons in Seahorse assay.

C-H) Analysis of mitochondrial respiration phases for R607* and CTRL-F1 iNeurons. (C) basal respiration, (D) ATP production, (E) proton leak from mitochondria, (F) maximal respiration from mitochondria, (G) non-mitochondrial oxygen consumption, (H) spare respiratory capacity. CTRL-F1 (n=45 wells) and R607* (n=45 wells), 3 viral transductions recorded at DIV 14. Data represent means ± SEM. *$p < 0.05$, **$p < 0.01$, ***$p < 0.001$, ****$p < 0.0001$, Student's t-test.

I-N) Analysis of mitochondrial respiration phases for G1744* and CTRL-F2 iNeurons. (I) basal respiration, (J) ATP production, (K) proton leak from mitochondria, (L) maximal respiration from mitochondria, (M) non-mitochondrial oxygen consumption, (N) spare respiratory capacity. CTRL-F2 (n=45 wells) and G1744* (n=45 wells), 3 viral transductions recorded at DIV 14. Data represent means ± SEM. *$p < 0.05$, **$p < 0.01$, ***$p < 0.001$, ****$p < 0.0001$, Student's t-test.
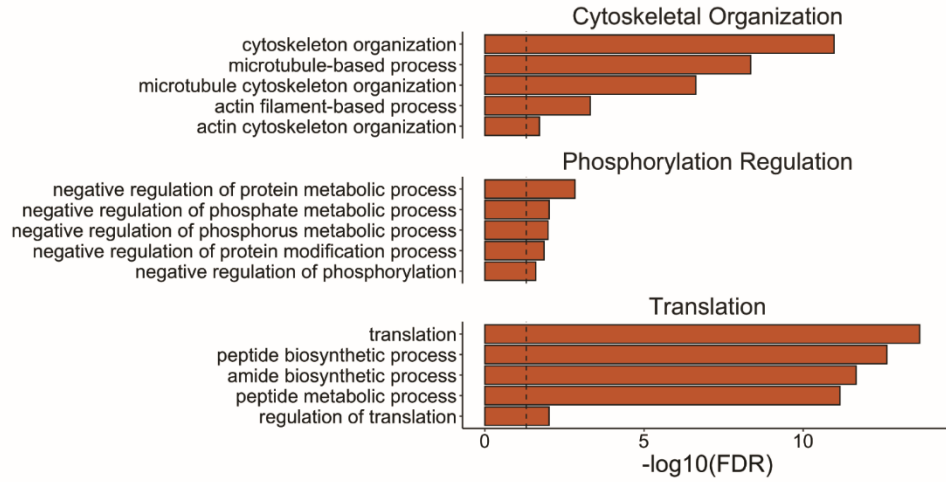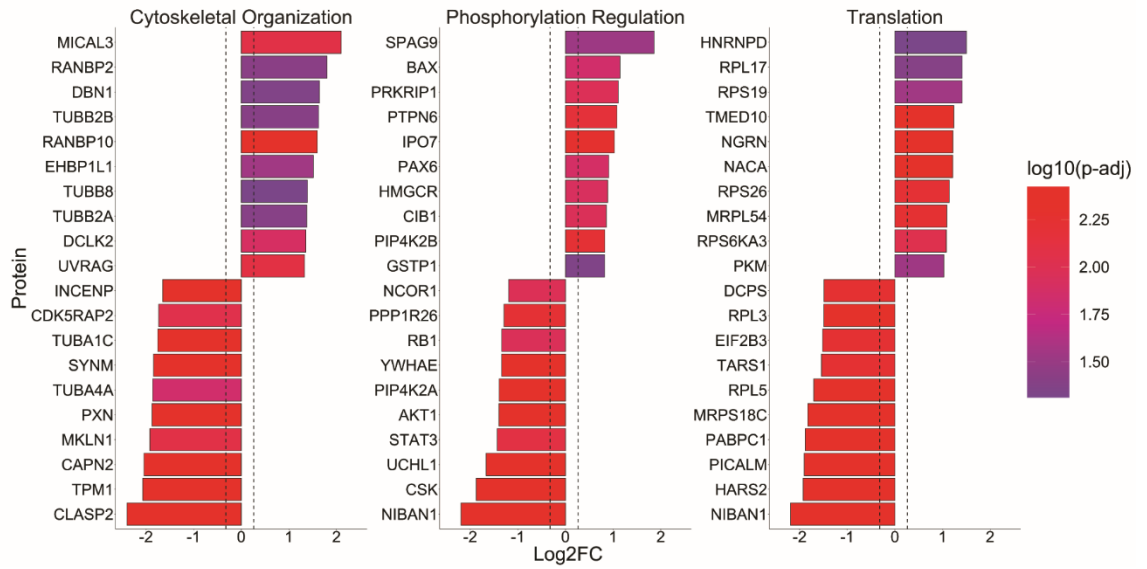
Figure S1. Alternative disrupted cellular signaling pathways in SCN2A$^{+/p.R607*}$

iNeurons.

A) GO term analysis of clusters of interest identified from Figure 2A displaying selected

GO:BP terms.

B) Top differentially expressed proteins from clusters examined in Figure S1A.

3.6 References

Begemann, A., Acuña, M.A., Zweier, M., Vincent, M., Steindl, K., Bachmann-Gagescu, R., Hackenberg, A., Abela, L., Plecko, B., Kroell-Seger, J., et al. (2019). Further corroboration of distinct functional features in SCN2A variants causing intellectual disability or epileptic phenotypes. Mol. Med. *25*, 6.

Bélanger, M., Allaman, I., and Magistretti, P.J. (2011). Brain energy metabolism: Focus on Astrocyte-neuron metabolic cooperation. Cell Metab. *14*, 724–738.

Ben-Shalom, R., Keeshen, C.M., Berrios, K.N., An, J.Y., Sanders, S.J., and Bender, K.J. (2017). Opposing Effects on NaV1.2 Function Underlie Differences Between SCN2A Variants Observed in Individuals With Autism Spectrum Disorder or Infantile Seizures. Biol. Psychiatry *82*, 224–232.

Catterall, W.A., Schmidt, J.W., Messner, D.J., and Feller, D.J. (1986). Structure and Biosynthesis of Neuronal Sodium Channels. Ann. N. Y. Acad. Sci. *479*, 186–203.

Chen, H., Detmer, S.A., Ewald, A.J., Griffin, E.E., Fraser, S.E., and Chan, D.C. (2003). Mitofusins Mfn1 and Mfn2 coordinately regulate mitochondrial fusion and are essential for embryonic development. J. Cell Biol. *160*, 189–200.

Cicaloni, V., Pecorelli, A., Tinti, L., Rossi, M., Benedusi, M., Cervellati, C., Spiga, O., Santucci, A., Hayek, J., Salvini, L., et al. (2020). Proteomic profiling reveals mitochondrial alterations in Rett syndrome. Free Radic. Biol. Med. *155*, 37–48.

Cioni, J.M., Lin, J.Q., Holtermann, A. V., Koppers, M., Jakobs, M.A.H., Azizi, A.,

Turner-Bridger, B., Shigeoka, T., Franze, K., Harris, W.A., et al. (2019). Late Endosomes Act as mRNA Translation Platforms and Sustain Mitochondria in Axons. Cell *176*, 56-72.e15.

Coleman, M., and Blass, J.P. (1985). Autism and lactic acidosis. J. Autism Dev. Disord. *15*, 1–8.

Crivellari, I., Pecorelli, A., Cordone, V., Marchi, S., Pinton, P., Hayek, J., Cervellati, C., and Valacchi, G. (2021). Impaired mitochondrial quality control in Rett Syndrome. Arch. Biochem. Biophys. *700*, 108790.

Dayon, L., Hainard, A., Licker, V., Turck, N., Kuhn, K., Hochstrasser, D.F., Burkhard, P.R., and Sanchez, J.C. (2008). Relative quantification of proteins in human cerebrospinal fluids by MS/MS using 6-plex isobaric tags. Anal. Chem. *80*, 2921–2931.

Deneault, E., White, S.H., Rodrigues, D.C., Ross, P.J., Faheem, M., Zaslavsky, K., Wang, Z., Alexandrova, R., Pellecchia, G., Wei, W., et al. (2018). Complete Disruption of Autism-Susceptibility Genes by Gene Editing Predominantly Reduces Functional Connectivity of Isogenic Human Neurons. Stem Cell Reports *11*, 1211–1225.

Deneault, E., Faheem, M., White, S.H., Rodrigues, D.C., Sun, S., Wei, W., Piekna, A., Thompson, T., Howe, J.L., Chalil, L., et al. (2019). CNTN5-/+or EHMT2-/+human iPSC-derived neurons from individuals with autism develop hyperactive neuronal networks. Elife *8*, 1–26.

Divakaruni, S.S., Van Dyke, A.M., Chandra, R., LeGates, T.A., Contreras, M.,

Dharmasri, P.A., Higgs, H.N., Lobo, M.K., Thompson, S.M., and Blanpied, T.A. (2018). Long-Term Potentiation Requires a Rapid Burst of Dendritic Mitochondrial Fission during Induction. Neuron.

Ebrahimi-Fakhari, D., Saffari, A., Wahlster, L., Di Nardo, A., Turner, D., Lewis, T.L., Conrad, C., Rothberg, J.M., Lipton, J.O., Kölker, S., et al. (2016). Impaired Mitochondrial Dynamics and Mitophagy in Neuronal Models of Tuberous Sclerosis Complex. Cell Rep. *17*, 1053–1070.

Echevarria-Cooper, D.M., Hawkins, N.A., Misra, S.N., Huffman, A., Thaxton, T., Thompson, C.H., Ben-Shalom, R., Nelson, A.D., Lipkin, A.M., George, A.L., et al. (2021). Cellular and behavioral effects of altered NaV1.2 sodium channel ion permeability in Scn2aK1422E mice. BioRxiv 2021.07.19.452930.

Filadi, R., Greotti, E., Turacchio, G., Luini, A., Pozzan, T., and Pizzo, P. (2015). Mitofusin 2 ablation increases endoplasmic reticulum–mitochondria coupling. Proc. Natl. Acad. Sci. *112*, E2174–E2181.

Filadi, R., Pendin, D., and Pizzo, P. (2018). Mitofusin 2: from functions to disease. Cell Death Dis. 2018 93 *9*, 1–13.

Franco-Iborra, S., Vila, M., and Perier, C. (2018). Mitochondrial quality control in neurodegenerative diseases: Focus on Parkinson's disease and Huntington's disease. Front. Neurosci. *12*.

Frye, R.E. (2020). Mitochondrial Dysfunction in Autism Spectrum Disorder: Unique

Abnormalities and Targeted Treatments. Semin. Pediatr. Neurol. *35*, 100829.

Fukumitsu, K., Hatsukano, T., Yoshimura, A., Heuser, J., Fujishima, K., and Kengaku, M. (2016). Mitochondrial fission protein Drp1 regulates mitochondrial transport and dendritic arborization in cerebellar Purkinje cells. Mol. Cell. Neurosci. *71*, 56–65.

Gebara, E., Zanoletti, O., Ghosal, S., Grosse, J., Schneider, B.L., Knott, G., Astori, S., and Sandi, C. (2021). Mitofusin-2 in the Nucleus Accumbens Regulates Anxiety and Depression-like Behaviors Through Mitochondrial and Neuronal Actions. Biol. Psychiatry *89*, 1033–1044.

Gupta, J.P., and Jenkins, P.M. (2022). Ankyrin-B is lipid-modified by S-palmitoylation to promote dendritic membrane scaffolding of voltage-gated sodium channel Nav1.2 in neurons. BioRxiv 2022.06.01.494444.

Haas, R.H. (2010). Autism and mitochondrial disease. Dev. Disabil. Res. Rev. *16*, 144–153.

He, M., Jenkins, P., and Bennett, V. (2012). Cysteine 70 of ankyrin-G is S-palmitoylated and is required for function of ankyrin-G in membrane domain assembly. J. Biol. Chem. *287*, 43995–44005.

Iwata, R., Casimir, P., and Vanderhaeghen, P. (2020). Mitochondrial dynamics in postmitotic cells regulate neurogenesis. Science (80-.). *369*, 858–862.

Klein Gunnewiek, T.M., Van Hugte, E.J.H., Frega, M., Guardia, G.S., Foreman, K., Panneman, D., Mossink, B., Linda, K., Keller, J.M., Schubert, D., et al. (2020). m.3243A

> G-Induced Mitochondrial Dysfunction Impairs Human Neuronal Development and Reduces Neuronal Network Activity and Synchronicity. Cell Rep. *31*, 107538.

Knobloch, M., and Jessberger, S. (2017). Metabolism and neurogenesis. Curr. Opin. Neurobiol. *42*, 45–52.

Kucera, M., Isserlin, R., Arkhangorodsky, A., and Bader, G.D. (2016). AutoAnnotate: A Cytoscape app for summarizing networks with semantic annotations. F1000Research *5*.

Kwan, V., Rosa, E., Xing, S., Murtaza, N., Singh, K., Holzapfel, N.T., Berg, T., Lu, Y., and Singh, K.K. (2020). Proteomic Analysis Reveals Autism-Associated Gene DIXDC1 Regulates Proteins Associated with Mitochondrial Organization and Function. J. Proteome Res. *20*, 1052–1062.

Lee, A., Hirabayashi, Y., Kwon, S.-K., Lewis, T.L., and Polleux, F. (2018). Emerging roles of mitochondria in synaptic transmission and neurodegeneration. Curr. Opin. Physiol. *3*, 82–93.

Lewis, T.L., Kwon, S.K., Lee, A., Shaw, R., and Polleux, F. (2018). MFF-dependent mitochondrial fission regulates presynaptic release and axon branching by limiting axonal mitochondria size. Nat. Commun. *9*.

Li, Z., Okamoto, K.I., Hayashi, Y., and Sheng, M. (2004). The importance of dendritic mitochondria in the morphogenesis and plasticity of spines and synapses. Cell *119*, 873–887.

Liu, Y., Beyer, A., and Aebersold, R. (2016). On the Dependency of Cellular Protein

Levels on mRNA Abundance. Cell *165*, 535–550.

Magistretti, P.J., and Allaman, I. (2015). A Cellular Perspective on Brain Energy Metabolism and Functional Imaging. Neuron *86*, 883–901.

Merico, D., Isserlin, R., Stueker, O., Emili, A., and Bader, G.D. (2010). Enrichment Map: A Network-Based Method for Gene-Set Enrichment Visualization and Interpretation. PLoS One *5*.

Misko, A., Jiang, S., Wegorzewska, I., Milbrandt, J., and Baloh, R.H. (2010). Mitofusin 2 is necessary for transport of axonal mitochondria and interacts with the Miro/Milton complex. J. Neurosci. *30*, 4232–4240.

Mithal, D.S., and Chandel, N.S. (2020). Mitochondrial Dysfunction in Fragile-X Syndrome: Plugging the Leak May Save the Ship. Mol. Cell *80*, 381–383.

Nelson, A.D., Catalfio, A.M., Gupta, J.M., Min, L., Caballero-Floran, R.N., Dean, K.P., Elvira, C.C., Derderian, K.D., Kyoung, H., Sahagun, A., et al. (2022). Physical and functional convergence of the autism risk genes Scn2a and Ank2 in neocortical pyramidal cell dendrites. BioRxiv 2022.05.31.494205.

Palmieri, L., and Persico, A.M. (2010). Mitochondrial dysfunction in autism spectrum disorders: Cause or effect? Biochim. Biophys. Acta - Bioenerg. *1797*, 1130–1137.

Pecorelli, A., Ferrara, F., Messano, N., Cordone, V., Schiavone, M.L., Cervellati, F., Woodby, B., Cervellati, C., Hayek, J., and Valacchi, G. (2020). Alterations of mitochondrial bioenergetics, dynamics, and morphology support the theory of oxidative

damage involvement in autism spectrum disorder. FASEB J. *34*, 6521–6538.

Que, Z., Olivero-Acosta, M.I., Zhang, J., Eaton, M., Skarnes, W.C., and Yang, Y. (2021). Sodium channel Nav1.2-L1342P variant displaying complex biophysical properties renders hyperexcitability of cortical neurons derived from human iPSCs. BioRxiv 2021.01.18.427192.

Rangaraju, V., Lauterbach, M., and Schuman, E.M. (2019). Spatially Stable Mitochondrial Compartments Fuel Local Translation during Plasticity.

Reimand, J., Arak, T., Adler, P., Kolberg, L., Reisberg, S., Peterson, H., and Vilo, J. (2016). g:Profiler—a web server for functional interpretation of gene lists (2016 update). Nucleic Acids Res. *44*, W83.

Reimand, J., Isser, R., Voisin, V., Kucera, M., Tannus-Lopes, C., Rostamianfar, A., Wadi, L., Meyer, M., Wong, J., Xu, C., et al. (2019). Pathway enrichment analysis and visualization of omics data using g:Profiler, GSEA, Cytoscape and EnrichmentMap. Nat. Protoc. *14*, 482.

Rossignol, D.A., and Frye, R.E. (2012). Mitochondrial dysfunction in autism spectrum disorders: a systematic review and meta-analysis. Mol. Psychiatry *17*, 290.

Schmidt, J.W., and Catterall, W.A. (1986). Biosynthesis and processing of the α subunit of the voltage-sensitive sodium channel in rat brain neurons. Cell *46*, 437–445.

Shannon, P., Markiel, A., Ozier, O., Baliga, N.S., Wang, J.T., Ramage, D., Amin, N., Schwikowski, B., and Ideker, T. (2003). Cytoscape: A Software Environment for

Integrated Models of Biomolecular Interaction Networks. Genome Res. *13*, 2498.

Silva, C.A.P., Yalnizyan-Carson, A., Busch, M.V.F., van Zwieten, M., Verhage, M., and Lohmann, C. (2021). Activity-dependent regulation of mitochondrial motility in developing cortical dendrites. Elife *10*.

Solé, L., and Tamkun, M.M. (2020). Trafficking mechanisms underlying Nav channel subcellular localization in neurons. Channels *14*, 1.

Spillane, M., Ketschek, A., Merianda, T.T., Twiss, J.L., and Gallo, G. (2013). Mitochondria Coordinate Sites of Axon Branching through Localized Intra-axonal Protein Synthesis. Cell Rep. *5*, 1564–1575.

Spratt, P.W.E., Ben-Shalom, R., Keeshen, C.M., Burke, K.J., Clarkson, R.L., Sanders, S.J., and Bender, K.J. (2019). The Autism-Associated Gene Scn2a Contributes to Dendritic Excitability and Synaptic Function in the Prefrontal Cortex. Neuron *103*, 673-685.e5.

Sung, J.Y., Engmann, O., Teylan, M.A., Nairn, A.C., Greengard, P., and Kim, Y. (2008). WAVE1 controls neuronal activity-induced mitochondrial distribution in dendritic spines. Proc. Natl. Acad. Sci. U. S. A. *105*, 3112–3116.

Zhang, J., Chen, X., Eaton, M., Lai, S., Park, A., Ahmad, T.S., Wu, J., Ma, Z., Que, Z., Lee, J.H., et al. (2021). Severe deficiency of voltage-gated sodium channel NaV1.2 elevates neuronal excitability in adult mice. BioRxiv 2021.02.02.429384.

Zhang, Y., Pak, C., Han, Y., Ahlenius, H., Zhang, Z., Chanda, S., Marro, S., Patzke, C.,

Acuna, C., Covy, J., et al. (2013). Rapid Single-Step Induction of Functional Neurons from Human Pluripotent Stem Cells. Neuron *78*, 785–798.

Zhang, Z., Marro, S.G., Zhang, Y., Arendt, K.L., Patzke, C., Zhou, B., Fair, T., Yang, N., Südhof, T.C., Wernig, M., et al. (2018). The fragile X mutation impairs homeostatic plasticity in human neurons by blocking synaptic retinoic acid signaling. *4338*, 1–16.

CHAPTER 4: ISOGENIC NEURONAL MODELLING OF THE *DE NOVO* SCN2A p.G1744* VARIANT IN HUMAN iPSC-DERIVED NEURONS

4.1 Preface

This chapter focuses on the genetic, cellular, and functional work I have done to further validate and delineate the phenotypes of the *SCN2A* G1744* patient variant on neuronal function. As previously mentioned, this *de novo* point variant was identified through our collaboration with Dr. Stephen Scherer (The Hospital for Sick Children). Unique to this variant, we reported that even though it is classified as a LoF variant, we observed enhancements in the action potential waveform and recovery of neuronal network activity in our MEA longitudinal study. To better understand how this LoF variant produces little to no deficits in our patch-clamp data and can recover neuronal network activity characteristics, we sought to create an isogenic model of this variant. With the guidance of Drs. Carole Shum, Tara Paton, and Guillermo Casallo from the Scherer lab/The Centre for Applied Genomics we generated and validated using *in silico* applications specific guide RNAs (gRNA), primers, and MGB® TaqMan gene expression probes for ddPCR. From this, we used the ribonucleotide protein (RNP) complex method of CRISPR-Cas9 to introduce the patient variant into a new control iPSC line. The iNeurons used in this chapter have undergone the same transduction and induction methods highlighted in Chapter 1 to generate the data represented here. All experiments, data collection, and analysis were performed by Chad Brown. The data generated in this chapter will also be included in the manuscript outlined in Chapters 1 and 2.

4.2 Introduction

Eukaryotic uses of the Clustered Regularly Interspaced Palindromic Repeats (CRISPR)-Cas system has revolutionized the study of genetic diseases. Gene editing technologies and their applications have exponentially expanded recently. Our current advancements in genetic engineering would not be where they are without the first discoveries of DNA ligation for DNA fragments, and restriction enzymes. Later, breakthroughs in creating recombinant DNA, transgenic mice, vaccines, and synthetic insulin all stemmed from these fundamental discoveries (Khan et al., 2016). Early strategies developed for precision genome editing include nucleases-meganucleases, Zinc finger nucleases (ZFN)s, and transcription activator-like effector nucleases (TALEN)s (Bogdanove and Voytas, 2011; Chevalier et al., 2001; Epinat et al., 2003; Urnov et al., 2005). The caveat of these three families of nucleases is the use of protein-DNA interactions for targeting. The DNA-binding domains can only acquire new targets with different sequences by being reprogrammed through protein engineering (Wang et al., 2020). Most Cas nucleases are however RNA-guided to target sequences, this has the additional benefit of being easily adjustable (Gaj et al., 2013). This provides an efficient platform to target multiple sequences with high efficiency.

4.2.2 CRISPR-Cas9 and ribonucleotide protein complexes

The CRISPR-Cas immune response in bacteria and archaea consists of an adaptation, expression, and interference stage. Briefly, during the adaptation stage, Cas proteins bind to target DNA by recognizing short motifs known as protospacer-adjacent motifs (PAM). The Cas complex then proceeds to cleave the protospacer as the target DNA

(Makarova et al., 2019). The protospacer excised is then integrated into the bacterial CRISPR array. In the expression stage, the CRISPR array is transcribed and processed into mature CRISPR RNAs (crRNA), each having the original protospacer sequence (Barrangou and Horvath, 2017; Koonin and Makarova, 2019; Mohanraju et al., 2016). At the interference stage, the crRNA is used as a guide to recognize similar protospacer sequences of pathogens (Makarova et al., 2019).

In the early-2010's the Cas9 nuclease system was first applied in mammalian cells for point mutagenesis experimentation (Cong et al., 2013; Mali et al., 2013). The most common Cas9 used in literature is derived from the *Streptococcus pyogenes* (SpCas9) system (Wang et al., 2020). This Cas protein recognizes the 5' NGG PAM sequence, indicating that the first basepair can be any nucleotide and the last two must be a Guanine. Unfortunately, SpCas9 is tolerable of basepair mismatches between the gRNA and target sequence adding to the likelihood of indels (Hsu et al., 2013). Additionally, due to the size of SpCas9 (~4.1 kb), the range of applications is limited. This spurred researchers to develop other orthologs of Cas9, that have better specificity and smaller sizes. As a type II CRISPR-Cas system, the major hallmarks include a single Cas9 protein, a crRNA, and a trans-activating crRNA (tracrRNA) (Mali et al., 2013; Wang et al., 2020). In addition to the widely used Type II systems, Type V and VI have been more recently used for targeting alternative PAM sites. Type V, known as the Cas12 family recognizes 5' TTN or TTTN depending on the bacterial host it is derived from (Dong et al., 2016). The cleavage of DNA from Cas12a is more robust than the Type II Cas' and generates sticky-end DNA double-stranded break (DSB)s instead of blunt-end DSBs. Members of the Type VI CRISPR-Cas

family are orthologs of the Cas13a protein. The distinction between this class and the others is the cleavage of single-stranded RNA instead of DNA (Abudayyeh et al., 2016).

Despite the low efficiency of gene editing in mammalian cells, CRISPR, and more specifically, CRISPR-Cas9 has had large success in genetically modifying genomes for various applications. One way to enhance the efficiency of site-specific mutagenesis is to provide the cells with enough machinery. Reports have found fusing other proteins or sequences to Cas proteins before delivery enhances the editing efficiency (Hackley, 2021; Li et al., 2021a; Zhang et al., 2021c). One strategy that we implored was by forming a ribonucleoprotein (RNP) complex before the delivery. Direct delivery of the RNP complex consisting of the Cas9 protein bound to the single guide RNA (sgRNA) has proven advantageous in reducing off-targets and increasing on-target efficiency. RNP delivery is also advantageous since it requires little to no transcription and translation activity from cells, reducing the stress and demand (Zhang et al., 2021c). This is in tandem with the electroporation delivery method, allowed for transient and stable transfection conditions, and provided a known platform for delivery into iPSCs.

4.2.3 Non-homologous end joining

Non-homologous end joining is a cellular pathway activated if a DSB occurs in the DNA. As a repair mechanism, DNA is not edited until this process responds. In response to DSBs, NHEJ activation can introduce insertions, deletions, translocations, and other DNA permutations (Jeggo, 1998). Even with the possibility of DNA abnormalities, mammalian cells prefer to use NHEJ when DSBs occur. In addition to NHEJ, homology-directed repair (HDR) exists as an opposing repair mechanism. The mechanisms of HDR

are described below. As HDR is widely used in the academic setting to alter DNA, the required auxiliary machinery needed from the cell creates an unfavourable situation, causing NHEJ to be more efficient (Rees and Liu, 2018). Moreover, since HDR is restricted to the G2 and S phases of the cell cycle HDR efficiency is often lower, as only actively dividing cells can undergo the process (Chapman et al., 2012; Cox et al., 2015; Paquet et al., 2016). The NHEJ repair pathway uses the KU70/80 to recognize DSBs, once recognized, DNA-dependent protein kinase catalytic subunit (DNA-PKcs) is recruited to form a complex (Chang et al., 2017). Polymerases μ and λ, nucleases Artemis and APLF, and DNA ligase IV, are major interactors during the repair process. Since DSBs are genotoxic, NHEJ is also favourable during the cell cycle since most DSBs arise during replication (Reid et al., 2015).

4.2.4 Homology-directed repair

To achieve site-specific repair of a DNA double-stranded break, Homology-directed repair (HDR) is needed. RNA-guided Cas9 nucleases create DSBs of the DNA, but to reduce the errors incurred by the cell preferred NHEJ repair, repair templates are required in the form of single-stranded oligodeoxynucleotides (ssODN) or double-stranded DNA (dsDNA) donors (Knott and Doudna, 2018; Nambiar et al., 2019). These repair templates provide precise sequences that include base substitutions, insertions, and deletions (Hsu et al., 2014). The success or efficiency of using HDR-mediated repair relies on the cell-specific pathways associated with repair. When DSBs occur, a process called DSB resection occurs where DSB ends are converted into 3' single-stranded DNA overhangs through a nucleolytic process (Nambiar et al., 2019; Symington, 2016). Like

NHEJ factors, there are HDR-promoting factors that enhance the selection of the DNA repair pathway. In addition, inhibiting crucial factors like KU70/80, 53BP1, DNA-PKcs, and ligase IV in the NHEJ pathway have been shown to increase the likelihood of using the HDR pathway (Canny et al., 2017; Chu et al., 2015; Guo et al., 2018; Maruyama et al., 2015). In mammalian cells, promoting the HDR pathway is more difficult which usually results in low efficiency of often a lack of an endogenous repair template (Sun et al., 2022). Because of this low efficiency, the generation of genetically edited mammalian cells that have your sequence of interest is time intensive. Colony selection, isolation, and expansion are required to obtain a uniform population of cells.

4.3 Materials and Methods

4.3.1 iPSC approval and validation

All pluripotent stem cell work was approved by the Canadian Institutes of Health Research Stem Cell Oversight Committee. Blood was taken from individuals with the approval from the SickKids Research Ethics Board after informed consent was obtained, REB approval file 1000050639. This study was also approved by the Hamilton Integrated Research Ethics Board, REB approval file #2707. In this Chapter, we used iPSCs that were named "19-2-2" and have been previously characterized and validated in our collaborator's work (Deneault et al., 2018). This iPSC line was reprogrammed from a healthy father with a child who carried the *de novo* 16p.11.2 microdeletion, associated with ASD. Further, WGS did not detect genetic abnormalities associated with ASD risk. iPSCs were generated from retrovirus reprogramming encoding OCT4, SOX2, KLF4, MYC on skin fibroblasts, and lentivirus vector encoding a pluripotency-GFP reporter with a puromycin resistance

gene were transduced (Deneault et al., 2018). After puromycin selection, colonies that were large enough were transferred to 1 well of a 12-well plate coated with irradiated MEFs and plated in iPSC media (DMEM/F12 supplemented with 10% KO serum, 1x non-essential amino acids, 1x GlutaMAX, 1mM β-mercaptoethanol, and 16ng/mL basic fibroblast growth factor (bFGF)). Once iPSCs were expanded and established they were transitioned to matrigel coated plates and grown in mTeSR1 (STEMCELL Technologies) and subsequent passaging continued to use ReLeSR (STEMCELL Technologies). iPSC lines without karyotypic abnormalities were used and this was verified by G-band karyotyping performed by the Centre for Applied Genomics (Hospital for Sick Children). To verify the expression of pluripotent markers OCT4 and NANOG, immunocytochemistry was performed.

4.3.2 iPSC and nucleofection preparation

For the nucleofection, reagents, and plates were prepared in advance. DNA oligos that included the gRNA (IDT) and ssODN (IDT) were prepared to a final concentration of 10 µM in sterile nuclease-free water (Corning) and stored in the -20°C freezer. 6-well plates were then coated with Matrigel (Corning) at a 1:60 dilution in DMEM/F-12 (Gibco) and incubated at room temperature. After 1 hour, Matrigel was aspirated off and mTeSR1 (STEMCELL Technologies), and ROCK inhibitor (STEMCELL Technologies, 10 µM, 1:1000) were added to the wells. We next prepared the RNP complex, this was done by creating a mastermix by adding 1 µL of 61 µM stock HiFi Cas9 (IDT), 11 µL of 10 µM gRNA, and 100 µL of the nucleofector solution with its' supplement (Lonza). After these reagents were added, an incubation of 20 minutes was required to form the RNP complex

between the Cas9 enzyme and gRNA. After the incubation, 22 µL of 10 µM ssODN (IDT) was added to the RNP mastermix. Following the preparation of the nucleofection mix, media from the cells were aspirated and washed once with dPBS (Gibco). Next, 200 µL of Accutase (STEMCELL Technologies) was added to each well and left at 37°C in the incubator for 6 minutes. After the incubation, cells were transferred from a 6-well plate to a 15 mL falcon tube for centrifugation. Samples were spun at 250 g for 3 minutes and the supernatant was removed. Cells were then resuspended in 1mL of mTeSR1+ROCK solution, and then 20 µL of cell suspension was taken and mixed 1:1 with trypan blue. From this, 20 µL of the mixed cell and trypan blue solution was taken and placed into a cell counter slide. Using the Auto T4 Cell Counter (Nexcelom), calculations to determine the concentration for 1 000 000 cells were needed. Once the calculations were completed a secondary cell suspension mixture was made with 1 000 000 cells in 1 mL of mTeSR1+ROCK solution. Cells were then centrifuged at 250 g again and the media was aspirated off after. During the centrifugation, the Amaxa Nucleofector 2b (Lonza) was turned on and programmed to the CA 137 for transfecting iPSCs. Once completed, the nucleofector solution mixture was then added to the cell pellet, mixed 3 times, and pipetted into a cuvette provided in the nucleofection kit. The cuvette was then placed into the nucleofector device and the program was started. Once completed, small bubbles in the cuvette can help to indicate if the electroporation was good. Cells were then incubated for 10 minutes after the nucleofection to provide a rest period. Next, cells were then plated at 500 000 cells/well in the previously prepared Matrigel 6-well plates. These wells contained the mTeSr1+ROCK solution. The plates were then placed into the incubator at 37°C for 24

hours undisturbed. After 24 hours, plates were then observed under the microscope to determine cell health and crude nucleofection efficiency.

4.3.3 Mutagenesis enrichment and purification

iPSCs with the most pmaxGFP expression and reached near 70% confluence post-nucleofection were treated were re-plated into a 96 well plate using 500 µL of Accutase and incubated at 37°C for 6 minutes to enzymatically unadhere the cells. Accutase was then neutralized with 1:1 mTeSR+ROCK and centrifuged at 250 g. The media was then aspirated and cells were evenly disturbed from the one well of a 6-well plate into four 24-well plates using mTeSR+ROCK. Once the 24-well plates were confluent, cells were split 1:2 into one eight 24-well plates, with each well having a sister well. Next, after the iPSCs reached 50% confluence in the 24-well plates, half of the plates were harvested for ddPCR (Bio-Rad). 50 µL/well of Accutase was added and incubated at 37°C for 6 minutes. Accutase was then neutralized with 50 µL/well DNA lysis buffer (10 mM Tris pH 7.5, 10 mM EDTA pH 8.0, 10 mM NaCl, 0.5% N-lauroylsarcosine, and freshly added 1 mg/mL proteinase K). Wells were then pipetted gently and transferred to a 96-well PCR plate. The PCR plate containing the cells and DNA lysis buffer was then sealed and placed in a thermocycler (Bio-rad) at 70°C for 10 minutes. Cells were then chilled on ice for 4 minutes, and 100 uL/well of a DNA precipitation solution (EtOH 95%, H_2O 5%, and a previously cooled NaCl 75 mM solution at -80°C). The PCR plate was then left at room temperature for 60 minutes, following this, the plate was spun at 1800 g for 4 minutes. The plate was then flicked quickly upside down to remove the supernatant. Two washes were performed where 100 µL/well of 70% EtOH was added slowly and quickly flicked off. The PCR plate

was then placed back into the thermocycler unsealed and incubated at 70°C for 3 minutes. DNA was resuspended in 20 uL of UltraPure™ Distilled Water (Invitrogen), heated at 70°C for 10 minutes, and vortexed briefly. Custom TaqMan® MGB probes (ThermoFisher) were designed and optimized according for our case use and the ddPCR's (Bio-Rad) recommendations. The TaqMan® MGB probes consisted of 20-21 basepair sequence that was complimentary to our DNA region of interest, one targeting the control DNA and the other targeting the point mutation. This ensured specificity, probes also underwent computational analysis in the Primer Express™ Software (ThermoFisher) to verify other paralogs were avoided. Further, the probes contained both a 5' fluorescent reporter dye (VIC-WT and 6FAM-MUT) and a 3' nonfluorescent quencher aiding in reduced background signal. The forward and reverse primers for ddPCR were designed to bind outside of the range of the ssODN, this would avoid partial amplicon products which may skew the probe binding. Primers were designed using the primer blast tool (www.ncbi.nlm.nih.gov/tools/primer-blast/). The ssODN was synthesized DNA that had 50 bp flanking homology arms on both sides of the point mutation (Benchling). Once the data was received from the ddPCR assay, the two highest edited frequencies were selected and colony selected. The corresponding sister wells to the data obtained were then plated at a low density (5000 cells/well) in a 6-well plate. When these cells grew into individual colonies larger enough to 'pick', we proceeded to colony pick 24 colonies from the top two edited frequencies, and place each colony into its own well of a 24-well plate. This process continued as described above until we obtained a pure population of heterozygous iPSC-edited cells.

4.3.4 Induction of iPSCs into glutamatergic neurons

Similar to Chapter 2, we needed to differentiate the newly generated iPSCs into excitatory neurons. To rapidly upscale experiments and focus on excitatory neurons, we used the previously published constitutive expression protocol of NGN2 to generate homogeneous populations of glutamatergic neurons (Zhang et al., 2013). These iNeurons displayed stable membrane, firing, and synaptic properties when co-cultured with mouse glial cells by DIV 21 (Zhang et al., 2013, 2018). Importantly as we previously described, this protocol provided consistent differentiation levels between cell lines derived from different participants (Deneault et al., 2018, 2019). We modified this protocol by inducing NGN2 for 3 days starting at DIV 1 and puromycin selecting for 2 days starting at DIV 2 and adding mouse glial cells at DIV 5. Half-iNeuron media (iNI) (Neurobasal media, 1x SM1, 1x GlutaMAX 1x pen/strep, 1μg/mL laminin, 10 ng/uL BDNF and 10 ng/uL GDNF) changes were performed every other day. Patch-clamp recordings were generated between DIV 24 and 27 post-NGN2-induction. Comparable bioelectric properties were previously reported (Deneault et al., 2018, 2019; Yi et al., 2016; Zhang et al., 2013, 2018).

4.3.5 Immunocytochemistry

On DIV 25, iNeurons were fixed at room temperature in 4% paraformaldehyde in PBS for 15 min. The cells were then washed 3 times for 10 min with PBS, then blocked and permeabilized (B/P) with a B/P solution containing (0.3% Triton-X, 10% Donkey Serum, and PBS) for 1 hr. The cells were then incubated overnight at 4°C with primary MAP2 and SYN1 antibodies in B/P solution. The next day, cells were washed 3 times for 10 min in PBS and incubated with secondary antibodies in B/P solution for 1.5 hours at

room temperature and covered with aluminum foil. The cells were then washed 3 times for 10 min and incubated with 300mM DAPI for 8 min. The cells were then washed 1 time with PBS for 10 min. Coverslips were then quickly dried with a Kimwipe, and mounted on VistaVision glass microscope slides (VWR) with 10 µL of Prolong Gold Anti-Fade mounting medium (Life Technologies). Mounted coverslips were allowed to cure overnight in a dark slide box at room temperature. Images were acquired using a Zeiss LSM700 confocal microscope.

4.3.6 Analysis of presynaptic puncta and primary dendrites

Synaptic morphology was processed and analyzed with ImageJ software. The SYN1 antibody was co-immunostained with MAP2 to determine dendrites with presynaptic puncta. Three biological replicates were used for each line with the data generated from five iNeurons per replicate per condition. A total of 15 iNeurons per condition per line were used with two dendrites of equal dimensions used per iNeuron. Data represent the number of synaptic puncta averaged by two dendrites per iNeuron within 30 µm segments. The same images were used to calculate dendrite complexity. This was determined by counting the number of MAP2-positive primary dendrites branching from the soma.

4.3.7 In vitro electrophysiology

iNeurons were replated on DIV 4 onto polyornithine/laminin-coated coverslips in a 24-well plate at a density of 100 000/well with 0.5 mL of iNI media. On DIV 5, primary mouse astrocytes were added at a density of 50 000/well to support iNeurons' viability and maturation. Half media changes were performed every other day and wells were maintained

until DIV 24 – 26 for recordings. At DIV 9, iNI was supplemented with 2.5% FBS which was adapted from (Zhang et al., 2013). Whole-cell patch-clamp recordings were performed at room temperature using Multiclamp 700B amplifier (Molecular Devices) from borosilicate patch electrodes (P-97 puller and P-1000 puller; Sutter Instruments) containing a potassium-based intracellular solution (in mM): 123 K-gluconate, 10 KCl, 10 HEPES; 1 EGTA, 1 MgCl2, 0.1 CaCl2, 1 Mg-ATP, and 0.2 Na4GTP (pH 7.2). 0.06% sulpharhodamine dye was added to the intracellular solution to confirm the selection of multipolar neurons. The extracellular solution consisted of (in mM): 140 NaCl, 5 KCl, 1.25 NaH_2PO_4, 1 $MgCl_2$, 2 $CaCl_2$, 10 glucose, and 10 HEPES (pH 7.4). Data were digitized at 10 – 20 kHz and low-pass filtered at 1 - 2 kHz. Recordings were omitted if access resistance was >30 MΩ. Whole-cell recordings were clamped at -70 mV and corrected for a calculated -10mV junction potential. Rheobase was determined by a step protocol with 5 pA increments, where the injected current had a 25 ms duration. Action potential waveform parameters were all analyzed in reference to the threshold. Repetitive firing step protocols ranged from -20 pA to +50 pA with 5 pA increments for the isogenic G1744* line. Data were analyzed using the Clampfit software (Molecular Devices), while phase-plane plots were generated in the OriginPro software (Origin Lab).

4.3.8 Statistical analysis

Data are expressed as mean ± SEM. Three viral NGN2 transductions were used as biological replicates for statistical analysis. We used the Student's unpaired t-test, two-way ANOVA, and post hoc Sidak tests in GraphPad Prism 8 statistical software for statistical analyses. Sidak was used to correct for multiple comparisons. Grubbs' test was used to

remove outliers. The p-values in the figure legends are from the specified tests, and $p < 0.05$ was considered statistically significant.

4.4 Results

4.4.1 Generation and validation of the p.G1744* variant in an isogenic model using CRISPR-Cas9

As mentioned previously in this chapter, we used the CRISPR-Cas9 system to genetically modify a control iPSC line and to introduce our variant of interest. After the upfront designing and computational validation of our gRNAs, ssODNs, primer sets, and TaqMan probes, we needed to test our nucleofection efficiency in the iPSCs. Using the RNP CRISPR-Cas9 system required us to optimize the amount of repair template and RNP complex to use since this was not a plasmid-based approach. From our collaborations with Dr. Stephen Scherers' group, we moved forward with one concentration in two different cell lines. Further, since Cas9 was not fused to a fluorescently labeled protein, we added a pmaxGFP vector that was independent of the RNP complex. This provided a qualitative inference of our nucleofection efficiency and confirm if the nucleofection worked. From our results, we found that the 19-2-2 iPSC line handled the nucleofection conditions better than the H1 ESC line. This was indicated by visual inspection of both cellular death and GFP expression 24 hours post-nucleofection (Figure S1A).

Following the nucleofection, colony picking was essential to enrich for our variant of interest in the iPSCS. As mentioned above in the workflow, iPSCs were collected and replated, and divided 1:2 to generate "sister-plates" that would express roughly the same population of cells (Figure 1A). To determine the variant expression in the population of

cells ddPCR was used. From previously published papers we knew a minimum of four rounds of enrichment were needed to generate a pure population of heterozygous or homozygous iPSCs. Our data indicated that after the initial nucleofection, we had an edited efficiency of approximately 4.5% in various wells (Figure 1B). This data was plotted using the fractional abundance of the variant DNA copies divided by the total DNA copies. Subsequent enrichment cycles are plotted to highlight the trajectory to a ~100% population purity (~50% target DNA/ total DNA) (Figure 1B). Additionally, 2D plots generated from ddPCR are shown to highlight the control and variant probe clusters, as they are purified in subsequent enrichment cycles (Figure 1C). Lastly, Sanger sequencing was performed as a supplemental validation to the ddPCR. Since MGB® TaqMan probes were designed to directly bind to a sequence that contained both the control and variant DNA sequence, fluorescent detection in their respective channels would confirm their presence. However, a readout of the bases is not provided as with Sanger. A representation of the sequence to confirm the heterozygosity of the variant is shown (Figure S1E). As a last quality control, we also karyotyped our iPSCs to determine if there were any major chromosomal abnormalities. Our results indicated that there were none identified in both CTRL-iso2 and iso-G1744* iPSCs (Figure S1C and D).

4.4.2 Synaptic and dendrite morphology are unaltered in isogenic iNeurons harbouring the p.G1774 variant*

To study the morphological effects of SCN2A perturbation on human glutamatergic neurons, we used iNeurons that were co-cultured with mouse glia from our varying models of SCN2A deficiency. To assess the differences between the deficiency severity, and

synaptic and dendritic morphology, we fixed our iNeuron co-cultures on DIV 25. This coincided with our electrophysiological recordings for this experiment. Our data indicate that MAP2+ primary dendrites' development is unaffected by the p.G1744* variant (Figure 1A and B). This was evident by scoring the MAP2+ dendrites, however, this analysis does not account for dendritic arborization which may still be affected.

We once again examined synapse formation in our genetically engineered isogenic iNeurons harbouring the G1744* variant (Figure 1C). Protocols for synaptic immunostaining are previously described in Chapter 2. Briefly, SYN1 was used to perform our analysis on the same samples used for the dendrite inquiry, thus providing a stronger correlation between any findings of dendrite and synapse morphology. From this, density and puncta size were extrapolated from the images. Each of which would describe a distinctive characteristic of the synapse. From our analysis, we found no differences in synapse density between CTRL-ISO2 and ISO-G1744* iNeurons (Figure 1D). This data suggests that iNeurons harbouring the p.G1744 variant do not suffer from impaired synaptic connection formation. When examining the presynaptic size, we also found no differences in CTRL-ISO and ISO-G1744* iNeurons (Figure 1D). This crudely suggests that ISO-G1744* iNeurons' presynaptic terminal dynamics were unaffected. Together, these data indicate that this *de novo* LoF variant is not sufficient to impair primary dendrite growth, synaptic connectivity, and synapse size.

4.4.3 Isogenic neuronal intrinsics are not impaired by the LoF variant p.G1744*

We once again used a whole-cell patch-clamp to probe our neuronal models of SCN2A deficiency. Further, we needed to use similar assays to validate our initial findings

from the patient-derived iNeurons harbouring the p.G1744* variants. Even though the control was a familial control and sex-matched, 50% of the genetic background differs; potentially leading to subtle or profound effects on iNeuron behaviour due to their expression profile or other common polymorphisms. Using our newly CRISPR/Cas9-edited iPSC-derived iNeurons as an isogenic model for the p.G1744* variant, we found generally the variant did not have deleterious effects. From our analysis of the bioelectric data, we found iso-G1744* iNeurons did not differ in their cell capacitance or input resistance, suggesting that their size was approximately the same, and, that the quantity and state of ion channels across the neuron were roughly the same, respectively (Figure 3A and B). The resting membrane potential also remained unchanged compared to CTRL-iso2 iNeurons (Figure 3C). All action potential characteristics also remained unchanged between CTRL-iso2 and iso-G1744* iNeurons, this consisted of the, rheobase, threshold of the action potential, ½ width, ½ width from the threshold, amplitude, maximum rise rate, maximum decay rate, and repetitive firing (Figure 3D-K). This all suggests that the action potential waveform is unaffected by the presence of this LoF variant, p.G1744*. Lastly, we examined the synaptic transmission of our isogenic iNeuron model. We observed no statistical difference between CTRL-iso2 and iso-G1744* for the frequency or amplitude of synaptic events (Figure 4A-C). This further reinforced the lack of deleterious effects on iNeurons from harbouring the p.G1744* variant.

4.5 Discussion

4.5.1 Expression of the de novo p.G1744* variant does not alter synapse or dendrite

morphology in isogenic modelling

The dendrite and synaptic morphology data obtained from our isogenic modelling of the p.G1744* variant was unexpected. Our initial predictions assumed that experiments performed in an isolated model would recapitulate the findings we saw in the CTRL-F2 and G1744* iNeurons (Chapter 2, Figure 2A-F). However, this was not the case, and in fact, decreases in puncta density and increases in puncta size in G1744* iNeurons were not present in the iso-G1744* iNeurons (Figure 2A). The foremost question that arises is, how could genetic background differences affect cellular phenotypes? Studies on genetic background and iPSCs have reported long-known associations (Rouhani et al., 2014). The transcriptional variance associated with iPSCs has been shown to affect the proliferation and differentiation of iPSCs into terminally differentiated cell types (Kyttälä et al., 2016). Further inter-individual variance analysis of iPSC and ESC cells accounts for ~38% of the differences (Rouhani et al., 2014). More recently, a report from the Human Induced Pluripotent Stem Cell Initiative increased the inter-individual differences up to 46% (Kilpinen et al., 2017). Many of these differences are specifically due to some epigenetic markers being retained during the reprogramming stages. One example is DNA methylation marks that are difficult to erase, these trace marks can alter the propensity for a cell line to differentiate (de Boni et al., 2018; Roost et al., 2017; Volpato and Webber, 2020). In addition to gene expression analysis, expression quantitative trait-associated loci (eQTL) analysis is done. eQTLs are genetic variants that are associated with changes in the

expression of the gene, this requires large-scale iPSC-based studies and is identified by GWAS (Carcamo-Orive et al., 2017). Gene expression variability in iPSC variability-associated eQTLs is directly involved in stem cell maintenance and differentiation efficiency (Carcamo-Orive et al., 2017; Kilpinen et al., 2017; Yamasaki et al., 2017). Many of these gene expressions produce cell morphology differences due to donor contribution, with up to 23% accounting for variation in cellular phenotypes (Kilpinen et al., 2017; Volpato and Webber, 2020). There are many approaches to reducing the variability caused by donor sources. Isolating reproducibility to donor-specific variables and not batch processing, protocol to protocol differences, or handling/ lab to lab differences genetic, points towards functional quality control. In our use case, WGS or WES of our genetically engineered iPSC line is needed to explore genetic differences that may have arouse from CRISPR-Cas9 genome editing. Additionally, this provides a platform to compare the genomes between the p.G1744* isogenic line and the associated proband and familial control to examine genetic variance.

Lastly, while the RNA-centric studies mentioned above provide crucial information in our understanding of gene regulatory mechanisms in the transcriptome, studies that investigate the proteome are needed. A paper published in 2020, followed up on the transcriptomic analysis mentioned prior, by analyzing 202 iPSC lines derived from 151 donors (Mirauta et al., 2020). They characterized major genetic and non-genetic determinants of proteome variance between iPSC lines, and evaluated important regulatory mechanisms affecting protein abundance. Similar to eQTLs, they identified 635 protein quantitative trait loci (pQTL) in iPSCs, with some variants linked to deviations in protein-

coding sequences and trans-regulatory effects. Together, these reports suggested that donor genetic variance and epigenetic factors often translate to phenotypes observed in human disease modelling, even among controls. Furthermore, the differences between iNeurons we observed in our synaptic and dendrite modelling may in large part be attributed to the aforementioned genetic causes.

4.5.2 Paradoxical electrophysiological phenotypes in the presence of the LoF p.G1744* variant

This investigation was done to functionally characterize the effects of iNeurons harbouring the *de novo* LoF p.G1744* variant in an isolated fashion. As we mentioned in Chapter 2, we observed unexpected results from the patch-clamp data, G1744* iNeurons showed an enhancement to the action potential waveform. However, this did not culminate into increased action potential trains or synaptic communication. To delineate our previous findings, we generated an isogenic model of the variant. We were able to genetically modify one of our in-house control lines to introduce our point mutation of interest. From our most recent data from this edited line, we determined that there were no differences between CTRL-iso2 and iso-G1744* in all parameters used to analyze the intrinsic and extrinsic parameters. This was both reassuring and confusing when extrapolating the interpretation of the data. As it stood, having a LoF variant that produced no deleterious effects on the iNeurons was novel and corroborated our previous findings (Chapter 2, Figure 2K-R). However, what was unexpected was the observation of no enhancement of the action potential waveform. Two main hypotheses were thought of to aid in explaining our findings. The first was genome instability after genetically modifying the DNA. It has

extensively been reported that CRISPR-Cas9 editing is most suitable for academic investigations and not clinical applications because of three main factors. These included the low efficiency in gene repair, mosaicism with unintended mutations, and the instability of the genome (Alanis-Lobato et al., 2021; Tang et al., 2017). Even though karyotyping was done and produced negative results, WGS was not once again done after the genetic manipulation. Since the process of electroporating and delivering a genetic payload to the cells is a stressful event, it is not uncommon to assume regions outside of our targeted area were affected by instability leading to other spontaneous off-target mutations. Further, Cas9 cleavage of unintended genomic sites is well known, PAM sites are numerous throughout the genome, and even with the gRNA annealing to the correct site, errors can still occur in regions with high homology outside of your intended target loci (Naeem et al., 2020). Due to the origins and original use case of the CRISPR-Cas9 system in bacteria, specificity was high in bacterial hosts because of the small genome size (Naeem et al., 2020). However, in the eukaryotic genome, which is 1000 times larger, specificity is decreased and errors are more common. Even with *in silico* analysis ahead of experimentation, there are still challenges for optimizing gene editing. Some difficulties include high homology regions due to paralogs, lack of the appropriate PAM site close to your edits, and G-C rich areas.

Secondly, upon further analysis of our data, we discovered a trend that may speak to the development of our iNeurons in our isogenic modelling of the p.G1744* variant. Previously in Chapter 2, we had performed the patch-clamp recordings for the iso-G1744* iNeurons between DIV 25 – 28. However, this time we slightly shifted the window two days earlier. When looking at the data longitudinally we observed indicators that may speak to the

further maturation of the iNeurons. When examining the data, we noticed that CTRL-iso2 iNeurons that were recorded on DIV 23 and 24 were more robust in their characteristics, especially in the action potential parameters (Figure S2). Even though this data was not statistically significant, it pointed towards a potential increase in maturation compared to the iso-G1744* iNeurons. Data analyzed on DIV 25 for most if not all intrinsic parameters showed that the means of both CTRL-iso2 and iso-G1744* iNeurons were identical, suggesting that iso-G1744* iNeurons made subtle but important increases. On the last day of recording DIV 26 iNeurons reversed in most parameters recapitulating the enhancements observed from the previous data (Figure S2). Unfortunately, since the sample size is decreased when splitting the data into recording days, the power of the experiment is decreased due to the smaller sample size. This trend was promising since the trajectory of neuronal development of iso-G1744* iNeurons could be explained via the MEA data (Chapter 2, Figure 4). The MEA data highlighted that there were early impairments that reversed later in development; we suggested this reversal mimicked the clinical phenotypes of ASD with later development of seizures. In isogenic modelling, the data is suggestive that this could also be occurring, and that later recording timepoints would capture the robust enhancement.
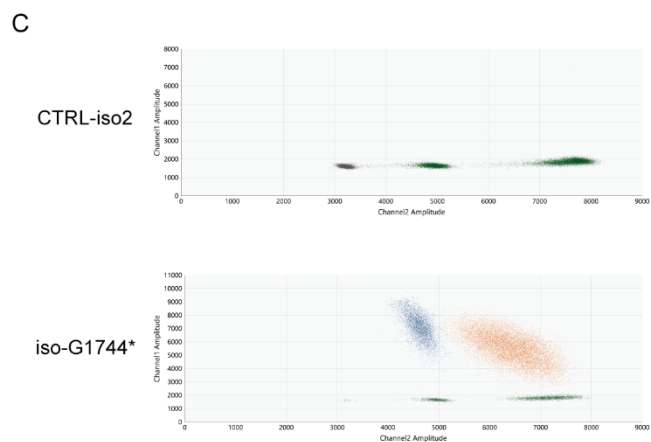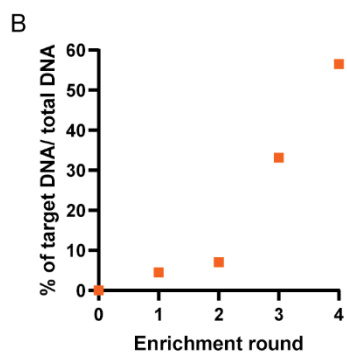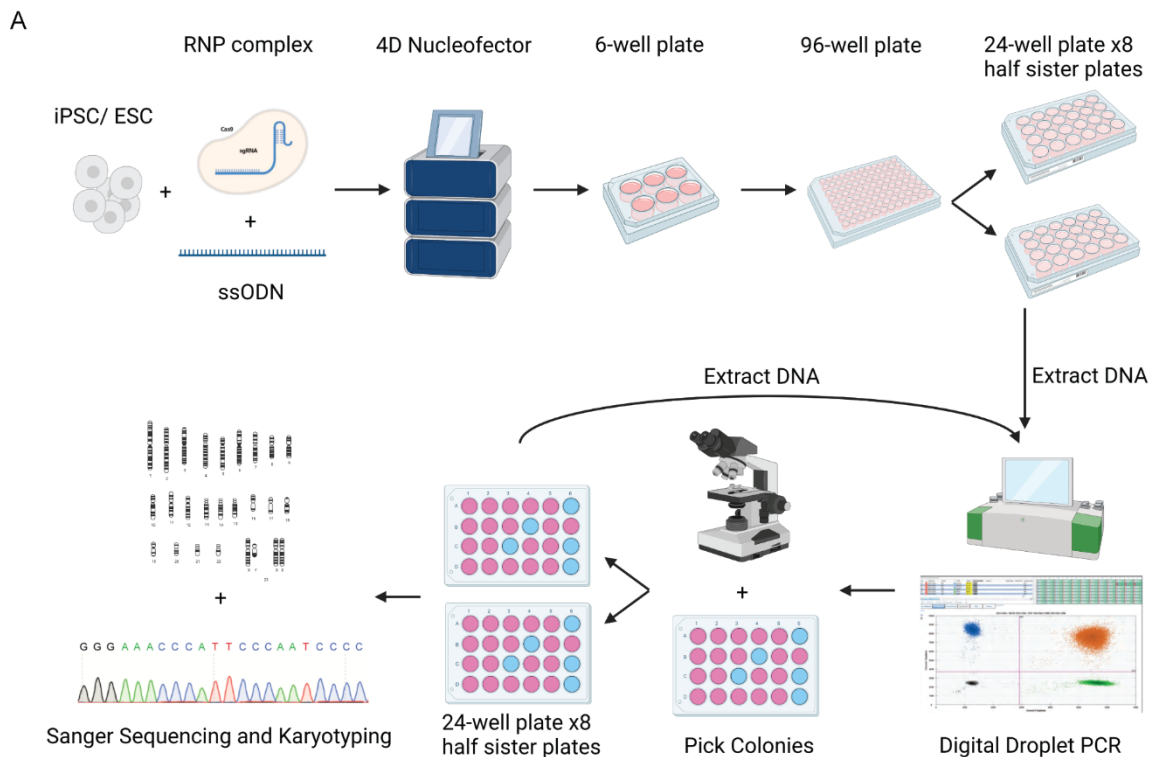
Figure 1. Mutagenesis workflow and validation of the p.G1744* variant in iPSCs.

A) Genetic engineering enrichment pipeline for iPSCs harbouring the p.G1744* variant.

B) Trajectory of the enrichment pipeline for iPSCs harbouring the p.G1744* variant.

C) 2D plot from ddPCR showing the detection of MGB® Taqman probes for the target

DNA. Top: represents the 2D plot wildtype DNA in the CTRL-iso2 iPSCs. Bottom:

represents the 2D plot for the variant basepair substitution in iso-G1744* iPSCs.
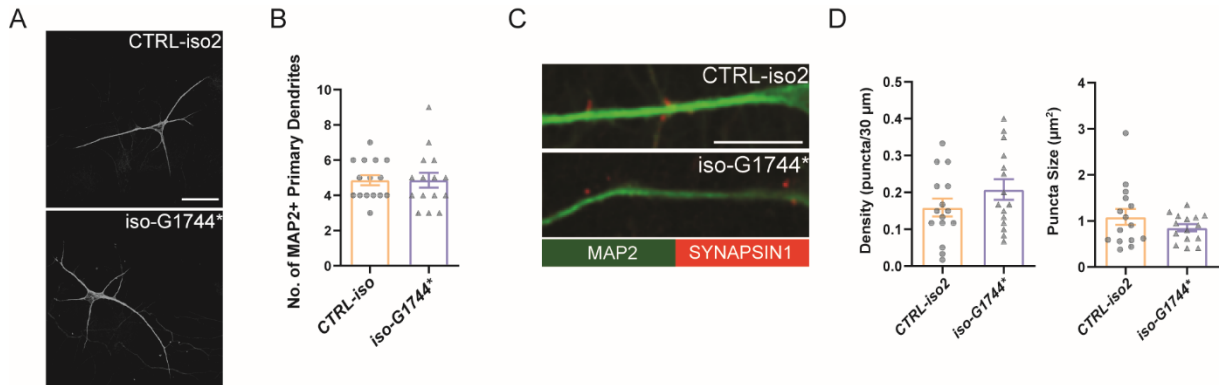
Figure 2. SCN2A$^{+/p.G1744*}$ variant's effects in isogenic iNeuron morphology.

A) Representative images of immunocytochemistry for dendrite complexity and analysis

of MAP2-positive primary dendrites.

B) Analysis of MAP2+ primary dendrites. CTRL-iso (n=15) and iso-G1744* (n=15)

iNeurons. 3 viral transductions. Scale bar, 40 μm.

C) Representative images and quantification of synaptic puncta density and size.

D) Analysis of synapse morphology for density and size of puncta along a MAP2+

dendrite. Left: synapse density, Right: puncta size. CTRL-iso (n=15) and iso-G1744*

(n=15) iNeurons. 3 viral transductions. Scale bar, 10 μm.
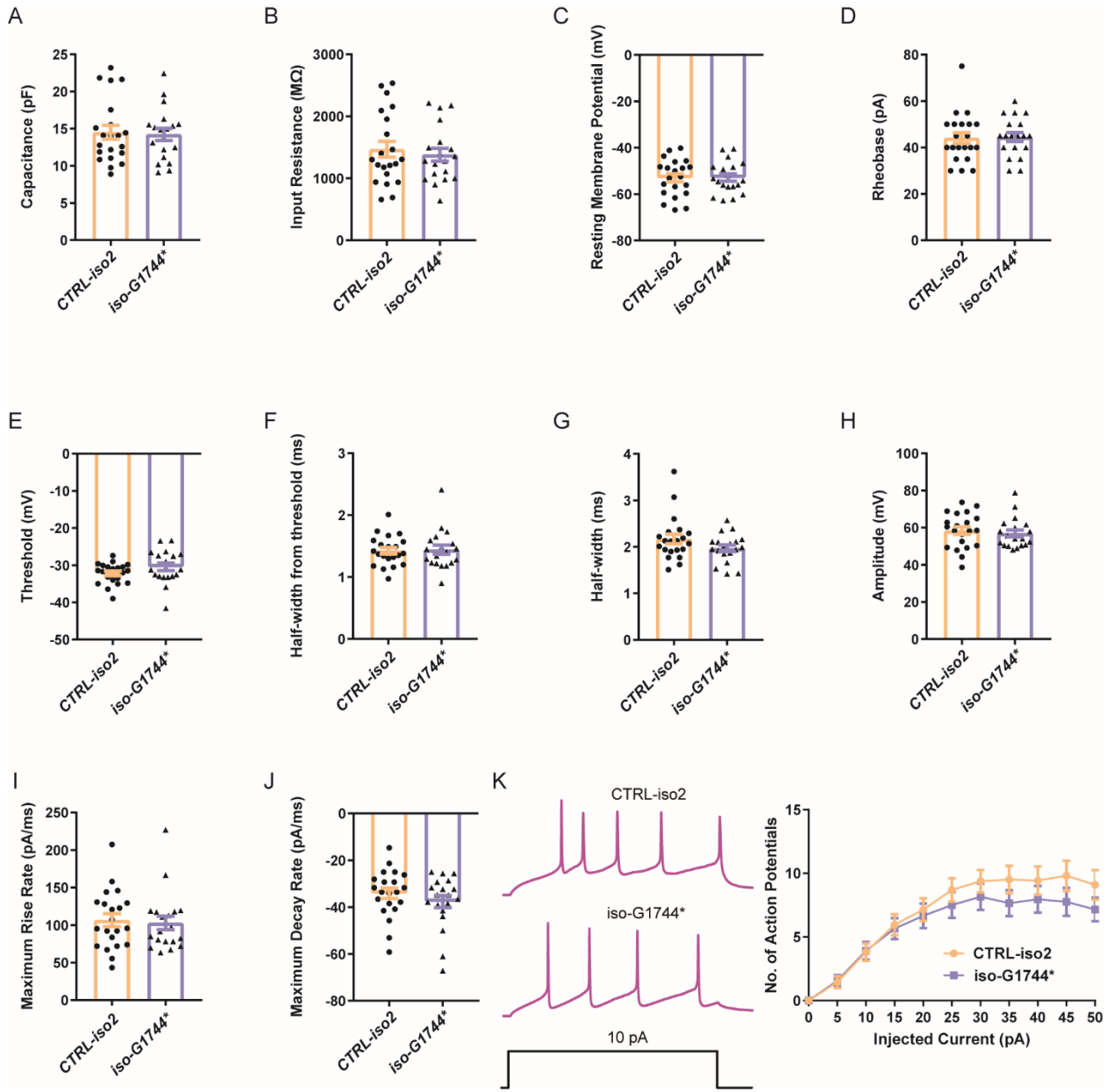
Figure 3. Bioelectric characteristics of isogenic *SCN2A* iNeurons harbouring the *de novo* p.G1744* variants.

A-J) Membrane and action potential properties of CTRL-iso2 and iso-G1744* iNeurons (n=21 and 19, respectively), 3 viral transductions. Data represent means ± SEM. *p < 0.05, **p < 0.01, Student's t-test. (A) cell capacitance, (B) input resistance, (C) resting membrane potential, (D), rheobase of action potential (E) threshold of the action potential, (F) half-width from threshold to amplitude, (G) half-width of the action potential, (H) amplitude of the action potential relative to threshold, (I) maximum rise rate from action potential threshold to amplitude, (J) maximum decay rate from action potential amplitude to threshold.

K) Repetitive firing properties of CTRL-iso2 and iso-G1744*. CTRL-iso2 (n=21) and iso-G1744* (n=19) iNeurons, 3 viral transductions. Data represent means ± SEM. *p < 0.05, **p < 0.01, Student's t-test.

Figure 4. Loss-of-function *SCN2A* variant p.G1744* has no effect on synaptic transmission.

A-C) Synaptic transmission representative traces and analysis of SCN2A deficient iNeurons. (A) Representative segment of synaptic transmission recording from CTRL-iso2 and iso-G1744* iNeurons. (B) sEPSC frequency from synaptic transmission. (C) sEPSC amplitude of synaptic transmission. CTRL-iso2 (n=21) and iso-G1744* (n=19) iNeurons. 3 viral transductions. Data represent means ± SEM. *p < 0.05, **p < 0.01, Student's t-test.
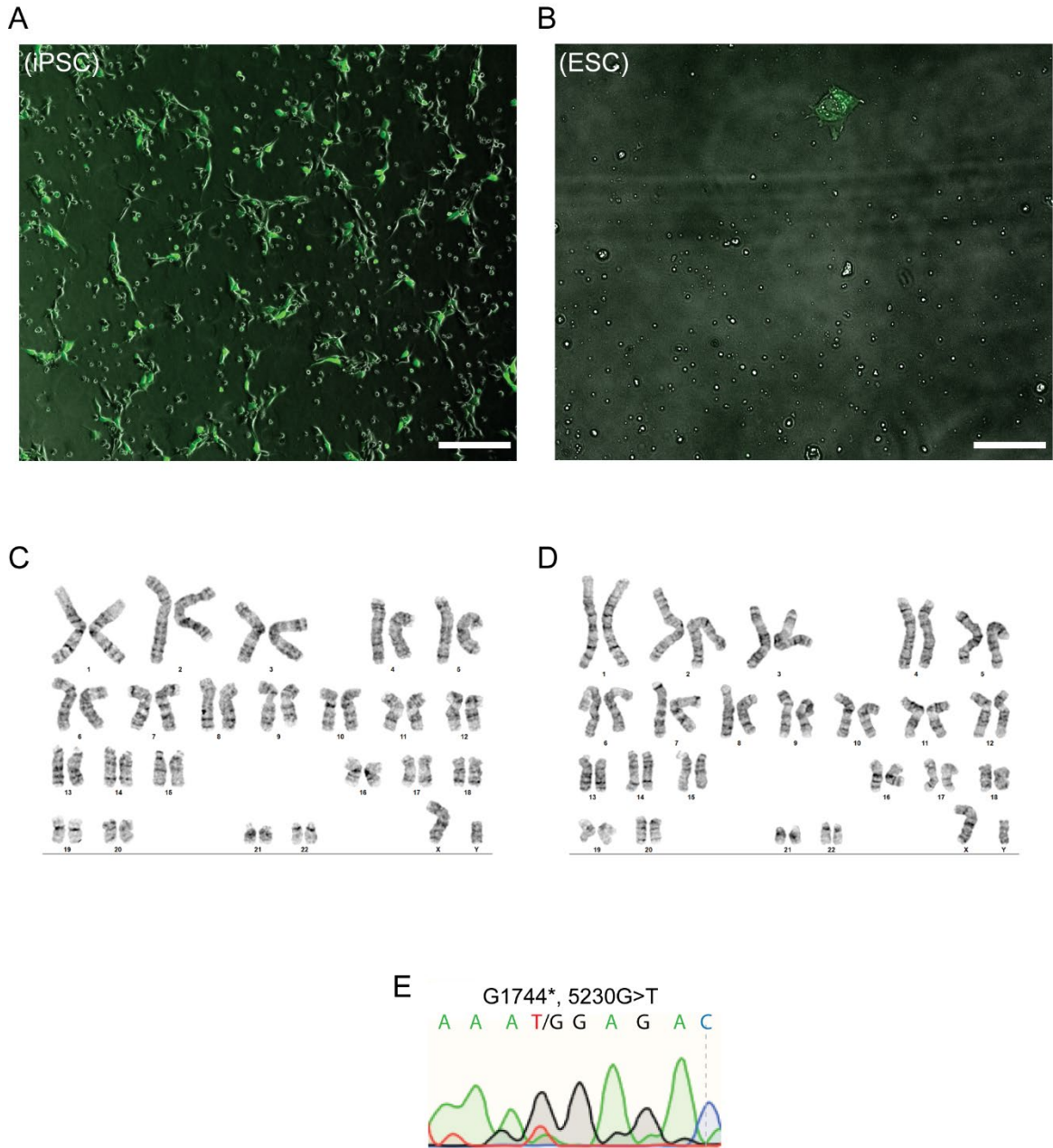
Figure S1. iPSC validations of two stem cell lines for the generation of an isogenic model.

A) Representative image of the 19-2-2 iPSCs 24 hr after nucleofection.

B) Representative image of the H1 ESCs 24 hr after nucleofection. Scale bar, 200 μm.

C) Karyotyping images of 19-2-2 (CTRL-iso2) iPSC chromosomes.

D) Karyotyping images of iso-G1744* iPSCs chromosomes.

E) Sanger sequencing results from iso-G1744* iPSCs indicating the point mutation.
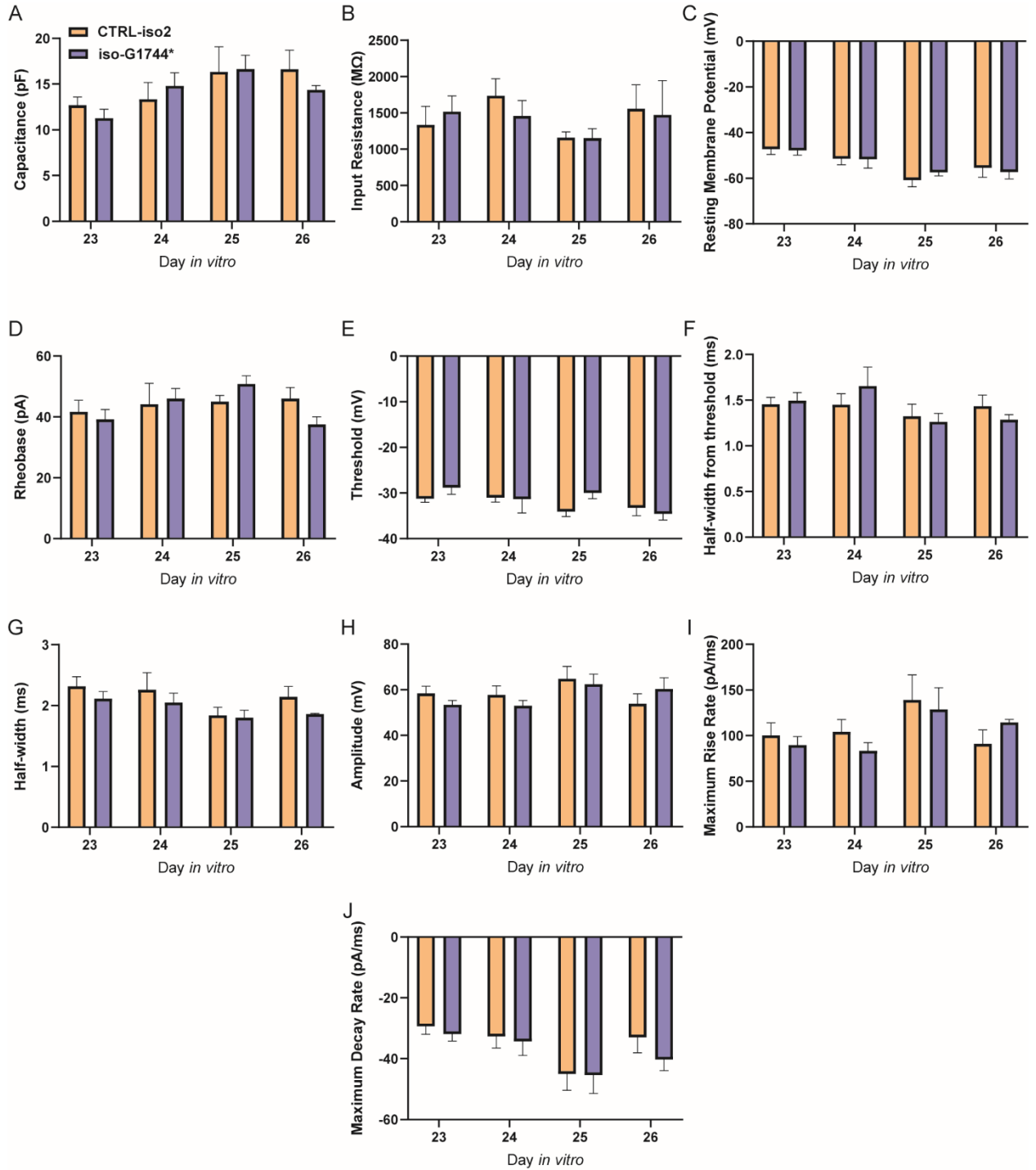
Figure S2. Developmental timeline of neuron intrinsics in isogenic $SCN2A^{+/p.G1744*}$

iNeurons suggests time-dependent phenotypes.

A-J) Membrane and action potential properties of CTRL-iso2 and iso-G1744* iNeurons

(N=21 and 19, respectively, per time point n = 2-6), 3 viral transductions. Data represent

means ± SEM. No statistical analysis done. (A) cell capacitance, (B) input resistance, (C)

resting membrane potential, (D), rheobase of action potential (E) threshold of the action

potential, (F) half-width from threshold to amplitude, (G) half-width of the action

potential, (H) amplitude of the action potential relative to threshold, (I) maximum rise

rate from action potential threshold to amplitude, (J) maximum decay rate from action

potential amplitude to threshold.

CHAPTER 5: SIGNIFICANCE AND FUTURE DIRECTIONS

5.1 Significance

With the evolution of NGS, the prevalence of ASD will continue to increase globally. Even with advancements in detection, our lack of knowledge of the etiology and molecular underpinnings of ASD impair our ability to resolve the cause. Functional sequencing studies have aided in highlighting high-risk gene targets for ASD, however functional experimentation is still needed to validate gene and protein function on a molecular and cellular level. To date, investigations of ASD-risk genes have had a uniform goal to determine convergence and divergence of molecular mechanisms, aiding in the grouping of genes by end phenotypes and mechanisms. However, SCN2A and the variants it harbours lag behind in experimental classification.

In the work presented in this thesis, we highlight two ASD-associated *de novo* truncating variants classified as LoF, one isogenic *SCN2A* KO model, and later one isogenic *SCN2A* variant model. We emphasized the need for a better classification system for *SCN2A* variants, as we demonstrated LoF variants can have null or enhancing effects on neurons. Moreover, changes in synaptic morphology but not dendrite morphology indicated altered *SCN2A* expression can in fact influence distal regions of neurons, in this case at the synapse. This was corroborated by electrophysiological recordings showing reductions in synaptic communication. Aside from the differential intrinsic parameters that were variant location dependent, activity-dependent gene and protein regulation were present in the most severe variant. Proteomic analysis of these iNeurons determined differential proteomic expression that clustered and enriched into various cellular pathways. Further, since we

were able to validate the mitochondrial function cluster from our proteomic analysis, a novel mechanism is now known and associated with SCN2A variants. This information may help future researchers expand their investigations beyond the traditional ion channel characterization. This work adds to our understanding of how *SCN2A* variant location and classification may determine cellular phenotypes, and how downstream signalling is altered because of atypical neuronal activity.

5.2 Exploring promising ASD therapeutic interventions for voltage-gated sodium channels

ASD represents a group of highly heterogeneous NDDs with a poor understanding of the etiology. Yet, investigations on many ASD-risk genes have provided insight into uncharacterized gene functions, and variant validations from sequencing studies. The work presented in this thesis revealed the importance of understanding how (1) current classifications of variants and mutations need to be less simplistic, and (2) changes in neuronal activity can have profound changes in the proteome and downstream cellular signalling. In many of the well-known ASD-risk gene studies focusing on human cellular models, rescues are more forthcoming to perform due to the resulting proteins' function in gene expression regulation, scaffolding, and cellular communication. However, cellular rescues targeting ion channels, in particular sodium channels, are drastically more difficult to perform. Studies have long pursued to discover pharmacological and chemical agents to alter voltage-gated sodium channel function, with some becoming Food and Drug Administration (FDA) approved with specific use cases (Nardi et al., 2012). In the CNS, there are nine drugs targeted at epilepsy that overlap with other neuropathologies including

Parkinson's disease, and bipolar disorder. Moreover, drugs in the same classification can have significant differences. For example, Lamotrigine, an anticonvulsant is reported to be effective against absence seizures, were phenytoin, another anticonvulsant, is not (Nardi et al., 2012). A similar concept was experimentally investigated where they created an isogenic line using CRISPR-Cas9 for the L1342P variant in iPSCs (Que et al., 2021b). This variant is a recurrent variant associated with early-onset encephalopathy and intractable seizures. Neurons harbouring this variant revealed increases in many intrinsic parameters including rheobase, threshold, and amplitude. Furthermore, they saw increases in the whole-cell inward currents, repetitive firing, and bursting events in their MEA assay. Clinical reports indicated that patients with this variant had minimal response to commonly used antiepileptic drugs (Hackenberg et al., 2014). They were able to recapitulate these reports in their cellular model using the previously mentioned anticonvulsant phenytoin. Phenytoin is a non-specific sodium channel blocker that is used to inhibit high-frequency spiking in seizure episodes (Boerma et al., 2016; Braakman et al., 2017; Gardella et al., 2018; Gorman and King, 2017). Their study showed that phenytoin was only useful at unsafe concentrations in neurons with the L1342P variant, while at lower concentrations control neuron firing was reduced. This spoke to the variance of general sodium channel blockers as the efficacy can drastically change across patients and their variants. Lastly, blockers that target Navs, aren't isoform-specific for Nav1.2; in addition, many openers and blockers of Nav1.2 are neurotoxins and are only useful for proof of concept and not clinical applications.

Researchers have completed many rescues experiments for proof-of-concept investigations that are important to understanding the underlying pathophysiology of *SCN2A* variants. In a recent study, researchers found that in gene trap *Scn2a* KO mice (resembling ~70% gene expression reduction), hyperexcitability was present (Zhang et al., 2021a). This included an enhancement in the number of action potentials consecutively fired, and more depolarized resting membrane potential. Further, they determined that the hyperexcitable phenotype was potassium current dependent. Specifically, the gene expression of $K_V1.1$, $K_V1.2$, and other potassium channels was decreased in mouse *Scn2a* KO medium spiny neurons. In a co-submission, another article found similar deficiencies in potassium currents in *Scn2a* KO pyramidal neurons (Spratt et al., 2021). They rescued their phenotypes using a dynamic clamp and injecting 200 nS of $K_V1.2$. This partially rescued the high-frequency bursting occurring in the first 50 ms of the firing/current curve but not the other 250 ms in their KO neurons. Once again, this proved to be an academic exercise in rescuing a phenotype but clinical applications would be difficult. Antisense oligonucleotide (ASO) therapies are promising for clinical applications and surmounting the difficulties that are associated with targeting ion channels. ASOs are synthetic single-stranded nucleotides that target and bind complementary to the mRNA of a gene of interest (Bajan and Hutvagner, 2020; Dhuri et al., 2020; Hill and Meisler, 2021). The binding of ASOs disrupts mRNA function by preventing translation. Because of this sequence specificity, ASOs are highly specific with low off-targets, making proteins that are difficult to target with drugs accessible through expression targeting (Hill and Meisler, 2021). Further, patient variant targeting is specific since sequences of the ASO are often 13 – 20

bp. Recently, a recurrent *de novo* heterozygous p.R1872W patient variant in *Scn8a* was expressed in mice, with known phenotypes of early seizure onset and premature death (Lenk et al., 2020). In cases where missense variants increase neuronal activity and have a clinically associated diagnosis of EE, expression of the protein needs to be decreased. This group administered *Scn8a* mutant mice with an ASD through intracerebroventricular injection and postnatal day 2, before symptoms. It was reported that *Scn8a* mutant mice receiving two treatments of ASO lived for 9 weeks, where untreated mice lived for 2 weeks. Remarkably, *Scn8a* transcript levels were reduced to control levels after three weeks of treatment. Additionally, they found that survivability was ASO dose-dependent. A similar application was used to study a recurring human p.R188Q missense variant associated with developmental and EE (Li et al., 2021b). Genetically engineered mice harboured this variant, and results followed suite with the prior SCN8A investigation. *Scn2a* mRNA levels were reduced after intracerebroventricular ASO administration at P1-2, and increased life span and reduced seizure occurrence were reported. As of early 2022, there are 15 approved ASO therapies approved by the FDA for rare diseases and four for Duchenne muscular dystrophy. In the case of core ASD phenotypes associated with SCN2A LoF variants, ASOs would need to increase gene expression to negate the hypoexcitable phenotype often reported. Moving forward, advances are needed to investigate ASOs that increase transcript and protein expression in a NDD context. Modified ASOs that bind to mRNA in upstream of the open reading frames have been shown to increase protein expression *in vivo* (Liang et al., 2016). More effort and resources are need to investigate the use cases of these ASOs in patient variants that do not have an epileptic spectrum regarding Navs.

5.3 Future Directions

Future studies should continue to experimentally validate many of the computation studies of *SCN2A* variants. More recent papers have begun to genetically edit iPSC lines and create isogenic models of known variants to better elucidate their pathophysiology (Que et al., 2021a). As human cellular modelling capabilities advance, one area that is currently lacking in *SCN2A* investigations, is the human development aspect. *SCN2A* reports and those of the variants it harbours have focused solely on postnatal neurons, with only iPSC-derived neurons recapitulating embryonic timepoints due to their maturation plateau. Studies like the one we presented here showcase that activity-dependent gene and protein regulation of signaling pathways can happen early. Currently, we have no insights into the initial onset of dysfunction, and what signalling outcomes are disrupted from that onset. Furthermore, questions of altered cellular fate and fitness arise since SCN2A is solely expressed for excitation in the cortex until perinatal periods. Capturing the developmental stages of the cortex can be helpful when isolating variants, and this is where 3D modelling using organoids can be advantageous. Adding in a spatiotemporal aspect provides a better platform to investigate many stages of development including micro (proliferation and differentiation) to macro (cortical layer development) phenotypes. To date, there are no *SCN2A* human brain organoid papers. This highlights the necessity for further application of human cellular models toward SCN2A channelopathies and their variants.

REFERENCES

Abrahams, B.S., Arking, D.E., Campbell, D.B., Mefford, H.C., Morrow, E.M., Weiss, L.A., Menashe, I., Wadkins, T., Banerjee-Basu, S., and Packer, A. (2013). SFARI Gene 2.0: A community-driven knowledgebase for the autism spectrum disorders (ASDs). Mol. Autism *4*, 1–3.

Abudayyeh, O.O., Gootenberg, J.S., Konermann, S., Joung, J., Slaymaker, I.M., Cox, D.B.T., Shmakov, S., Makarova, K.S., Semenova, E., Minakhin, L., et al. (2016). C2c2 is a single-component programmable RNA-guided RNA-targeting CRISPR effector. Science (80-.). *353*.

Acab, A., and Muotri, A.R. (2015). The Use of Induced Pluripotent Stem Cell Technology to Advance Autism Research and Treatment. Neurotherapeutics *12*, 534–545.

Agrawal, S., Rao, S.C., Bulsara, M.K., and Patole, S.K. (2018). Prevalence of autism spectrum disorder in preterm infants: A meta-Analysis. Pediatrics *142*, 20180134.

Aitken, C.E., and Lorsch, J.R. (2012). A mechanistic overview of translation initiation in eukaryotes. Nat. Struct. Mol. Biol. *19*, 568–576.

Alanis-Lobato, G., Zohren, J., McCarthy, A., Fogarty, N.M.E., Kubikova, N., Hardman, E., Greco, M., Wells, D., Turner, J.M.A., and Niakan, K.K. (2021). Frequent loss of heterozygosity in CRISPR-Cas9-edited early human embryos. Proc. Natl. Acad. Sci. U. S. A. *118*, e2004832117.

Amin, N.D., and Paşca, S.P. (2018). Building Models of Brain Disorders with Three-

Dimensional Organoids. Neuron *100*, 389–405.

Amorim, I.S., Lach, G., and Gkogkas, C.G. (2018). The Role of the Eukaryotic Translation Initiation Factor 4E (eIF4E) in Neuropsychiatric Disorders. Front. Genet. *9*, 23.

An, J.Y., Lin, K., Zhu, L., Werling, D.M., Dong, S., Brand, H., Wang, H.Z., Zhao, X., Schwartz, G.B., Collins, R.L., et al. (2018). Genome-wide de novo risk score implicates promoter variation in autism spectrum disorder. Science (80-.). *362*.

Antion, M.D., Merhav, M., Hoeffer, C.A., Reis, G., Kozma, S.C., Thomas, G., Schuman, E.M., Rosenblum, K., and Klann, E. (2008). Removal of S6K1 and S6K2 leads to divergent alterations in learning, memory, and synaptic plasticity. Learn. Mem. *15*, 29–38.

Anttila, V., Bulik-Sullivan, B., Finucane, H.K., Walters, R.K., Bras, J., Duncan, L., Escott-Price, V., Falcone, G.J., Gormley, P., Malik, R., et al. (2018). Analysis of shared heritability in common disorders of the brain. Science (80-.). *360*.

Ashrafi, G., and Schwarz, T.L. (2013). The pathways of mitophagy for quality control and clearance of mitochondria. Cell Death Differ. *20*, 31–42.

Ashrafi, G., Schlehe, J.S., LaVoie, M.J., and Schwarz, T.L. (2014). Mitophagy of damaged mitochondria occurs locally in distal neuronal axons and requires PINK1 and Parkin. J. Cell Biol. *206*, 655–670.

Autism Spectrum Disorders Working Group of The Psychiatric Genomics Consortium

(2017). Meta-analysis of GWAS of over 16,000 individuals with autism spectrum disorder highlights a novel locus at 10q24.32 and a significant overlap with schizophrenia. Mol. Autism *8*, 21.

Bagley, J.A., Reumann, D., Bian, S., Lévi-Strauss, J., and Knoblich, J.A. (2017). Fused cerebral organoids model interactions between brain regions. Nat. Methods 2017 147 *14*, 743–751.

Bagni, C., Tassone, F., Neri, G., and Hagerman, R. (2012). Fragile X syndrome: Causes, diagnosis, mechanisms, and therapeutics. J. Clin. Invest. *122*, 4314–4322.

Bai, D., Yip, B.H.K., Windham, G.C., Sourander, A., Francis, R., Yoffe, R., Glasson, E., Mahjani, B., Suominen, A., Leonard, H., et al. (2019). Association of Genetic and Environmental Factors With Autism in a 5-Country Cohort. JAMA Psychiatry.

Baio, J., Wiggins, L., Christensen, D.L., Maenner, M.J., Daniels, J., Warren, Z., Kurzius-Spencer, M., Zahorodny, W., Rosenberg, C.R., White, T., et al. (2018). Prevalence of autism spectrum disorder among children aged 8 Years - Autism and developmental disabilities monitoring network, 11 Sites, United States, 2014. MMWR Surveill. Summ.

Bajan, S., and Hutvagner, G. (2020). RNA-Based Therapeutics: From Antisense Oligonucleotides to miRNAs. Cells *9*.

Banerjee, A., Ifrim, M.F., Valdez, A.N., Raj, N., and Bassell, G.J. (2018). Aberrant RNA translation in fragile X syndrome: From FMRP mechanisms to emerging therapeutic strategies. Brain Res. *1693*, 24–36.

Banko, J.L., Poulin, F., Hou, L., DeMaria, C.T., Sonenberg, N., and Klann, E. (2005). The translation repressor 4E-BP2 is critical for eIF4F complex formation, synaptic plasticity, and memory in the hippocampus. J. Neurosci. *25*, 9581–9590.

Banko, J.L., Merhav, M., Stern, E., Sonenberg, N., Rosenblum, K., and Klann, E. (2007). Behavioral alterations in mice lacking the translation repressor 4E-BP2. Neurobiol. Learn. Mem. *87*, 248–256.

Barrangou, R., and Horvath, P. (2017). A decade of discovery: CRISPR functions and applications. Nat. Microbiol. 2017 27 *2*, 1–9.

Barretto, N., Zhang, H., Powell, S.K., Fernando, M.B., Zhang, S., Flaherty, E.K., Ho, S.-M., Slesinger, P.A., Duan, J., and Brennand, K.J. (2020). ASCL1- and DLX2-induced GABAergic neurons from hiPSC-derived NPCs. J. Neurosci. Methods *334*, 108548.

Bateup, H.S., Johnson, C.A., Denefrio, C.L., Saulnier, J.L., Kornacker, K., and Sabatini, B.L. (2013). Excitatory/Inhibitory Synaptic Imbalance Leads to Hippocampal Hyperexcitability in Mouse Models of Tuberous Sclerosis. Neuron *78*, 510–522.

Baudouin, S.J., Gaudias, J., Gerharz, S., Hatstatt, L., Zhou, K., Punnakkal, P., Tanaka, K.F., Spooren, W., Hen, R., De Zeeuw, C.I., et al. (2012). Shared synaptic pathophysiology in syndromic and nonsyndromic rodent models of autism. Science (80-.). *338*, 128–132.

Baxter, A.J., Brugha, T.S., Erskine, H.E., Scheurer, R.W., Vos, T., and Scott, J.G. (2015). The epidemiology and global burden of autism spectrum disorders. Psychol. Med. *45*,

601–613.

Bear, M.F., Huber, K.M., and Warren, S.T. (2004). The mGluR theory of fragile X mental retardation. Trends Neurosci. *27*, 370–377.

Bechara, E.G., Didiot, M.C., Melko, M., Davidovic, L., Bensaid, M., Martin, P., Castets, M., Pognonec, P., Khandjian, E.W., Moine, H., et al. (2009). A novel function for fragile X mental retardation protein in translational activation. PLoS Biol. *7*.

Begemann, A., Acuña, M.A., Zweier, M., Vincent, M., Steindl, K., Bachmann-Gagescu, R., Hackenberg, A., Abela, L., Plecko, B., Kroell-Seger, J., et al. (2019). Further corroboration of distinct functional features in SCN2A variants causing intellectual disability or epileptic phenotypes. Mol. Med. *25*, 6.

El Bekay, R., Romero-Zerbo, Y., Decara, J., Sanchez-Salido, L., Del Arco-Herrera, I., Rodríguez-De Fonseca, F., and De Diego-Otero, Y. (2007). Enhanced markers of oxidative stress, altered antioxidants and NADPH-oxidase activation in brains from Fragile X mental retardation 1-deficient mice, a pathological model for Fragile X syndrome. Eur. J. Neurosci. *26*, 3169–3180.

Bélanger, M., Allaman, I., and Magistretti, P.J. (2011). Brain energy metabolism: Focus on Astrocyte-neuron metabolic cooperation. Cell Metab. *14*, 724–738.

Belkadi, A., Bolze, A., Itan, Y., Cobat, A., Vincent, Q.B., Antipenko, A., Shang, L., Boisson, B., Casanova, J.L., and Abel, L. (2015). Whole-genome sequencing is more powerful than whole-exome sequencing for detecting exome variants. Proc. Natl. Acad.

Sci. U. S. A. *112*, 5473–5478.

Belyeu, J.R., Brand, H., Wang, H., Zhao, X., Pedersen, B.S., Feusier, J., Gupta, M., Nicholas, T.J., Brown, J., Baird, L., et al. (2021). De novo structural mutation rates and gamete-of-origin biases revealed through genome sequencing of 2,396 families. Am. J. Hum. Genet. *108*, 597–607.

Ben-Shalom, R., Keeshen, C.M., Berrios, K.N., An, J.Y., Sanders, S.J., and Bender, K.J. (2017). Opposing Effects on NaV1.2 Function Underlie Differences Between SCN2A Variants Observed in Individuals With Autism Spectrum Disorder or Infantile Seizures. Biol. Psychiatry *82*, 224–232.

Bender, K.J., and Trussell, L.O. (2012). The Physiology of the Axon Initial Segment. Annu. Rev. Neurosci. *35*, 249–265.

Bender, A.C., Morse, R.P., Scott, R.C., Holmes, G.L., and Lenck-Santini, P.P. (2012). SCN1A mutations in Dravet syndrome: Impact of interneuron dysfunction on neural networks and cognitive outcome. Epilepsy Behav. *23*, 177–186.

Bhattacharya, A., Kaphzan, H., Alvarez-Dieppa, A.C., Murphy, J.P., Pierre, P., and Klann, E. (2012). Genetic Removal of p70 S6 Kinase 1 Corrects Molecular, Synaptic, and Behavioral Phenotypes in Fragile X Syndrome Mice. Neuron *76*, 325–337.

Bhattacharya, A., Mamcarz, M., Mullins, C., Choudhury, A., Boyle, R.G., Smith, D.G., Walker, D.W., and Klann, E. (2016). Targeting Translation Control with p70 S6 Kinase 1 Inhibitors to Reverse Phenotypes in Fragile X Syndrome Mice.

Neuropsychopharmacology *41*, 1991–2000.

Birey, F., Andersen, J., Makinson, C.D., Islam, S., Wei, W., Huber, N., Fan, H.C., Metzler, K.R.C., Panagiotakos, G., Thom, N., et al. (2017). Assembly of functionally integrated human forebrain spheroids. Nature *545*, 54–59.

Boerma, R.S., Braun, K.P., van de Broek, M.P.H., van Berkestijn, F.M.C., Swinkels, M.E., Hagebeuk, E.O., Lindhout, D., van Kempen, M., Boon, M., Nicolai, J., et al. (2016). Remarkable Phenytoin Sensitivity in 4 Children with SCN8A-related Epilepsy: A Molecular Neuropharmacological Approach. Neurotherapeutics *13*, 192–197.

Bogdanove, A.J., and Voytas, D.F. (2011). TAL Effectors: Customizable Proteins for DNA Targeting. Science (80-.). *333*, 1843–1846.

Boiko, T., Van Wart, A., CaldWell, J.H., Levinson, S.R., Trimmer, J.S., and Matthews, G. (2003). Functional Specialization of the Axon Initial Segment by Isoform-Specific Sodium Channel Targeting. J. Neurosci. *23*, 2306.

de Boni, L., Gasparoni, G., Haubenreich, C., Tierling, S., Schmitt, I., Peitz, M., Koch, P., Walter, J., Wüllner, U., and Brüstle, O. (2018). DNA methylation alterations in iPSC- and hESC-derived neurons: Potential implications for neurological disease modeling. Clin. Epigenetics *10*, 1–13.

Bozdagi, O., Tavassoli, T., and Buxbaum, J.D. (2013). Insulin-like growth factor-1 rescues synaptic and motor deficits in a mouse model of autism and developmental delay. Mol. Autism *4*, 9.

Braakman, H.M., Verhoeven, J.S., Erasmus, C.E., Haaxma, C.A., Willemsen, M.H., and Schelhaas, H.J. (2017). Phenytoin as a last-resort treatment in SCN8A encephalopathy. Epilepsia Open *2*, 343–344.

Brandler, W.M., Antaki, D., Gujral, M., Noor, A., Rosanio, G., Chapman, T.R., Barrera, D.J., Lin, G.N., Malhotra, D., Watts, A.C., et al. (2016). Frequency and Complexity of De Novo Structural Mutation in Autism. Am. J. Hum. Genet. *98*, 667–679.

Brentani, H., de Paula, C.S., Bordini, D., Rolim, D., Sato, F., Portolese, J., Pacifico, M.C., and McCracken, J.T. (2013). Autism spectrum disorders: an overview on diagnosis and treatment. Brazilian J. Psychiatry *35*, S62–S72.

Brian, J.A., Zwaigenbaum, L., and Ip, A. (2019). Standards of diagnostic assessment for autism spectrum disorder. Paediatr. Child Health *24*, 444–451.

Buiting, K., Williams, C., and Horsthemke, B. (2016). Angelman syndrome — insights into a rare neurogenetic disorder. Nat. Rev. Neurol. 2016 1210 *12*, 584–593.

Bunton-Stasyshyn, R.K.A., Saccon, R.A., Fratta, P., and Fisher, E.M.C. (2015). SOD1 Function and Its Implications for Amyotrophic Lateral Sclerosis Pathology: New and Renascent Themes. Neuroscientist *21*, 519–529.

Cakir, B., Xiang, Y., Tanaka, Y., Kural, M.H., Parent, M., Kang, Y.J., Chapeton, K., Patterson, B., Yuan, Y., He, C.S., et al. (2019). Engineering of human brain organoids with a functional vascular-like system. Nat. Methods 2019 1611 *16*, 1169–1175.

Canny, M.D., Moatti, N., Wan, L.C.K., Fradet-Turcotte, A., Krasner, D., Mateos-Gomez,

P.A., Zimmermann, M., Orthwein, A., Juang, Y.C., Zhang, W., et al. (2017). Inhibition of 53BP1 favors homology-dependent DNA repair and increases CRISPR–Cas9 genome-editing efficiency. Nat. Biotechnol. 2017 361 *36*, 95–102.

Carcamo-Orive, I., Hoffman, G.E., Cundiff, P., Beckmann, N.D., D'Souza, S.L., Knowles, J.W., Patel, A., Papatsenko, D., Abbasi, F., Reaven, G.M., et al. (2017). Analysis of Transcriptional Variability in a Large Human iPSC Library Reveals Genetic and Non-genetic Determinants of Heterogeneity. Cell Stem Cell *20*, 518-532.e9.

Carroll, L.S., Woolf, R., Ibrahim, Y., Williams, H.J., Dwyer, S., Walters, J., Kirov, G., O'Donovan, M.C., and Owen, M.J. (2016). Mutation screening of SCN2A in schizophrenia and identification of a novel loss-of-function mutation. Psychiatr. Genet. *26*, 60.

Chambers, S.M., Fasano, C.A., Papapetrou, E.P., Tomishima, M., Sadelain, M., and Studer, L. (2009). Highly efficient neural conversion of human ES and iPS cells by dual inhibition of SMAD signaling. Nat. Biotechnol. *27*, 275–280.

Chang, H.H.Y., Pannunzio, N.R., Adachi, N., and Lieber, M.R. (2017). Non-homologous DNA end joining and alternative pathways to double-strand break repair. Nat. Rev. Mol. Cell Biol. 2017 188 *18*, 495–506.

Chapman, J.R., Taylor, M.R.G., and Boulton, S.J. (2012). Playing the End Game: DNA Double-Strand Break Repair Pathway Choice. Mol. Cell *47*, 497–510.

Cheng, N., Rho, J.M., and Masino, S.A. (2017). Metabolic dysfunction underlying autism

spectrum disorder and potential treatment approaches. Front. Mol. Neurosci. *10*, 34.

Chevalier, B.S., Monnat, R.J., and Stoddard, B.L. (2001). The homing endonuclease I-CreI uses three metals, one of which is shared between the two active sites. Nat. Struct. Biol. 2001 84 *8*, 312–316.

Choi, K.-D., and Choi, J.-H. (2016). Episodic Ataxias: Clinical and Genetic Features. J. Mov. Disord. *9*, 129.

Choi, L., and An, J.Y. (2021). Genetic architecture of autism spectrum disorder: Lessons from large-scale genomic studies. Neurosci. Biobehav. Rev. *128*, 244–257.

Christensen, D.L., Braun, K.V.N., Baio, J., Bilder, D., Charles, J., Constantino, J.N., Daniels, J., Durkin, M.S., Fitzgerald, R.T., Kurzius-Spencer, M., et al. (2018). Prevalence and Characteristics of Autism Spectrum Disorder Among Children Aged 8 Years — Autism and Developmental Disabilities Monitoring Network, 11 Sites, United States, 2012. MMWR Surveill. Summ. *65*, 1.

Chu, V.T., Weber, T., Wefers, B., Wurst, W., Sander, S., Rajewsky, K., and Kühn, R. (2015). Increasing the efficiency of homology-directed repair for CRISPR-Cas9-induced precise gene editing in mammalian cells. Nat. Biotechnol. 2015 335 *33*, 543–548.

Chung, C., Ha, S., Kang, H., Lee, J., Um, S.M., Yan, H., Yoo, Y.E., Yoo, T., Jung, H., Lee, D., et al. (2019). Early Correction of N-Methyl-D-Aspartate Receptor Function Improves Autistic-like Social Behaviors in Adult Shank2 −/− Mice. Biol. Psychiatry *85*, 534–543.

Cioni, J.M., Lin, J.Q., Holtermann, A. V., Koppers, M., Jakobs, M.A.H., Azizi, A., Turner-Bridger, B., Shigeoka, T., Franze, K., Harris, W.A., et al. (2019). Late Endosomes Act as mRNA Translation Platforms and Sustain Mitochondria in Axons. Cell *176*, 56-72.e15.

Coker, S.B., and Melnyk, A.R. (1991). Rett Syndrome and Mitochondrial Enzyme Deficiencies. J. Child Neurol. *6*, 164–166.

Coleman, M., and Blass, J.P. (1985). Autism and lactic acidosis. J. Autism Dev. Disord. *15*, 1–8.

Cong, L., Ran, F.A., Cox, D., Lin, S., Barretto, R., Habib, N., Hsu, P.D., Wu, X., Jiang, W., Marraffini, L.A., et al. (2013). Multiplex genome engineering using CRISPR/Cas systems. Science (80-.). *339*, 819–823.

Costa-Mattioli, M., Sossin, W.S., Klann, E., and Sonenberg, N. (2009). Translational Control of Long-Lasting Synaptic Plasticity and Memory. Neuron *61*, 10–26.

Courchesne, E., Pramparo, T., Gazestani, V.H., Lombardo, M. V., Pierce, K., and Lewis, N.E. (2018). The ASD Living Biology: from cell proliferation to clinical phenotype. Mol. Psychiatry 2018 241 *24*, 88–107.

Cox, D.B.T., Platt, R.J., and Zhang, F. (2015). Therapeutic genome editing: prospects and challenges. Nat. Med. 2015 212 *21*, 121–131.

Crawford, K., Xian, J., Helbig, K.L., Galer, P.D., Parthasarathy, S., Lewis-Smith, D., Kaufman, M.C., Fitch, E., Ganesan, S., O'Brien, M., et al. (2021). Computational

analysis of 10,860 phenotypic annotations in individuals with SCN2A-related disorders. Genet. Med. 2021 237 *23*, 1263–1272.

Croen, L.A., Qian, Y., Ashwood, P., Zerbo, O., Schendel, D., Pinto-Martin, J., Daniele Fallin, M., Levy, S., Schieve, L.A., Yeargin-Allsopp, M., et al. (2019). Infection and Fever in Pregnancy and Autism Spectrum Disorders: Findings from the Study to Explore Early Development. Autism Res. *12*, 1551.

Culotta, L., and Penzes, P. (2020). Exploring the mechanisms underlying excitation/inhibition imbalance in human iPSC-derived models of ASD. Mol. Autism *11*.

Davuluri, R. V., Suzuki, Y., Sugano, S., Plass, C., and Huang, T.H.M. (2008). The functional consequences of alternative promoter use in mammalian genomes. Trends Genet. *24*, 167–177.

Deneault, E., White, S.H., Rodrigues, D.C., Ross, P.J., Faheem, M., Zaslavsky, K., Wang, Z., Alexandrova, R., Pellecchia, G., Wei, W., et al. (2018). Complete Disruption of Autism-Susceptibility Genes by Gene Editing Predominantly Reduces Functional Connectivity of Isogenic Human Neurons. Stem Cell Reports *11*, 1211–1225.

Deneault, E., Faheem, M., White, S.H., Rodrigues, D.C., Sun, S., Wei, W., Piekna, A., Thompson, T., Howe, J.L., Chalil, L., et al. (2019). CNTN5-/+or EHMT2-/+human iPSC-derived neurons from individuals with autism develop hyperactive neuronal networks. Elife *8*, 1–26.

Dhuri, K., Bechtold, C., Quijano, E., Pham, H., Gupta, A., Vikram, A., and Bahal, R.

(2020). Antisense Oligonucleotides: An Emerging Area in Drug Discovery and Development. J. Clin. Med. *9*, 1–24.

Dickinson, D., Straub, R.E., Trampush, J.W., Gao, Y., Feng, N., Xie, B., Shin, J.H., Lim, H.K., Ursini, G., Bigos, K.L., et al. (2014). Differential Effects of Common Variants in SCN2A on General Cognitive Ability, Brain Physiology, and messenger RNA Expression in Schizophrenia Cases and Control Individuals. JAMA Psychiatry *71*, 647–656.

De Diego-Otero, Y., Romero-Zerbo, Y., Bekay, R. El, Decara, J., Sanchez, L., Fonseca, F.R. De, and Arco-Herrera, I. Del (2009). α-Tocopherol protects against oxidative stress in the fragile X knockout mouse: An experimental therapeutic approach for the Fmr1 deficiency. Neuropsychopharmacology *34*, 1011–1026.

Divakaruni, S.S., Van Dyke, A.M., Chandra, R., LeGates, T.A., Contreras, M., Dharmasri, P.A., Higgs, H.N., Lobo, M.K., Thompson, S.M., and Blanpied, T.A. (2018). Long-Term Potentiation Requires a Rapid Burst of Dendritic Mitochondrial Fission during Induction. Neuron.

Dölen, G., Osterweil, E., Rao, B.S.S., Smith, G.B., Auerbach, B.D., Chattarji, S., and Bear, M.F. (2007). Correction of Fragile X Syndrome in Mice. Neuron *56*, 955–962.

Dong, D., Ren, K., Qiu, X., Zheng, J., Guo, M., Guan, X., Liu, H., Li, N., Zhang, B., Yang, D., et al. (2016). The crystal structure of Cpf1 in complex with CRISPR RNA. Nat. 2016 5327600 *532*, 522–526.

Ten Donkelaar, H.J., and van der Vliet, T. (2006). Overview of the Development of the

Human Brain and Spinal Cord. Clin. Neuroembryology 1–45.

Ten Donkelaar, H.J., Yamada, S., Shiota, K., and Van Der Vliet, T. (2014). Overview of the development of the human brain and spinal cord. Clin. Neuroembryology Dev. Dev. Disord. Hum. Cent. Nerv. Syst. 1–52.

Eaton, M., Zhang, J., Ma, Z., Park, A.C., Lietzke, E., Romero, C.M., Liu, Y., Coleman, E.R., Chen, X., Xiao, T., et al. (2021). Generation and basic characterization of a gene-trap knockout mouse model of Scn2a with a substantial reduction of voltage-gated sodium channel Nav1.2 expression. Genes, Brain Behav. *20*, e12725.

Ebert, D.H., and Greenberg, M.E. (2013). Activity-dependent neuronal signalling and autism spectrum disorder. Nat. 2013 4937432 *493*, 327.

Ebrahimi-Fakhari, D., Saffari, A., Wahlster, L., Di Nardo, A., Turner, D., Lewis, T.L., Conrad, C., Rothberg, J.M., Lipton, J.O., Kölker, S., et al. (2016). Impaired Mitochondrial Dynamics and Mitophagy in Neuronal Models of Tuberous Sclerosis Complex. Cell Rep. *17*, 1053–1070.

Echevarria-Cooper, D.M., Hawkins, N.A., Misra, S.N., Huffman, A., Thaxton, T., Thompson, C.H., Ben-Shalom, R., Nelson, A.D., Lipkin, A.M., George, A.L., et al. (2021). Cellular and behavioral effects of altered NaV1.2 sodium channel ion permeability in Scn2aK1422E mice. BioRxiv 2021.07.19.452930.

Eeg-Olofsson, O., Al-Zuhair, A.G.H., Teebi, A.S., and Al-Essa, M.M.N. (1989). Rett syndrome: Genetic clues based on mitochondrial changes in muscle. Am. J. Med. Genet.

32, 142–144.

Ehninger, D., Han, S., Shilyansky, C., Zhou, Y., Li, W., Kwiatkowski, D.J., Ramesh, V., and Silva, A.J. (2008). Reversal of learning deficits in a Tsc2+/- mouse model of tuberous sclerosis. Nat. Med. *14*, 843–848.

Epinat, J.C., Amould, S., Chames, P., Rochaix, P., Desfontaines, D., Puzin, C., Patin, A., Zanghellini, A., Pâques, F., and Lacroix, E. (2003). A novel engineered meganuclease induces homologous recombination in yeast and mammalian cells. Nucleic Acids Res. *31*, 2952–2962.

Espuny-Camacho, I., Michelsen, K.A., Gall, D., Linaro, D., Hasche, A., Bonnefont, J., Bali, C., Orduz, D., Bilheu, A., Herpoel, A., et al. (2013). Pyramidal Neurons Derived from Human Pluripotent Stem Cells Integrate Efficiently into Mouse Brain Circuits In Vivo. Neuron *77*, 440–456.

Ey, E., Yang, M., Katz, A.M., Woldeyohannes, L., Silverman, J.L., Leblond, C.S., Faure, P., Torquet, N., Le Sourd, A.M., Bourgeron, T., et al. (2012). Absence of deficits in social behaviors and ultrasonic vocalizations in later generations of mice lacking neuroligin4. Genes, Brain Behav. *11*, 928–941.

Falkmer, T., Anderson, K., Falkmer, M., and Horlin, C. (2013). Diagnostic procedures in autism spectrum disorders: A systematic literature review. Eur. Child Adolesc. Psychiatry *22*, 329–340.

Farley, M.A., McMahon, W.M., Fombonne, E., Jenson, W.R., Miller, J., Gardner, M.,

Block, H., Pingree, C.B., Ritvo, E.R., Ritvo, R.A., et al. (2009). Twenty-year outcome for individuals with autism and average or near-average cognitive abilities. Autism Res. *2*, 109–118.

Fernandez, A., Meechan, D.W., Karpinski, B.A., Paronett, E.M., Bryan, C.A., Rutz, H.L., Radin, E.A., Lubin, N., Bonner, E.R., Popratiloff, A., et al. (2019). Mitochondrial Dysfunction Leads to Cortical Under-Connectivity and Cognitive Impairment. Neuron *102*, 1127-1142.e3.

De Filippis, M., and Wagner, K.D. (2016). Treatment of Autism Spectrum Disorder in Children and Adolescents. Psychopharmacol. Bull. *46*, 18.

Flaherty, E., Zhu, S., Barretto, N., Cheng, E., Deans, P.J.M., Fernando, M.B., Schrode, N., Francoeur, N., Antoine, A., Alganem, K., et al. (2019). Neuronal impact of patient-specific aberrant NRXN1α splicing. Nat. Genet. *51*, 1679–1690.

Folstein, S., and Rutter, M. (1977). Infantile autism: a genetic study of 21 twin pairs. J. Child Psychol. Psychiatry. *18*, 297–321.

Franco-Iborra, S., Vila, M., and Perier, C. (2018). Mitochondrial quality control in neurodegenerative diseases: Focus on Parkinson's disease and Huntington's disease. Front. Neurosci. *12*.

Freitag, C.M., Staal, W., Klauck, S.M., Duketis, E., and Waltes, R. (2010). Genetics of autistic disorders: review and clinical implications. Eur. Child Adolesc. Psychiatry *19*, 169–178.

Fromer, M., Pocklington, A.J., Kavanagh, D.H., Williams, H.J., Dwyer, S., Gormley, P., Georgieva, L., Rees, E., Palta, P., Ruderfer, D.M., et al. (2014). De novo mutations in schizophrenia implicate synaptic networks. Nat. 2014 5067487 *506*, 179–184.

Fukumitsu, K., Hatsukano, T., Yoshimura, A., Heuser, J., Fujishima, K., and Kengaku, M. (2016). Mitochondrial fission protein Drp1 regulates mitochondrial transport and dendritic arborization in cerebellar Purkinje cells. Mol. Cell. Neurosci. *71*, 56–65.

Gaily, E., Lommi, M., Lapatto, R., and Lehesjoki, A.E. (2016). Incidence and outcome of epilepsy syndromes with onset in the first year of life: A retrospective population-based study. Epilepsia *57*, 1594–1601.

Gaj, T., Gersbach, C.A., and Barbas, C.F. (2013). ZFN, TALEN, and CRISPR/Cas-based methods for genome engineering. Trends Biotechnol. *31*, 397–405.

Ganguly, K., Schinder, A.F., Wong, S.T., and Poo, M. ming (2001). GABA itself promotes the developmental switch of neuronal GABAergic responses from excitation to inhibition. Cell *105*, 521–532.

Gardella, E., Marini, C., Trivisano, M., Fitzgerald, M.P., Alber, M., Howell, K.B., Darra, F., Siliquini, S., Bölsterli, B.K., Masnada, S., et al. (2018). The phenotype of SCN8A developmental and epileptic encephalopathy. Neurology *91*, e1112–e1124.

Gaugler, T., Klei, L., Sanders, S.J., Bodea, C.A., Goldberg, A.P., Lee, A.B., Mahajan, M., Manaa, D., Pawitan, Y., Reichert, J., et al. (2014). Most genetic risk for autism resides with common variation. Nat. Genet. *46*, 881–885.

Gazina, E. V., Leaw, B.T.W., Richards, K.L., Wimmer, V.C., Kim, T.H., Aumann, T.D., Featherby, T.J., Churilov, L., Hammond, V.E., Reid, C.A., et al. (2015). 'Neonatal' Nav1.2 reduces neuronal excitability and affects seizure susceptibility and behaviour. Hum. Mol. Genet. *24*, 1457–1468.

Geschwind, D.H. (2011). Genetics of autism spectrum disorders. Trends Cogn. Sci. *15*, 409–416.

Geschwind, D.H., and Flint, J. (2015). Genetics and genomics of psychiatric disease. Science (80-.). *349*, 1489–1494.

Geschwind, D.H., and Rakic, P. (2013). Cortical evolution: Judge the brain by its cover. Neuron *80*, 633–647.

Gijtenbeek, M., Bogers, H., Groenenberg, I.A.L., Exalto, N., Willemsen, S.P., Steegers, E.A.P., Eilers, P.H.C., and Steegers-Theunissen, R.P.M. (2014). First trimester size charts of embryonic brain structures. Hum. Reprod. *29,* 201–207.

Gkogkas, C.G., Khoutorsky, A., Ran, I., Rampakakis, E., Nevarko, T., Weatherill, D.B., Vasuta, C., Yee, S., Truitt, M., Dallaire, P., et al. (2012). Autism-related deficits via dysregulated eIF4E-dependent translational control. Nature *493*, 371–377.

Goldmann, J.M., Wong, W.S.W., Pinelli, M., Farrah, T., Bodian, D., Stittrich, A.B., Glusman, G., Vissers, L.E.L.M., Hoischen, A., Roach, J.C., et al. (2016). Parent-of-origin-specific signatures of de novo mutations. Nat. Genet. 2016 488 *48*, 935–939.

Good, K. V., Vincent, J.B., and Ausió, J. (2021). MeCP2: The Genetic Driver of Rett

Syndrome Epigenetics. Front. Genet. *12*, 21.

Gordon, A., and Geschwind, D.H. (2020). Human in vitro models for understanding mechanisms of autism spectrum disorder. Mol. Autism *11*, 1–18.

Gordon, A., Yoon, S.J., Tran, S.S., Makinson, C.D., Park, J.Y., Andersen, J., Valencia, A.M., Horvath, S., Xiao, X., Huguenard, J.R., et al. (2021). Long-term maturation of human cortical organoids matches key early postnatal transitions. Nat. Neurosci. 2021 243 *24*, 331–342.

Gorman, K.M., and King, M.D. (2017). SCN2A p.Ala263Val Variant a Phenotype of Neonatal Seizures Followed by Paroxysmal Ataxia in Toddlers. Pediatr. Neurol. *67*, 111–112.

Graf, W.D., Marin-Garcia, J., Gao, H.G., Pizzo, S., Naviaux, R.K., Markusic, D., Barshop, B.A., Courchesne, E., and Haas, R.H. (2000). Autism associated with the mitochondrial DNA G8363A transfer RNA(Lys) mutation. J. Child Neurol. *15*, 357–361.

Großer, E., Hirt, U., Janc, O.A., Menzfeld, C., Fischer, M., Kempkes, B., Vogelgesang, S., Manzke, T.U., Opitz, L., Salinas-Riester, G., et al. (2012). Oxidative burden and mitochondrial dysfunction in a mouse model of Rett syndrome. Neurobiol. Dis. *48*, 102–114.

Grove, J., Ripke, S., Als, T.D., Mattheisen, M., Walters, R.K., Won, H., Pallesen, J., Agerbo, E., Andreassen, O.A., Anney, R., et al. (2019). Identification of common genetic risk variants for autism spectrum disorder. Nat. Genet. *51*, 431–444.

Guo, X., Bai, Y., Zhao, M., Zhou, M., Shen, Q., Yun, C.H., Zhang, H., Zhu, W.G., and Wang, J. (2018). Acetylation of 53BP1 dictates the DNA double strand break repair pathway. Nucleic Acids Res. *46*, 689–703.

Haas, R.H. (2010). Autism and mitochondrial disease. Dev. Disabil. Res. Rev. *16*, 144–153.

Hackenberg, A., Baumer, A., Sticht, H., Schmitt, B., Kroell-Seger, J., Wille, D., Joset, P., Papuc, S., Rauch, A., and Plecko, B. (2014). Infantile epileptic encephalopathy, transient choreoathetotic movements, and hypersomnia due to a de novo missense mutation in the scn2a gene. Neuropediatrics *45*, 261–264.

Hackley, C.R. (2021). A Novel Set of Cas9 Fusion Proteins to Stimulate Homologous Recombination: Cas9-HRs. Cris. J. *4*, 253–263.

Hallmayer, J., Cleveland, S., Torres, A., Phillips, J., Cohen, B., Torigoe, T., Miller, J., Fedele, A., Collins, J., Smith, K., et al. (2011). Genetic heritability and shared environmental factors among twin pairs with autism. Arch. Gen. Psychiatry *68*, 1095–1102.

Hayeems, R.Z., and Boycott, K.M. (2018). Genome-wide sequencing technologies: A primer for paediatricians. Paediatr. Child Health *23*, 191–197.

He, H.Y., and Cline, H.T. (2019). What Is Excitation/Inhibition and How Is It Regulated? A Case of the Elephant and the Wisemen. J. Exp. Neurosci. *13*.

Herlenius, E., Heron, S.E., Grinton, B.E., Keay, D., Scheffer, I.E., Mulley, J.C., and

Berkovic, S.F. (2007). SCN2A Mutations and Benign Familial Neonatal-Infantile Seizures: The Phenotypic Spectrum. Epilepsia *48*, 1138–1142.

Hill, S.F., and Meisler, M.H. (2021). Antisense Oligonucleotide Therapy for Neurodevelopmental Disorders. Dev. Neurosci. *43*, 247–252.

Ho, S.M., Hartley, B.J., TCW, J., Beaumont, M., Stafford, K., Slesinger, P.A., and Brennand, K.J. (2016). Rapid Ngn2-induction of excitatory neurons from hiPSC-derived neural progenitor cells. Methods *101*, 113.

Holland, L.Z., and Ocampo Daza, D. (2018). A new look at an old question: When did the second whole genome duplication occur in vertebrate evolution? Genome Biol. *19*, 1–4.

Hong, L., Zhang, M., Ly, O.T., Chen, H., Sridhar, A., Lambers, E., Chalazan, B., Youn, S.W., Maienschein-Cline, M., Feferman, L., et al. (2021). Human induced pluripotent stem cell-derived atrial cardiomyocytes carrying an SCN5A mutation identify nitric oxide signaling as a mediator of atrial fibrillation. Stem Cell Reports *16*, 1542–1554.

Hsu, P.D., Scott, D.A., Weinstein, J.A., Ran, F.A., Konermann, S., Agarwala, V., Li, Y., Fine, E.J., Wu, X., Shalem, O., et al. (2013). DNA targeting specificity of RNA-guided Cas9 nucleases. Nat. Biotechnol. 2013 319 *31*, 827–832.

Hsu, P.D., Lander, E.S., and Zhang, F. (2014). Development and applications of CRISPR-Cas9 for genome engineering. Cell *157*, 1262–1278.

Hu, B.Y., Weick, J.P., Yu, J., Ma, L.X., Zhang, X.Q., Thomson, J.A., and Zhang, S.C.

(2010). Neural differentiation of human induced pluripotent stem cells follows developmental principles but with variable potency. Proc. Natl. Acad. Sci. U. S. A. *107*, 4335–4340.

Hu, W., Tian, C., Li, T., Yang, M., Hou, H., and Shu, Y. (2009). Distinct contributions of Nav1.6 and Nav1.2 in action potential initiation and backpropagation. Nat. Neurosci. *12*, 996–1002.

Huang, C.Y.M., and Rasband, M.N. (2018). Axon initial segments: structure, function, and disease. Ann. N. Y. Acad. Sci. *1420*, 46.

Hulme, A.J., McArthur, J.R., Maksour, S., Miellet, S., Ooi, L., Adams, D.J., Finol-Urdaneta, R.K., and Dottori, M. (2020). Molecular and Functional Characterization of Neurogenin-2 Induced Human Sensory Neurons. Front. Cell. Neurosci. *0*, 425.

Husi, H., Ward, M.A., Choudhary, J.S., Blackstock, W.P., and Grant, S.G.N. (2000). Proteomic analysis of NMDA receptor-adhesion protein signaling complexes. Nat. Neurosci. *3*, 661–669.

Iakoucheva, L.M., Muotri, A.R., and Sebat, J. (2019). Getting to the Cores of Autism. Cell *178*, 1287–1298.

Iossifov, I., O'Roak, B.J., Sanders, S.J., Ronemus, M., Krumm, N., Levy, D., Stessman, H.A., Witherspoon, K.T., Vives, L., Patterson, K.E., et al. (2014). The contribution of de novo coding mutations to autism spectrum disorder. Nature *515*, 216–221.

Ip, J.P.K., Mellios, N., and Sur, M. (2018). Rett syndrome: insights into genetic,

molecular and circuit mechanisms. Nat. Rev. Neurosci. 2018 196 *19*, 368–382.

Jacquemont, S., Pacini, L., Jønch, A.E., Cencelli, G., Rozenberg, I., He, Y., D'Andrea, L., Pedini, G., Eldeeb, M., Willemsen, R., et al. (2018). Protein synthesis levels are increased in a subset of individuals with fragile X syndrome. Hum. Mol. Genet. *27*, 2039–2051.

Janc, O.A., and Müller, M. (2014). The free radical scavenger Trolox dampens neuronal hyperexcitability, reinstates synaptic plasticity, and improves hypoxia tolerance in a mouse model of Rett syndrome. Front. Cell. Neurosci. *8*.

Jeggo, P.A. (1998). 5 DNA Breakage and Repair. Adv. Genet. *38*, 185–218.

Jones, J.M., Dionne, L., Dell'Orco, J., Parent, R., Krueger, J.N., Cheng, X., Dib-Hajj, S.D., Bunton-Stasyshyn, R.K., Sharkey, L.M., Dowling, J.J., et al. (2016). Single amino acid deletion in transmembrane segment D4S6 of sodium channel Scn8a (Nav1.6) in a mouse mutant with a chronic movement disorder. Neurobiol. Dis. *89*, 36–45.

Jónsson, H., Sulem, P., Kehr, B., Kristmundsdottir, S., Zink, F., Hjartarson, E., Hardarson, M.T., Hjorleifsson, K.E., Eggertsson, H.P., Gudjonsson, S.A., et al. (2017). Parental influence on human germline de novo mutations in 1,548 trios from Iceland. Nat. 2017 5497673 *549*, 519–522.

Kathuria, A., Lopez-Lengowski, K., Vater, M., McPhie, D., Cohen, B.M., and Karmacharya, R. (2020). Transcriptome analysis and functional characterization of cerebral organoids in bipolar disorder. Genome Med. 2020 121 *12*, 1–16.

Kelleher, R.J., and Bear, M.F. (2008). The Autistic Neuron: Troubled Translation? Cell

135, 401–406.

Kelly, E., Schaeffer, S.M., Dhamne, S.C., Lipton, J.O., Lindemann, L., Honer, M., Jaeschke, G., Super, C.E., Lammers, S.H., Modi, M.E., et al. (2018). MGluR5 Modulation of Behavioral and Epileptic Phenotypes in a Mouse Model of Tuberous Sclerosis Complex. Neuropsychopharmacology *43*, 1457–1465.

Kepecs, A., and Fishell, G. (2014). Interneuron cell types are fit to function. Nature *505*, 318–326.

Khan, S., Ullah, M.W., Siddique, R., Nabi, G., Manan, S., Yousaf, M., and Hou, H. (2016). Role of Recombinant DNA Technology to Improve Life. Int. J. Genomics *2016*.

Kilpinen, H., Goncalves, A., Leha, A., Afzal, V., Alasoo, K., Ashford, S., Bala, S., Bensaddek, D., Casale, F.P., Culley, O.J., et al. (2017). Common genetic variation drives molecular heterogeneity in human iPSCs. Nat. 2017 5467658 *546*, 370–375.

Kim, J., Koo, B.K., and Knoblich, J.A. (2020). Human organoids: model systems for human biology and medicine. Nat. Rev. Mol. Cell Biol. *21*, 571–584.

Kim, J.H., Lee, H.K., Takamiya, K., and Huganir, R.L. (2003). The role of synaptic GTPase-activating protein in neuronal development and synaptic plasticity. J. Neurosci. *23*, 1119–1124.

Knott, G.J., and Doudna, J.A. (2018). CRISPR-Cas guides the future of genetic engineering. Science (80-.). *361*, 866–869.

Kohlnhofer, B., Liu, Y., Woodruff, G., Lovenberg, T., Bonaventure, P., and Harrington,

A.. (2021). The Schizophrenia Variant V1282F in SCN2A Causes Functional Impairment of NaV1.2. J. Schizophr. Res.

Kole, M.H.P., and Stuart, G.J. (2008). Is action potential threshold lowest in the axon? Nat. Neurosci. 2008 1111 *11*, 1253–1255.

Kole, M.H.P., and Stuart, G.J. (2012). Signal Processing in the Axon Initial Segment. Neuron *73*, 235–247.

Kole, M.H.P., Ilschner, S.U., Kampa, B.M., Williams, S.R., Ruben, P.C., and Stuart, G.J. (2008). Action potential generation requires a high sodium channel density in the axon initial segment. Nat. Neurosci. 2008 112 *11*, 178–186.

Kong, A., Frigge, M.L., Masson, G., Besenbacher, S., Sulem, P., Magnusson, G., Gudjonsson, S.A., Sigurdsson, A., Jonasdottir, A., Jonasdottir, A., et al. (2012). Rate of de novo mutations and the importance of father's age to disease risk. Nat. 2012 4887412 *488*, 471–475.

Koonin, E. V., and Makarova, K.S. (2019). Origins and evolution of CRISPR-Cas systems. Philos. Trans. R. Soc. B *374*.

Kriaucionis, S., Paterson, A., Curtis, J., Guy, J., MacLeod, N., and Bird, A. (2006). Gene Expression Analysis Exposes Mitochondrial Abnormalities in a Mouse Model of Rett Syndrome. Mol. Cell. Biol. *26*, 5033–5042.

Krumm, N., Turner, T.N., Baker, C., Vives, L., Mohajeri, K., Witherspoon, K., Raja, A., Coe, B.P., Stessman, H.A., He, Z.X., et al. (2015). Excess of rare, inherited truncating

mutations in autism. Nat. Genet. 2015 476 *47*, 582–588.

Kruth, K.A., Grisolano, T.M., Ahern, C.A., and Williams, A.J. (2020). SCN2A channelopathies in the autism spectrum of neuropsychiatric disorders: A role for pluripotent stem cells? Mol. Autism *11*, 1–11.

Kyttälä, A., Moraghebi, R., Valensisi, C., Kettunen, J., Andrus, C., Pasumarthy, K.K., Nakanishi, M., Nishimura, K., Ohtaka, M., Weltner, J., et al. (2016). Genetic Variability Overrides the Impact of Parental Cell Type and Determines iPSC Differentiation Potential. Stem Cell Reports *6*, 200–212.

De La Torre-Ubieta, L., Won, H., Stein, J.L., and Geschwind, D.H. (2016). Advancing the understanding of autism disease mechanisms through genetics. Nat. Med. *22*, 345–361.

Lancaster, M.A., and Knoblich, J.A. (2014). Generation of cerebral organoids from human pluripotent stem cells. Nat. Protoc. 2014 910 *9*, 2329–2340.

Lancaster, M.A., Renner, M., Martin, C.A., Wenzel, D., Bicknell, L.S., Hurles, M.E., Homfray, T., Penninger, J.M., Jackson, A.P., and Knoblich, J.A. (2013). Cerebral organoids model human brain development and microcephaly. Nature *501*, 373–379.

Lee, K.M., Hawi, Z.H., Parkington, H.C., Parish, C.L., Kumar, P. V., Polo, J.M., Bellgrove, M.A., and Tong, J. (2019). The application of human pluripotent stem cells to model the neuronal and glial components of neurodevelopmental disorders. Mol. Psychiatry 2019 252 *25*, 368–378.

Léna, I., and Mantegazza, M. (2019). NaV1.2 haploinsufficiency in Scn2a knock-out mice causes an autistic-like phenotype attenuated with age. Sci. Reports 2019 91 *9*, 1–14.

Lenk, G.M., Jafar-Nejad, P., Hill, S.F., Huffman, L.D., Smolen, C.E., Wagnon, J.L., Petit, H., Yu, W., Ziobro, J., Bhatia, K., et al. (2020). Scn8a Antisense Oligonucleotide Is Protective in Mouse Models of SCN8A Encephalopathy and Dravet Syndrome. Ann. Neurol. *87*, 339–346.

Lewis, T.L., Kwon, S.K., Lee, A., Shaw, R., and Polleux, F. (2018). MFF-dependent mitochondrial fission regulates presynaptic release and axon branching by limiting axonal mitochondria size. Nat. Commun. *9*.

Li, S., and Sheng, Z.H. (2021). Energy matters: presynaptic metabolism and the maintenance of synaptic transmission. Nat. Rev. Neurosci. 2021 231 *23*, 4–22.

Li, G., Wang, H., Zhang, X., Wu, Z., and Yang, H. (2021a). A Cas9-transcription factor fusion protein enhances homology-directed repair efficiency. J. Biol. Chem. *296*, 100525–100526.

Li, J., Ryan, S.K., Deboer, E., Cook, K., Fitzgerald, S., Lachman, H.M., Wallace, D.C., Goldberg, E.M., and Anderson, S.A. (2019). Mitochondrial deficits in human iPSC-derived neurons from patients with 22q11.2 deletion syndrome and schizophrenia. Transl. Psychiatry *9*, 1–10.

Li, M., Jancovski, N., Jafar-Nejad, P., Burbano, L.E., Rollo, B., Richards, K., Drew, L., Sedo, A., Heighway, J., Pachernegg, S., et al. (2021b). Antisense oligonucleotide therapy

reduces seizures and extends life span in an SCN2A gain-of-function epilepsy model. J. Clin. Invest. *131*.

Li, Y., Wang, H., Muffat, J., Cheng, A.W., Orlando, D.A., Lovén, J., Kwok, S.M., Feldman, D.A., Bateup, H.S., Gao, Q., et al. (2013). Global transcriptional and translational repression in human-embryonic- stem-cell-derived rett syndrome neurons. Cell Stem Cell *13*, 446–458.

Li, Z., Okamoto, K.I., Hayashi, Y., and Sheng, M. (2004). The importance of dendritic mitochondria in the morphogenesis and plasticity of spines and synapses. Cell *119*, 873–887.

Liang, X.H., Shen, W., Sun, H., Migawa, M.T., Vickers, T.A., and Crooke, S.T. (2016). Translation efficiency of mRNAs is increased by antisense oligonucleotides targeting upstream open reading frames. Nat. Biotechnol. 2016 348 *34*, 875–880.

Liao, Y., Anttonen, A.K., Liukkonen, E., Gaily, E., Maljevic, S., Schubert, S., Bellan-Koch, A., Petrou, S., Ahonen, V.E., Lerche, H., et al. (2010). SCN2A mutation associated with neonatal epilepsy, late-onset episodic ataxia, myoclonus, and pain. Neurology *75*, 1454–1458.

Lim, E.T., Uddin, M., De Rubeis, S., Chan, Y., Kamumbu, A.S., Zhang, X., D'Gama, A.M., Kim, S.N., Hill, R.S., Goldberg, A.P., et al. (2017). Rates, distribution and implications of postzygotic mosaic mutations in autism spectrum disorder. Nat. Neurosci. 2017 209 *20*, 1217–1224.

Lin, H.-C., He, Z., Ebert, S., Schörnig, M., Santel, M., Nikolova, M.T., Weigert, A., Hevers, W., Kasri, N.N., Taverna, E., et al. (2021). NGN2 induces diverse neuron types from human pluripotency. Stem Cell Reports.

Liu, M.-L., Zang, T., Zou, Y., Chang, J.C., Gibson, J.R., Huber, K.M., and Zhang, C.-L. (2013). Small molecules enable neurogenin 2 to efficiently convert human fibroblasts into cholinergic neurons. Nat. Commun. *4*, 2183.

Loebrich, S., and Nedivi, E. (2009). The function of activity-regulated genes in the nervous system. Physiol. Rev. *89*, 1079–1103.

Lu, X., Yang, J., and Xiang, Y. (2022). Modeling human neurodevelopmental diseases with brain organoids. Cell Regen. *11*, 1–13.

Ma, D., Salyakina, D., Jaworski, J.M., Konidari, I., Whitehead, P.L., Andersen, A.N., Hoffman, J.D., Slifer, S.H., Hedges, D.J., Cukier, H.N., et al. (2009). A genome-wide association study of autism reveals a common novel risk locus at 5p14.1. Ann. Hum. Genet. *73*, 263.

Ma, R., Deng, L., Xia, Y., Wei, X., Cao, Y., Guo, R., Zhang, R., Guo, J., Liang, D., and Wu, L. (2017). A clear bias in parental origin of de novo pathogenic CNVs related to intellectual disability, developmental delay and multiple congenital anomalies. Sci. Reports 2017 71 *7*, 1–9.

Ma, Z., Eaton, M., Liu, Y., Zhang, J., Chen, X., Tu, X., Shi, Y., Que, Z., Wettschurack, K., Zhang, Z., et al. (2022). Deficiency of autism-related Scn2a gene in mice disrupts

sleep patterns and circadian rhythms. Neurobiol. Dis. *168*, 105690.

Maenner, M.J., Shaw, K.A., Bakian, A. V., Bilder, D.A., Durkin, M.S., Esler, A., Furnier, S.M., Hallas, L., Hall-Lande, J., Hudson, A., et al. (2021). Prevalence and Characteristics of Autism Spectrum Disorder Among Children Aged 8 Years — Autism and Developmental Disabilities Monitoring Network, 11 Sites, United States, 2018. MMWR Surveill. Summ. *70*, 1.

Magistretti, P.J., and Allaman, I. (2015). A Cellular Perspective on Brain Energy Metabolism and Functional Imaging. Neuron *86*, 883–901.

Makarova, K.S., Wolf, Y.I., Iranzo, J., Shmakov, S.A., Alkhnbashi, O.S., Brouns, S.J.J., Charpentier, E., Cheng, D., Haft, D.H., Horvath, P., et al. (2019). Evolutionary classification of CRISPR–Cas systems: a burst of class 2 and derived variants. Nat. Rev. Microbiol. 2019 182 *18*, 67–83.

Mali, P., Yang, L., Esvelt, K.M., Aach, J., Guell, M., DiCarlo, J.E., Norville, J.E., and Church, G.M. (2013). RNA-guided human genome engineering via Cas9. Science (80-.). *339*, 823–826.

Malkova, N. V., Yu, C.Z., Hsiao, E.Y., Moore, M.J., and Patterson, P.H. (2012). Maternal immune activation yields offspring displaying mouse versions of the three core symptoms of autism. Brain. Behav. Immun. *26*, 607.

Marro, S.G., Chanda, S., Yang, N., Janas, J.A., Valperga, G., Trotter, J., Zhou, B., Merrill, S., Yousif, I., Shelby, H., et al. (2019). Neuroligin-4 Regulates Excitatory

Synaptic Transmission in Human Neurons. Neuron *103*, 617-626.e6.

Maruyama, T., Dougan, S.K., Truttmann, M.C., Bilate, A.M., Ingram, J.R., and Ploegh, H.L. (2015). Increasing the efficiency of precise genome editing with CRISPR-Cas9 by inhibition of nonhomologous end joining. Nat. Biotechnol. 2015 335 *33*, 538–542.

Matsui, T.K., Tsuru, Y., Hasegawa, K., and Kuwako, K. ichiro (2021). Vascularization of human brain organoids. Stem Cells *39*, 1017–1024.

McMahon, A.C., Barnett, M.W., O'Leary, T.S., Stoney, P.N., Collins, M.O., Papadia, S., Choudhary, J.S., Komiyama, N.H., Grant, S.G.N., Hardingham, G.E., et al. (2012). SynGAP isoforms exert opposing effects on synaptic strength. Nat. Commun. *3*, 1–9.

Meijer, M., Rehbach, K., Brunner, J.W., Classen, J.A., Lammertse, H.C.A., van Linge, L.A., Schut, D., Krutenko, T., Hebisch, M., Cornelisse, L.N., et al. (2019). A Single-Cell Model for Synaptic Transmission and Plasticity in Human iPSC-Derived Neurons. Cell Rep. *27*, 2199-2211.e6.

Meisler, M.H., Hill, S.F., and Yu, W. (2021). Sodium channelopathies in neurodevelopmental disorders. Nat. Rev. Neurosci. 2021 223 *22*, 152–166.

Middleton, S.J., Kneller, E.M., Chen, S., Ogiwara, I., Montal, M., Yamakawa, K., and McHugh, T.J. (2018). Altered hippocampal replay is associated with memory impairment in mice heterozygous for the Scn2a gene. Nat. Neurosci. *21*, 996–1003.

Mierau, S.B., and Neumeyer, A.M. (2019). Metabolic interventions in Autism Spectrum Disorder. Neurobiol. Dis. *132*, 104544.

Miles, J.H. (2011). Autism spectrum disorders—A genetics review. Genet. Med. 2011 134 *13*, 278–294.

Mirauta, B.A., Seaton, D.D., Bensaddek, D., Brenes, A., Bonder, M.J., Kilpinen, H., Agu, C.A., Alderton, A., Danecek, P., Denton, R., et al. (2020). Population-scale proteome variation in human induced pluripotent stem cells. Elife *9*, 1–22.

Misko, A., Jiang, S., Wegorzewska, I., Milbrandt, J., and Baloh, R.H. (2010). Mitofusin 2 is necessary for transport of axonal mitochondria and interacts with the Miro/Milton complex. J. Neurosci. *30*, 4232–4240.

Miura, Y., Li, M.Y., Birey, F., Ikeda, K., Revah, O., Thete, M.V., Park, J.Y., Puno, A., Lee, S.H., Porteus, M.H., et al. (2020). Generation of human striatal organoids and cortico-striatal assembloids from human pluripotent stem cells. Nat. Biotechnol. 2020 3812 *38*, 1421–1430.

Miura, Y., Li, M.Y., Revah, O., Yoon, S.J., Narazaki, G., and Paşca, S.P. (2022). Engineering brain assembloids to interrogate human neural circuits. Nat. Protoc. 2022 171 *17*, 15–35.

Mohanraju, P., Makarova, K.S., Zetsche, B., Zhang, F., Koonin, E. V., and Van Der Oost, J. (2016). Diverse evolutionary roots and mechanistic variations of the CRISPR-Cas systems. Science (80-.). *353*.

Muhia, M., Yee, B.K., Feldon, J., Markopoulos, F., and Knuesel, I. (2010). Disruption of hippocampus-regulated behavioural and cognitive processes by heterozygous constitutive

deletion of SynGAP. Eur. J. Neurosci. *31*, 529–543.

Muller, F.L., Liu, Y., and Van Remmen, H. (2004). Complex III releases superoxide to both sides of the inner mitochondrial membrane. J. Biol. Chem. *279*, 49064–49073.

Naeem, M., Majeed, S., Hoque, M.Z., and Ahmad, I. (2020). Latest Developed Strategies to Minimize the Off-Target Effects in CRISPR-Cas-Mediated Genome Editing. Cells *9*.

Nambiar, T.S., Billon, P., Diedenhofen, G., Hayward, S.B., Taglialatela, A., Cai, K., Huang, J.W., Leuzzi, G., Cuella-Martin, R., Palacios, A., et al. (2019). Stimulation of CRISPR-mediated homology-directed repair by an engineered RAD18 variant. Nat. Commun. 2019 101 *10*, 1–13.

Napoli, E., Wong, S., and Giulivi, C. (2013). Evidence of reactive oxygen species-mediated damage to mitochondrial DNA in children with typical autism. Mol. Autism *4*, 1–8.

Napoli, I., Mercaldo, V., Boyl, P.P., Eleuteri, B., Zalfa, F., De Rubeis, S., Di Marino, D., Mohr, E., Massimi, M., Falconi, M., et al. (2008). The Fragile X Syndrome Protein Represses Activity-Dependent Translation through CYFIP1, a New 4E-BP. Cell *134*, 1042–1054.

Nardi, A., Damann, N., Hertrampf, T., and Kless, A. (2012). Corrigendum: Advances in Targeting Voltage-Gated Sodium Channels with Small Molecules. ChemMedChem *7*, 1874–1874.

Nehme, R., Zuccaro, E., Ghosh, S.D., Li, C., Sherwood, J.L., Pietilainen, O., Barrett,

L.E., Limone, F., Worringer, K.A., Kommineni, S., et al. (2018). Combining NGN2 Programming with Developmental Patterning Generates Human Excitatory Neurons with NMDAR-Mediated Synaptic Transmission. Cell Rep. *23*, 2509–2523.

Nelson, S.B., and Valakh, V. (2015). Excitatory/Inhibitory Balance and Circuit Homeostasis in Autism Spectrum Disorders. Neuron *87*, 684–698.

Neves-Pereira, M., Muller, B., Massie, D., Williams, J.H.G., O'Brien, P.C.M., Hughes, A., Shen, S.-B., Clair, D.S., and Miedzybrodzka, Z. (2009). Deregulation of EIF4E: a novel mechanism for autism. J. Med. Genet. *46*, 759–765.

Niyazov, D.M., Kahler, S.G., and Frye, R.E. (2016). Primary Mitochondrial Disease and Secondary Mitochondrial Dysfunction: Importance of Distinction for Diagnosis and Treatment. Mol. Syndromol. *7*, 122–137.

Ogiwara, I., Miyamoto, H., Tatsukawa, T., Yamagata, T., Nakayama, T., Atapour, N., Miura, E., Mazaki, E., Ernst, S.J., Cao, D., et al. (2018). Nav1.2 haplodeficiency in excitatory neurons causes absence-like seizures in mice. Commun. Biol. *1*, 96.

Osorio, N., Alcaraz, G., Padilla, F., Couraud, F., Delmas, P., and Crest, M. (2005). Differential targeting and functional specialization of sodium channels in cultured cerebellar granule cells. J. Physiol. *569*, 801–816.

Pacheco, N.L., Heaven, M.R., Holt, L.M., Crossman, D.K., Boggio, K.J., Shaffer, S.A., Flint, D.L., and Olsen, M.L. (2017). RNA sequencing and proteomics approaches reveal novel deficits in the cortex of Mecp2-deficient mice, a model for Rett syndrome. Mol.

Autism *8*, 56.

Pak, C., Danko, T., Zhang, Y., Aoto, J., Anderson, G., Maxeiner, S., Yi, F., Wernig, M., and Südhof, T.C. (2015). Human Neuropsychiatric Disease Modeling using Conditional Deletion Reveals Synaptic Transmission Defects Caused by Heterozygous Mutations in NRXN1. Cell Stem Cell *17*, 316–328.

Palmieri, L., and Persico, A.M. (2010). Mitochondrial dysfunction in autism spectrum disorders: Cause or effect? Biochim. Biophys. Acta - Bioenerg. *1797*, 1130–1137.

Paquet, D., Kwart, D., Chen, A., Sproul, A., Jacob, S., Teo, S., Olsen, K.M., Gregg, A., Noggle, S., and Tessier-Lavigne, M. (2016). Efficient introduction of specific homozygous and heterozygous mutations using CRISPR/Cas9. Nature *533*, 125–129.

Paşca, S.P. (2019). Assembling human brain organoids. Science *363*, 126–127.

Paşca, A.M., Sloan, S.A., Clarke, L.E., Tian, Y., Makinson, C.D., Huber, N., Kim, C.H., Park, J.-Y., O'Rourke, N.A., Nguyen, K.D., et al. (2015). Functional cortical neurons and astrocytes from human pluripotent stem cells in 3D culture. Nat. Methods *12*, 671–678.

Pejhan, S., and Rastegar, M. (2021). Role of DNA Methyl-CpG-Binding Protein MeCP2 in Rett Syndrome Pathobiology and Mechanism of Disease. Biomol. 2021, Vol. 11, Page 75 *11*, 75.

Petreanu, L., Mao, T., Sternson, S.M., and Svoboda, K. (2009). The subcellular organization of neocortical excitatory connections. Nature *457*, 1142–1145.

Planells-Cases, R., Caprini, M., Zhang, J., Rockenstein, E.M., Rivera, R.R., Murre, C.,

Masliah, E., and Montal, M. (2000). Neuronal Death and Perinatal Lethality in Voltage-Gated Sodium Channel αII-Deficient Mice. Biophys. J. *78*, 2878–2891.

Pons, R., Andreu, A.L., Checcarelli, N., Vilà, M.R., Engelstad, K., Sue, C.M., Shungu, D., Haggerty, R., De Vivo, D.C., and DiMauro, S. (2004). Mitochondrial DNA abnormalities and autistic spectrum disorders. J. Pediatr. *144*, 81–85.

Primavera, D., Bandecchi, C., Lepori, T., Sanna, L., Nicotra, E., and Carpiniello, B. (2012). Does duration of untreated psychosis predict very long term outcome of schizophrenic disorders? results of a retrospective study. Ann. Gen. Psychiatry *11*, 1–6.

Qian, X., Jacob, F., Song, M.M., Nguyen, H.N., Song, H., and Ming, G.L. (2018). Generation of human brain region–specific organoids using a miniaturized spinning bioreactor. Nat. Protoc. 2018 133 *13*, 565–580.

Qian, X., Song, H., and Ming, G.L. (2019). Brain organoids: Advances, applications and challenges. Dev. *146*.

Qian, X., Su, Y., Adam, C.D., Deutschmann, A.U., Pather, S.R., Goldberg, E.M., Su, K., Li, S., Lu, L., Jacob, F., et al. (2020). Sliced Human Cortical Organoids for Modeling Distinct Cortical Layer Formation. Cell Stem Cell *26*, 766-781.e9.

Que, Z., Olivero-Acosta, M.I., Zhang, J., Eaton, M., Tukker, A.M., Chen, X., Wu, J., Xie, J., Xiao, T., Wettschurack, K., et al. (2021a). Hyperexcitability and Pharmacological Responsiveness of Cortical Neurons Derived from Human iPSCs Carrying Epilepsy-Associated Sodium Channel Nav1.2-L1342P Genetic Variant. J. Neurosci. *41*, 10194–

10208.

Que, Z., Olivero-Acosta, M.I., Zhang, J., Eaton, M., Skarnes, W.C., and Yang, Y. (2021b). Sodium channel Nav1.2-L1342P variant displaying complex biophysical properties renders hyperexcitability of cortical neurons derived from human iPSCs. BioRxiv 2021.01.18.427192.

Rakic, P. (2009). Evolution of the neocortex: a perspective from developmental biology. Nat. Rev. Neurosci. 2009 1010 *10*, 724–735.

Randall, M., Egberts, K.J., Samtani, A., Scholten, R.J.P.M., Hooft, L., Livingstone, N., Sterling-Levis, K., Woolfenden, S., and Williams, K. (2018). Diagnostic tests for autism spectrum disorder (ASD) in preschool children. Cochrane Database Syst. Rev. *2018*.

Rangaraju, V., Lauterbach, M., and Schuman, E.M. (2019). Spatially Stable Mitochondrial Compartments Fuel Local Translation during Plasticity.

Raybaud, C. (2010). Normal and abnormal embryology and development of the intracranial vascular system. Neurosurg. Clin. N. Am. *21*, 399–426.

Rees, H.A., and Liu, D.R. (2018). Base editing: precision chemistry on the genome and transcriptome of living cells. Nat. Rev. Genet. 2018 1912 *19*, 770–788.

Reid, D.A., Keegan, S., Leo-Macias, A., Watanabe, G., Strande, N.T., Chang, H.H., Oksuz, B.A., Fenyo, D., Lieber, M.R., Ramsden, D.A., et al. (2015). Organization and dynamics of the nonhomologous end-joining machinery during DNA double-strand break repair. Proc. Natl. Acad. Sci. U. S. A. *112*, E2575–E2584.

Rhee, H.J., Shaib, A.H., Rehbach, K., Lee, C., Seif, P., Thomas, C., Gideons, E., Guenther, A., Krutenko, T., Hebisch, M., et al. (2019). An Autaptic Culture System for Standardized Analyses of iPSC-Derived Human Neurons. Cell Rep. *27*, 2212-2228.e7.

Richter, J.D., and Zhao, X. (2021). The molecular biology of FMRP: new insights into fragile X syndrome. Nat. Rev. Neurosci. 2021 224 *22*, 209–222.

Richter, J.D., Bassell, G.J., and Klann, E. (2015). Dysregulation and restoration of translational homeostasis in fragile X syndrome. Nat. Rev. Neurosci. *16*, 595–605.

Rodrigues, D.C., Mufteev, M., Weatheritt, R.J., Djuric, U., Ha, K.C.H., Ross, P.J., Wei, W., Piekna, A., Sartori, M.A., Byres, L., et al. (2020). Shifts in Ribosome Engagement Impact Key Gene Sets in Neurodevelopment and Ubiquitination in Rett Syndrome. Cell Rep. *30*, 4179-4196.e11.

Ronen, G.M., Penney, S., and Andrews, W. (1999). The epidemiology of clinical neonatal seizures in Newfoundland: a population-based study. J. Pediatr. *134*, 71–75.

Roost, M.S., Slieker, R.C., Bialecka, M., Van Iperen, L., Gomes Fernandes, M.M., He, N., Suchiman, H.E.D., Szuhai, K., Carlotti, F., De Koning, E.J.P., et al. (2017). DNA methylation and transcriptional trajectories during human development and reprogramming of isogenic pluripotent stem cells. Nat. Commun. 2017 81 *8*, 1–11.

Rossignol, D.A., and Frye, R.E. (2012). Mitochondrial dysfunction in autism spectrum disorders: a systematic review and meta-analysis. Mol. Psychiatry *17*, 290.

Rouhani, F., Kumasaka, N., de Brito, M.C., Bradley, A., Vallier, L., and Gaffney, D.

(2014). Genetic Background Drives Transcriptional Variation in Human Induced Pluripotent Stem Cells. PLoS Genet. *10*, 1004432.

De Rubeis, S., He, X., Goldberg, A.P., Poultney, C.S., Samocha, K., Ercument Cicek, A., Kou, Y., Liu, L., Fromer, M., Walker, S., et al. (2014). Synaptic, transcriptional and chromatin genes disrupted in autism. Nature *515*, 209–215.

Rubenstein, J.L.R., and Merzenich, M.M. (2003). Model of autism: Increased ratio of excitation/inhibition in key neural systems. Genes, Brain Behav. *2*, 255–267.

Ruch, A., Kurczynski, T.W., and Velasco, M.E. (1989). Mitochondrial alterations in Rett syndrome. Pediatr. Neurol. *5*, 320–323.

Rumbaugh, G., Adams, J.P., Kim, J.H., and Huganir, R.L. (2006). SynGAP regulates synaptic strength and mitogen-activated protein kinases in cultured neurons. Proc. Natl. Acad. Sci. U. S. A. *103*, 4344–4351.

Sanders, S.J., Murtha, M.T., Gupta, A.R., Murdoch, J.D., Raubeson, M.J., Willsey, A.J., Ercan-Sencicek, A.G., DiLullo, N.M., Parikshak, N.N., Stein, J.L., et al. (2012). De novo mutations revealed by whole-exome sequencing are strongly associated with autism. Nature *485*, 237–241.

Sanders, S.J., He, X., Willsey, A.J., Ercan-Sencicek, A.G., Samocha, K.E., Cicek, A.E., Murtha, M.T., Bal, V.H., Bishop, S.L., Dong, S., et al. (2015). Insights into Autism Spectrum Disorder Genomic Architecture and Biology from 71 Risk Loci. Neuron *87*, 1215–1233.

Sanders, S.J., Campbell, A.J., Cottrell, J.R., Moller, R.S., Wagner, F.F., Auldridge, A.L., Bernier, R.A., Catterall, W.A., Chung, W.K., Empfield, J.R., et al. (2018). Progress in Understanding and Treating SCN2A-Mediated Disorders. Trends Neurosci. *41*, 442–456.

Sandin, S., Lichtenstein, P., Kuja-Halkola, R., Larsson, H., Hultman, C.M., and Reichenberg, A. (2014). The Familial Risk of Autism. JAMA *311*, 1770–1777.

Sanjurjo-Soriano, C., Erkilic, N., Mamaeva, D., and Kalatzis, V. (2022). CRISPR/Cas9-Mediated Genome Editing to Generate Clonal iPSC Lines. Methods Mol. Biol. *2454*, 589–606.

Santini, E., Huynh, T.N., MacAskill, A.F., Carter, A.G., Pierre, P., Ruggero, D., Kaphzan, H., and Klann, E. (2013). Exaggerated translation causes synaptic and behavioural aberrations associated with autism. Nature *493*, 411–415.

Santini, E., Huynh, T.N., Longo, F., Koo, S.Y., Mojica, E., D'Andrea, L., Bagni, C., and Klann, E. (2017). Reducing eIF4E-eIF4G interactions restores the balance between protein synthesis and actin dynamics in fragile X syndrome model mice. Sci. Signal. *10*.

Sasani, T.A., Pedersen, B.S., Gao, Z., Baird, L., Przeworski, M., Jorde, L.B., and Quinlan, A.R. (2019). Large, three-generation human families reveal post-zygotic mosaicism and variability in germline mutation accumulation. Elife *8*.

Satterstrom, F.K., Kosmicki, J.A., Wang, J., Breen, M.S., De Rubeis, S., An, J.-Y., Peng, M., Collins, R., Grove, J., Klei, L., et al. (2020). Large-Scale Exome Sequencing Study Implicates Both Developmental and Functional Changes in the Neurobiology of Autism.

Cell.

Saxena, A., and Chahrour, M. (2017). Autism Spectrum Disorder. Genomic Precis. Med. Prim. Care Third Ed. 301–316.

Saxton, R.A., and Sabatini, D.M. (2017). mTOR Signaling in Growth, Metabolism, and Disease. Cell *168*, 960–976.

Schieve, L.A., Tian, L.H., Drews-Botsch, C., Windham, G.C., Newschaffer, C., Daniels, J.L., Lee, L.C., Croen, L.A., and Danielle Fallin, M. (2018). Autism Spectrum Disorder and Birth Spacing: Findings from the Study to Explore Early Development (SEED). Autism Res. *11*, 81.

Schwarz, N., Bast, T., Gaily, E., Golla, G., Gorman, K.M., Griffiths, L.R., Hahn, A., Hukin, J., King, M., Korff, C., et al. (2019). Clinical and genetic spectrum of SCN2A-associated episodic ataxia. Eur. J. Paediatr. Neurol. *23*, 438–447.

Scult, M.A., Trampush, J.W., Zheng, F., Conley, E.D., Lencz, T., Malhotra, A.K., Dickinson, D., Weinberger, D.R., and Hariri, A.R. (2015). A Common Polymorphism in SCN2A Predicts General Cognitive Ability Through Effects on Prefrontal Cortex Physiology. J. Cogn. Neurosci. *27*, 1766.

Sebat, J., Lakshmi, B., Malhotra, D., Troge, J., Lese-Martin, C., Walsh, T., Yamrom, B., Yoon, S., Krasnitz, A., Kendall, J., et al. (2007). Strong association of de novo copy number mutations with autism. Science (80-.). *316*, 445–449.

Shendure, J., and Akey, J.M. (2015). The origins, determinants, and consequences of

human mutations. Science (80-.). *349*, 1478–1483.

Shi, R., Redman, P., Ghose, D., Liu, Y., Ren, X., Ding, L.J., Liu, M., Jones, K.J., and Xu, W. (2017). Shank proteins differentially regulate synaptic transmission. ENeuro *4*.

Shi, Y., Kirwan, P., and Livesey, F.J. (2012a). Directed differentiation of human pluripotent stem cells to cerebral cortex neurons and neural networks. Nat. Protoc. 2012 710 *7*, 1836–1846.

Shi, Y., Kirwan, P., Smith, J., Robinson, H.P.C., and Livesey, F.J. (2012b). Human cerebral cortex development from pluripotent stem cells to functional excitatory synapses. Nat. Neurosci. 2012 153 *15*, 477–486.

Shi, Y., Sun, L., Wang, M., Liu, J., Zhong, S., Li, R., Li, P., Guo, L., Fang, A., Chen, R., et al. (2020). Vascularized human cortical organoids (vOrganoids) model cortical development in vivo. PLOS Biol. *18*, e3000705.

Simkin, D., Papakis, V., Bustos, B.I., Ambrosi, C.M., Ryan, S.J., Baru, V., Williams, L.A., Dempsey, G.T., McManus, O.B., Landers, J.E., et al. (2022). Homozygous might be hemizygous: CRISPR/Cas9 editing in iPSCs results in detrimental on-target defects that escape standard quality controls. Stem Cell Reports *17*, 993–1008.

Skarnes, W.C., Rosen, B., West, A.P., Koutsourakis, M., Bushell, W., Iyer, V., Mujica, A.O., Thomas, M., Harrow, J., Cox, T., et al. (2011). A conditional knockout resource for the genome–wide study of mouse gene function. Nature *474*, 337.

Soliman, M.A., Aboharb, F., Zeltner, N., and Studer, L. (2017). Pluripotent stem cells in

neuropsychiatric disorders. Mol. Psychiatry *22*, 1241.

Spencer, C.M., Alekseyenko, O., Hamilton, S.M., Thomas, A.M., Serysheva, E., Yuva-Paylor, L.A., and Paylor, R. (2011). Modifying behavioral phenotypes in Fmr1KO mice: genetic background differences reveal autistic-like responses. Autism Res. *4*, 40–56.

Spillane, M., Ketschek, A., Merianda, T.T., Twiss, J.L., and Gallo, G. (2013). Mitochondria Coordinate Sites of Axon Branching through Localized Intra-axonal Protein Synthesis. Cell Rep. *5*, 1564–1575.

Spratt, P.A.W., Alexander, R.P., Ben-Shalom, R., Keeshen, C.M., Sanders, S.J., Bender Correspondence, K.J., Spratt, P.W., Sahagun, A., Kyoung, H., and Bender, K.J. (2021). Paradoxical hyperexcitability from NaV1.2 sodium channel loss in neocortical pyramidal cells. Cell Rep. *36*, 109483.

Spratt, P.W.E., Ben-Shalom, R., Keeshen, C.M., Burke, K.J., Clarkson, R.L., Sanders, S.J., and Bender, K.J. (2019). The Autism-Associated Gene Scn2a Contributes to Dendritic Excitability and Synaptic Function in the Prefrontal Cortex. Neuron *103*, 673-685.e5.

Srivastava, S., Love-Nichols, J.A., Dies, K.A., Ledbetter, D.H., Martin, C.L., Chung, W.K., Firth, H. V., Frazier, T., Hansen, R.L., Prock, L., et al. (2019). Meta-analysis and multidisciplinary consensus statement: exome sequencing is a first-tier clinical diagnostic test for individuals with neurodevelopmental disorders. Genet. Med. *21*, 2413–2421.

Steinhausen, H.C., Mohr Jensen, C., and Lauritsen, M.B. (2016). A systematic review and

meta-analysis of the long-term overall outcome of autism spectrum disorders in adolescence and adulthood. Acta Psychiatr. Scand. *133*, 445–452.

Sullivan, P.F., and Geschwind, D.H. (2019). Defining the Genetic, Genomic, Cellular, and Diagnostic Architectures of Psychiatric Disorders. Cell *177*, 162–183.

Sun, W., Liu, H., Yin, W., Qiao, J., Zhao, X., and Liu, Y. (2022). Strategies for Enhancing the Homology-Directed Repair Efficiency of CRISPR-Cas Systems. Cris. J. *5*, 7–18.

Symington, L.S. (2016). Mechanism and regulation of DNA end resection in eukaryotes. Http://Dx.Doi.Org/10.3109/10409238.2016.1172552 *51*, 195–212.

Tai, C., Abe, Y., Westenbroek, R.E., Scheuer, T., and Catterall, W.A. (2014). Impaired excitability of somatostatin- and parvalbumin-expressing cortical interneurons in a mouse model of Dravet syndrome. Proc. Natl. Acad. Sci. U. S. A. *111*, E3139–E3148.

Takahashi, K., Tanabe, K., Ohnuki, M., Narita, M., Ichisaka, T., Tomoda, K., and Yamanaka, S. (2007). Induction of Pluripotent Stem Cells from Adult Human Fibroblasts by Defined Factors. Cell *131*, 861–872.

Talkowski, M.E., Rosenfeld, J.A., Blumenthal, I., Pillalamarri, V., Chiang, C., Heilbut, A., Ernst, C., Hanscom, C., Rossin, E., Lindgren, A.M., et al. (2012). Sequencing Chromosomal Abnormalities Reveals Neurodevelopmental Loci that Confer Risk across Diagnostic Boundaries. Cell *149*, 525–537.

Tang, L., Zeng, Y., Du, H., Gong, M., Peng, J., Zhang, B., Lei, M., Zhao, F., Wang, W.,

Li, X., et al. (2017). CRISPR/Cas9-mediated gene editing in human zygotes using Cas9 protein. Mol. Genet. Genomics *292*, 525–533.

Tatsukawa, T., Raveau, M., Ogiwara, I., Hattori, S., Miyamoto, H., Mazaki, E., Itohara, S., Miyakawa, T., Montal, M., and Yamakawa, K. (2019). Scn2a haploinsufficient mice display a spectrum of phenotypes affecting anxiety, sociability, memory flexibility and ampakine CX516 rescues their hyperactivity. Mol. Autism *10*, 15.

Tebbenkamp, A.T.N., Varela, L., Choi, J., Paredes, M.I., Giani, A.M., Song, J.E., Sestan-Pesa, M., Franjic, D., Sousa, A.M.M., Liu, Z.W., et al. (2018). The 7q11.23 Protein DNAJC30 Interacts with ATP Synthase and Links Mitochondria to Brain Development. Cell *175*, 1088-1104.e23.

Testa, G., Schaft, J., Van Der Hoeven, F., Glaser, S., Anastassiadis, K., Zhang, Y., Hermann, T., Stremmel, W., and Stewart, A.F. (2004). A reliable lacZ expression reporter cassette for multipurpose, knockout-first alleles. Genesis *38*, 151–158.

Thapar, A., and Cooper, M. (2013). Copy Number Variation: What Is It and What Has It Told Us About Child Psychiatric Disorders? J. Am. Acad. Child Adolesc. Psychiatry *52*, 772.

Tidball, A.M., Lopez-Santiago, L.F., Yuan, Y., Glenn, T.W., Margolis, J.L., Clayton Walker, J., Kilbane, E.G., Miller, C.A., Martina Bebin, E., Scott Perry, M., et al. (2020). Variant-specific changes in persistent or resurgent sodium current in SCN8A-related epilepsy patient-derived neurons. Brain *143*, 3025–3040.

Topol, A., Tran, N.N., and Brennand, K.J. (2015). A guide to generating and using hiPSC derived NPCs for the study of neurological diseases. J. Vis. Exp. e52495.

Tsai, P.T., Hull, C., Chu, Y., Greene-Colozzi, E., Sadowski, A.R., Leech, J.M., Steinberg, J., Crawley, J.N., Regehr, W.G., and Sahin, M. (2012). Autistic-like behaviour and cerebellar dysfunction in Purkinje cell Tsc1 mutant mice. Nature *488*, 647–651.

Turner, T.N., Coe, B.P., Dickel, D.E., Hoekzema, K., Nelson, B.J., Zody, M.C., Kronenberg, Z.N., Hormozdiari, F., Raja, A., Pennacchio, L.A., et al. (2017). Genomic Patterns of De Novo Mutation in Simplex Autism. Cell *171*, 710-722.e12.

Tyzio, R., Nardou, R., Ferrari, D.C., Tsintsadze, T., Shahrokhi, A., Eftekhari, S., Khalilov, I., Tsintsadze, V., Brouchoud, C., Chazal, G., et al. (2014). Oxytocin-mediated GABA inhibition during delivery attenuates autism pathogenesis in rodent offspring. Science (80-.). *343*, 675–679.

Urnov, F.D., Miller, J.C., Lee, Y.L., Beausejour, C.M., Rock, J.M., Augustus, S., Jamieson, A.C., Porteus, M.H., Gregory, P.D., and Holmes, M.C. (2005). Highly efficient endogenous human gene correction using designed zinc-finger nucleases. Nat. 2005 4357042 *435*, 646–651.

Vaher, U., Nõukas, M., Nikopensius, T., Kals, M., Annilo, T., Nelis, M., Õunap, K., Reimand, T., Talvik, I., Ilves, P., et al. (2014). De Novo SCN8A mutation identified by whole-exome sequencing in a boy with neonatal epileptic encephalopathy, multiple congenital anomalies, and movement disorders. J. Child Neurol. *29*, NP202–NP206.

Vazquez, L.E., Chen, H.J., Sokolova, I., Knuesel, I., and Kennedy, M.B. (2004). SynGAP regulates spine formation. J. Neurosci. *24*, 8862–8872.

Volkmar, F.R., Jackson, S.L.J., and Hart, L. (2017). Transition Issues and Challenges for Youth with Autism Spectrum Disorders. Pediatr. Ann. *46*, e219–e223.

Volpato, V., and Webber, C. (2020). Addressing variability in iPSC-derived models of human disease: guidelines to promote reproducibility. Dis. Model. Mech. *13*.

Volpato, V., Smith, J., Sandor, C., Ried, J.S., Baud, A., Handel, A., Newey, S.E., Wessely, F., Attar, M., Whiteley, E., et al. (2018). Reproducibility of Molecular Phenotypes after Long-Term Differentiation to Human iPSC-Derived Neurons: A Multi-Site Omics Study. Stem Cell Reports *11*, 897.

Waltes, R., Gfesser, J., Haslinger, D., Schneider-Momm, K., Biscaldi, M., Voran, A., Freitag, C.M., and Chiocchetti, A.G. (2014). Common EIF4E variants modulate risk for autism spectrum disorders in the high-functioning range. J. Neural Transm. *121*, 1107–1116.

Wang, C., Geng, H., Liu, W., and Zhang, G. (2017). Prenatal, perinatal, and postnatal factors associated with autism: A meta-analysis. Medicine (Baltimore). *96*.

Wang, H.-G., Bavley, C.C., Li, A., Jones, R.M., Hackett, J.E., Bayleyen, Y., Lee, F.S., Rajadhyaksha, A.M., and Pitt, G.S. (2021). Scn2a severe hypomorphic mutation decreases excitatory synaptic input and causes autism-associated behaviors. JCI Insight.

Wang, J., Zhang, C., and Feng, B. (2020). The rapidly advancing Class 2 CRISPR-Cas

technologies: A customizable toolbox for molecular manipulations. J. Cell. Mol. Med. *24*, 3256.

Weiss, L.A., Arking, D.E., Daly, M.J., Chakravarti, A., Brune, C.W., West, K., O'Connor, A., Hilton, G., Tomlinson, R.L., West, A.B., et al. (2009). A genome-wide linkage and association scan reveals novel loci for autism. Nat. 2009 4617265 *461*, 802–808.

Weissman, J.R., Kelley, R.I., Bauman, M.L., Cohen, B.H., Murray, K.F., Mitchell, R.L., Kern, R.L., and Natowicz, M.R. (2008). Mitochondrial disease in autism spectrum disorder patients: A cohort analysis. PLoS One *3*.

Werling, D.M., Brand, H., An, J.Y., Stone, M.R., Zhu, L., Glessner, J.T., Collins, R.L., Dong, S., Layer, R.M., Markenscoff-Papadimitriou, E., et al. (2018). An analytical framework for whole-genome sequence association studies and its implications for autism spectrum disorder. Nat. Genet. *50*, 727–736.

Wilfert, A.B., Turner, T.N., Murali, S.C., Hsieh, P.H., Sulovari, A., Wang, T., Coe, B.P., Guo, H., Hoekzema, K., Bakken, T.E., et al. (2021). Recent ultra-rare inherited variants implicate new autism candidate risk genes. Nat. Genet. 2021 538 *53*, 1125–1134.

Wolff, M., Johannesen, K.M., Hedrich, U.B.S., Masnada, S., Rubboli, G., Gardella, E., Lesca, G., Ville, D., Milh, M., Villard, L., et al. (2017). Genetic and phenotypic heterogeneity suggest therapeutic implications in SCN2A-related disorders. Brain *140*, 1316–1336.

Xiang, Y., Tanaka, Y., Patterson, B., Kang, Y.J., Govindaiah, G., Roselaar, N., Cakir, B., Kim, K.Y., Lombroso, A.P., Hwang, S.M., et al. (2017). Fusion of Regionally Specified hPSC-Derived Organoids Models Human Brain Development and Interneuron Migration. Cell Stem Cell *21*, 383-398.e7.

Xie, Y., Ng, N.N., Safrina, O.S., Ramos, C.M., Ess, K.C., Schwartz, P.H., Smith, M.A., and O'Dowd, D.K. (2020). Comparisons of dual isogenic human iPSC pairs identify functional alterations directly caused by an epilepsy associated SCN1A mutation. Neurobiol. Dis. *134*, 104627.

Xu, B., Roos, J.L., Levy, S., Van Rensburg, E.J., Gogos, J.A., and Karayiorgou, M. (2008). Strong association of de novo copy number mutations with sporadic schizophrenia. Nat. Genet. 2008 407 *40*, 880–885.

Yamagata, T., Raveau, M., Kobayashi, K., Miyamoto, H., Tatsukawa, T., Ogiwara, I., Itohara, S., Hensch, T.K., and Yamakawa, K. (2020). CRISPR/dCas9-based Scn1a gene activation in inhibitory neurons ameliorates epileptic and behavioral phenotypes of Dravet syndrome model mice. Neurobiol. Dis. *141*, 104954.

Yamasaki, A.E., Panopoulos, A.D., and Belmonte, J.C.I. (2017). Understanding the genetics behind complex human disease with large-scale iPSC collections. Genome Biol. *18*, 1–3.

Yamatogi, Y., and Ohtahara, S. (2002). Early-infantile epileptic encephalopathy with suppression-bursts, Ohtahara syndrome; its overview referring to our 16 cases. Brain Dev. *24*, 13–23.

Yi, F., Danko, T., Botelho, S.C., Patzke, C., Pak, C., Wernig, M., and Südhof, T.C. (2016). Autism-associated SHANK3 haploinsufficiency causes Ih channelopathy in human neurons. Science (80-.). *352*, aaf2669.

Yoon, S.-J., Elahi, L.S., Pașca, A.M., Marton, R.M., Gordon, A., Revah, O., Miura, Y., Walczak, E.M., Holdgate, G.M., Fan, H.C., et al. (2018). Reliability of human cortical organoid generation. Nat. Methods 2018 161 *16*, 75–78.

Yuen, R.K.C., Thiruvahindrapuram, B., Merico, D., Walker, S., Tammimies, K., Hoang, N., Chrysler, C., Nalpathamkalam, T., Pellecchia, G., Liu, Y., et al. (2015). Whole-genome sequencing of quartet families with autism spectrum disorder. Nat. Med. *21*, 185–191.

Yuen, R.K.C., Merico, D., Cao, H., Pellecchia, G., Alipanahi, B., Thiruvahindrapuram, B., Tong, X., Sun, Y., Cao, D., Zhang, T., et al. (2016). Genome-wide characteristics of de novo mutations in autism. Npj Genomic Med. 2016 11 *1*, 1–10.

Yuen, R.K.C., Merico, D., Bookman, M., Howe, J.L., Thiruvahindrapuram, B., Patel, R. V., Whitney, J., Deflaux, N., Bingham, J., Wang, Z., et al. (2017). Whole genome sequencing resource identifies 18 new candidate genes for autism spectrum disorder. Nat. Neurosci. *20*, 602–611.

Zakon, H.H. (2012). Adaptive evolution of voltage-gated sodium channels: The first 800 million years. Proc. Natl. Acad. Sci. U. S. A. *109*, 10619.

Zaman, T., Helbig, I., Božović, I.B., DeBrosse, S.D., Bergqvist, A.C., Wallis, K., Medne,

L., Maver, A., Peterlin, B., Helbig, K.L., et al. (2018). Mutations in SCN3A cause early infantile epileptic encephalopathy. Ann. Neurol. *83*, 703.

Zhang, J., Chen, X., Lanman, N.A., Skarnes, W.C., Correspondence, Y.Y., Eaton, M., Wu, J., Ma, Z., Lai, S., Park, A., et al. (2021a). Severe deficiency of the voltage-gated sodium channel Na V 1.2 elevates neuronal excitability in adult mice ll Severe deficiency of the voltage-gated sodium channel Na V 1.2 elevates neuronal excitability in adult mice. Cell Rep. *36*, 109495.

Zhang, S., Shen, J., Li, D., and Cheng, Y. (2021b). Strategies in the delivery of Cas9 ribonucleoprotein for CRISPR/Cas9 genome editing. Theranostics *11*, 614.

Zhang, Y., Pak, C., Han, Y., Ahlenius, H., Zhang, Z., Chanda, S., Marro, S., Patzke, C., Acuna, C., Covy, J., et al. (2013). Rapid Single-Step Induction of Functional Neurons from Human Pluripotent Stem Cells. Neuron *78*, 785–798.

Zhang, Z., Marro, S.G., Zhang, Y., Arendt, K.L., Patzke, C., Zhou, B., Fair, T., Yang, N., Südhof, T.C., Wernig, M., et al. (2018). The fragile X mutation impairs homeostatic plasticity in human neurons by blocking synaptic retinoic acid signaling. *4338*, 1–16.

Zhao, X., and Bhattacharyya, A. (2018). Human Models Are Needed for Studying Human Neurodevelopmental Disorders. Am. J. Hum. Genet. *103*, 829.

Zhao, R.Z., Jiang, S., Zhang, L., and Yu, Z. Bin (2019). Mitochondrial electron transport chain, ROS generation and uncoupling (Review). Int. J. Mol. Med. *44*, 3–15.

Zhu, J.J., Qin, Y., Zhao, M., Van Aelst, L., and Malinow, R. (2002). Ras and Rap control

AMPA receptor trafficking during synaptic plasticity. Cell *110*, 443–455.

Ziats, C.A., Patterson, W.G., and Friez, M. (2021). Syndromic Autism Revisited: Review of the Literature and Lessons Learned. Pediatr. Neurol. *114*, 21–25.

Zwaigenbaum, L., and Penner, M. (2018). Autism spectrum disorder: advances in diagnosis and evaluation. BMJ *361*.